Mascle, J., Lohmann, G.P., Clift, P.D., et al., 1996
Proceedings of the Ocean Drilling Program, Initial Reports, Vol. 159

7. SITE 961[1]

Shipboard Scientific Party[2]

HOLE 961A

Date occupied: 4 February 1995

Date departed: 7 February 1995

Time on hole: 3 days, 21 hr

Position: 3°26.542′N, 3°3.513′W

Bottom felt (drill pipe measurement from rig floor, m): 3303.6

Distance between rig floor and sea level (m): 11.6

Water depth (drill pipe measurement from sea level, m): 3292.0

Total depth (from rig floor, m): 3612.3

Penetration (m): 308.7

Number of cores (including cores having no recovery): 35

Total length of cored section (m): 308.7

Total core recovered (m): 60.42

Core recovery (%): 19.6

Oldest sediment cored:
Depth (mbsf): 308.7
Lithology: clayey siltstone
Age: pre-late Paleocene; probably Aptian–Albian
Measured velocity (km/s): 2.728 at 159-961A-34R-1, 48 cm

HOLE 961B

Date occupied: 7 February 1995

Date departed: 12 February 1995

Time on hole: 4 days, 7 hr, 45 min

Position: 3°26.556′N, 3°3.560′W

Bottom felt (drill pipe measurement from rig floor, m): 3303.6

Distance between rig floor and sea level (m): 11.6

Water depth (drill pipe measurement from sea level, m): 3292.0

Total depth (from rig floor, m): 3678.2

Penetration (m): 374.6

Number of cores (including cores having no recovery): 19

Total length of cored section (m): 134.8

Total core recovered (m): 56.74

Core recovery (%): 42.1

Oldest sediment cored:
Depth (mbsf): 374.6
Lithology: siltstone
Age: pre-late Paleocene; probably Aptian–Albian
Measured velocity (km/s): 2.806 at 159-961B-16R-CC, 4 cm

Comments: Drilled: 0–216.3, 239–259.9, and 264.9–267.5 mbsf

Principal results: The vessel moved to Site 961 from Site 960 in dynamic positioning mode, while a PDC anti-whirl bit was made up to the bottom-hole assembly (BHA) with a mechanical bit release. Hole 961A was spudded at 1230 hr on 4 February and RCB cored to 308.7 mbsf. Recovery varied from 0% to 56%. ROP deteriorated during drilling due to bit balling and blockage of the jets despite increasing circulation. A free-fall funnel was dropped and the bit changed to a regular TCI cone bit. After a successful reentry, the coaxial cable retrieving the vibration-isolated television (VIT) frame broke. The VIT fell to the seafloor and could only be retrieved by tripping the pipe back to the surface, where the VIT was seen to have caught on the bit body. Rather than risk a second reentry, we decided to start Hole 961B. The bit was drilled ahead to 267.5 mbsf, taking four spot cores in the process. Continuous RCB coring took place from 267.5 to 369.9 mbsf, where coring was suspended due to deteriorating hole conditions. After reaming and circulation of mud, coring continued to 374.6 mbsf, where it was terminated because of hole conditions. The bit reached the rig floor at 0715 hr on 12 February.

A stratigraphic section 308.7 m long was cored in Hole 961A. In Hole 961B, the top 216.3 mbsf, and the intervals 239.0–259.9 mbsf and 264.9–267.5 mbsf, were drilled without coring.

Three lithologic units were identified at Site 961 (Fig. 1). lithologic Unit I (0–129.5 mbsf), comprises nannofossil ooze with foraminifers, which grades downhole into clayey nannofossil chalk and claystone. The unit is divided into two subunits: lithologic Subunit IA (Pleistocene to early Pliocene; 0–16 mbsf), having a darker color because of higher pyrite and organic matter content; and lithologic Subunit IB (early Pliocene to early Miocene; 16–129.5 mbsf). Lithologic Unit I at this site can be correlated with lithologic Unit I at Sites 959 and 960. The top boundary of lithologic Unit II (129.5–188.5 mbsf) is marked by the first significant appearance of siliceous microfossils in the sediments. This unit also is divided into two subunits. Lithologic Subunit IIA (129.5–148.1 mbsf) comprises early Miocene nannofossil chalk with radiolarians and glauconite, and claystone with glauconite. Lithologic Subunit IIB (148.1–188.5 mbsf) consists of chert interbedded with clayey porcellanite with micrite and zeolite, palygorskite/zeolite claystone, and glauconite-rich porcellanite (early Eocene to late Paleocene and older). Lithologic Unit II correlates with Unit II at Site 959, and with Units II and III at Site 960. Lithologic Unit III (188.5–374.6 mbsf), of late Paleocene or older age, consists of dark gray to black silty sandstone, sandy siltstone, clayey siltstone, and silty claystone, with local pyrite and siderite. This unit is correlative with lithologic Subunit VA at Site 960.

In Hole 961A little bedding data were recorded because of poor recovery and drilling disturbance. A few normal faults were observed in Hole 961A. Variable dips in Hole 961B can be attributed at least partly to synsedimentary disturbances (convolute bedding, slump fold) and faults. We observed sets of conjugated normal faults (Section 159-961B-18R-1) and steeply dipping shears (Core 159-961B-13R). In Core 159-961B-13R, the finely laminated bedding is affected by microfolds closely associated with small-scale shear planes. Calcite veining, infilling fractures and breccia, is found in the upper few cores of Hole 961B. Soft sedimentary defor-

[1]Mascle, J., Lohmann, G.P., Clift, P.D., et al., 1996. *Proc. ODP, Init. Repts.,* 159: College Station, TX (Ocean Drilling Program).
[2]Shipboard Scientific Party is given in the list preceding the Table of Contents.

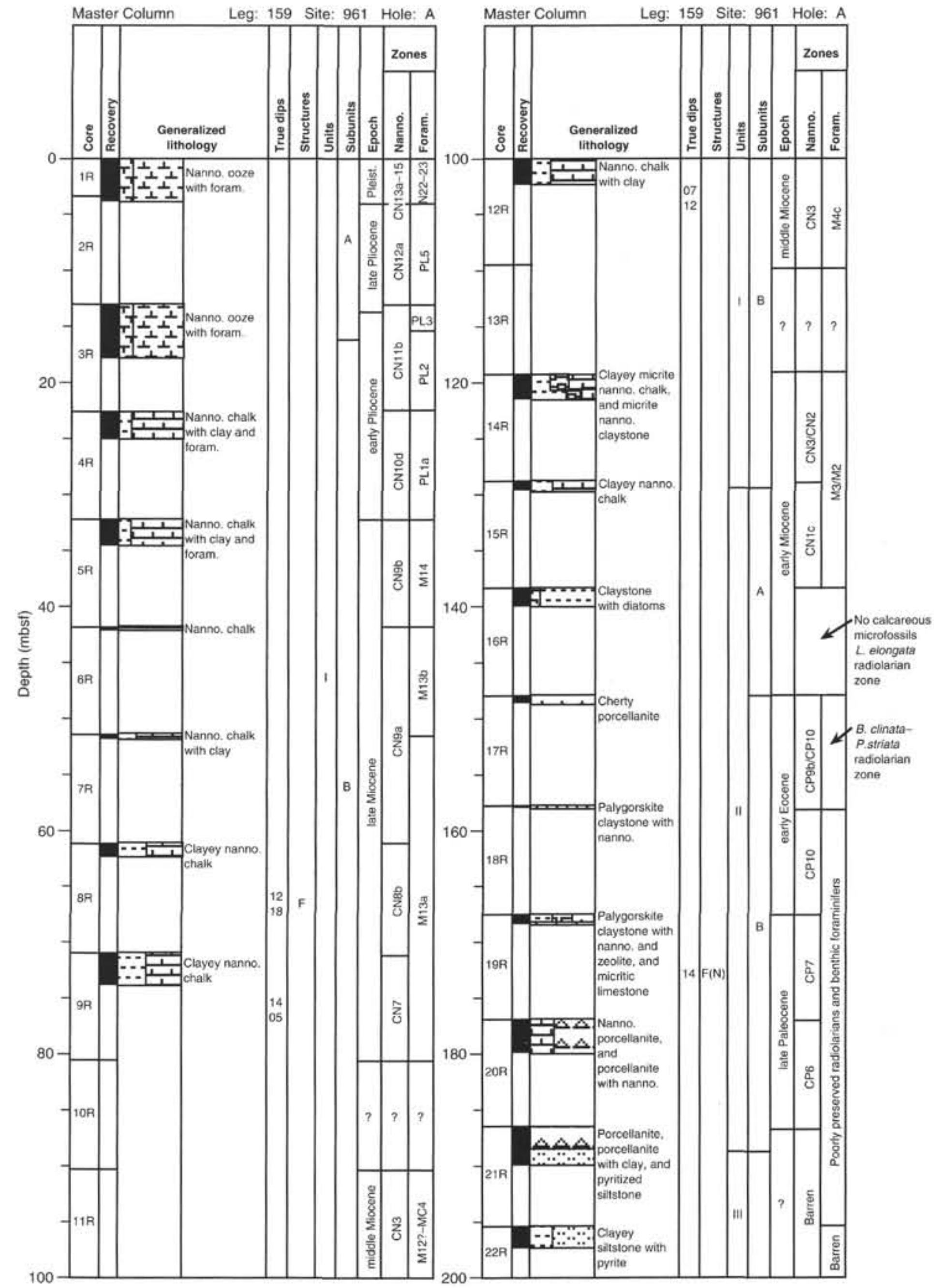

Figure 1. Site 961 master column.

mations were observed in both Holes 961A and 961B. They include a water escape structure and a sand pipe, slump folds, and wavy to convolute bedding.

Pleistocene sediments were recovered in Hole 961A at 3.4 mbsf. A Pliocene section extends from below 3.4 mbsf to the Miocene/Pliocene boundary at 32.3 mbsf. Below a middle to upper Miocene interval that extends to 148.1 mbsf, an unconformity has removed most or all of the Oligocene and middle to upper Eocene sediment. There also may be an unconformity or condensed interval in the upper middle Miocene at 81–100 mbsf. Lower Eocene sediment is present from 148.1 to 167.4 mbsf and upper Paleocene sediment from 177.0 to 186.7 mbsf. Below this, the section is barren of calcareous and siliceous microfossils. Hole 961B is barren of planktonic foraminifers. Only one species of calcareous nannofossil has been identified at 313.2 and 322.4 mbsf. This taxon ranges in age from the Bajocian through the Cretaceous. Calcareous microfossil preservation generally deteriorates downsection, and planktonic foraminifers are absent below the lower Miocene.

Changes in magnetic susceptibility mirror lithologic changes, with susceptibilities of 10×10^{-5} SI units encountered in lithologic Subunit IA and higher susceptibilities, between 10 and 50×10^{-5} SI units, in lithologic Subunit IB. Lithologic Unit II has low susceptibilities, $<15 \times 10^{-5}$ SI units, and lithologic Unit III has high susceptibilities, typically between 10 and 40×10^{-5} SI units. RCB coring caused a high degree of drilling disturbance, so measurements of the direction of magnetization have no geological significance. The variation of the intensity of NRM downhole shows a pattern similar to previous sites. NRM intensity increases from <10 mA/

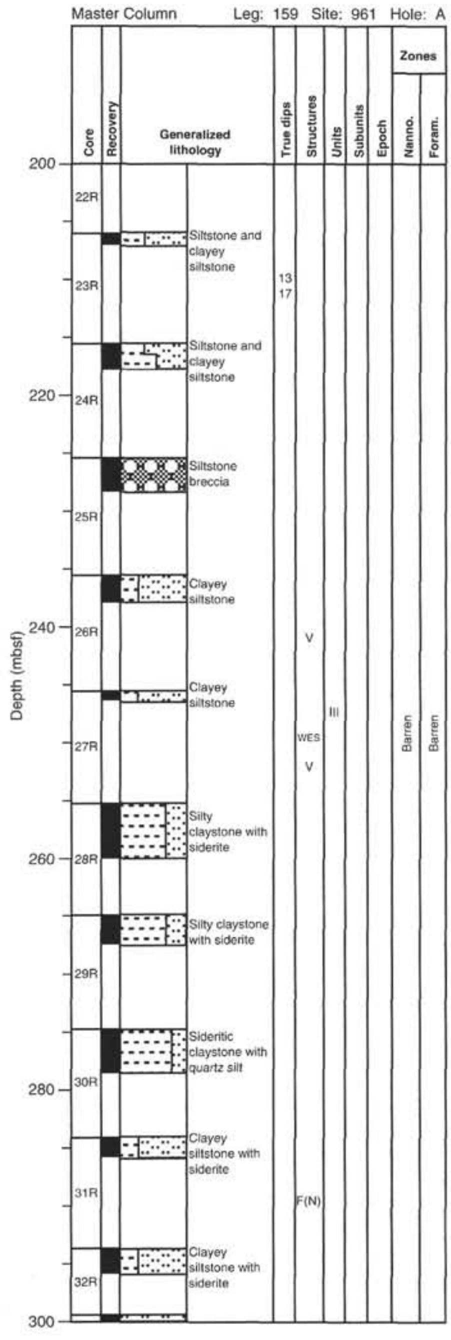

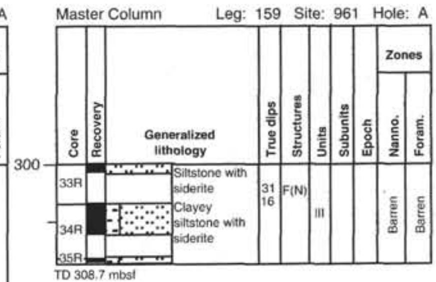

Figure 1 (continued).

m in Core 159-961A-1R to up to 50 mA/m in Core 159-961A-3R. This change occurs at the transition between lithologic Subunits IA and IB, within planktonic foraminifer Biozone M9. NRM intensities in lithologic Unit II are low (<1 mA/m) except for Cores 159-961-20R and 21R, which also show a marked reduction in palygorskite content. These cores have NRM values up to 10 mA/m. NRM values remain at this level throughout lithologic Unit III.

Eight interstitial-water samples were taken during coring operations at Site 961. In spite of the discontinuous sample suite, the data demonstrate a set of diagenetic reactions analogous to those documented at Sites 959 and 960. Sulfate, potassium, and magnesium concentrations decrease with increasing depth, while the concentrations of calcium and ammonium increase with increasing depth in the sediment. Appreciable pore-fluid sulfate concentrations, approximately 6 mM, persist below the depth in the sediment where methane concentrations rise above background levels. These results are suggestive of contamination of the deep (>250 mbsf) interstitial-water samples with seawater. However, none of the pore-water profiles show the large degree of scatter that is expected to be associated with large and variable amounts of seawater contamination.

Generally lower carbonate and organic carbon content in Holes 961A and 961B compared to Sites 959 and 960 are related to the more pelagic depositional conditions. Pliocene to Pleistocene deposits display highest carbonate content (up to 50 wt%). Evidence for intense organic matter degradation was found in the upper 70 mbsf by a continuous exponential decrease in organic carbon content with depth. Paleocene through Miocene sediments have low carbonate and organic carbon contents (below

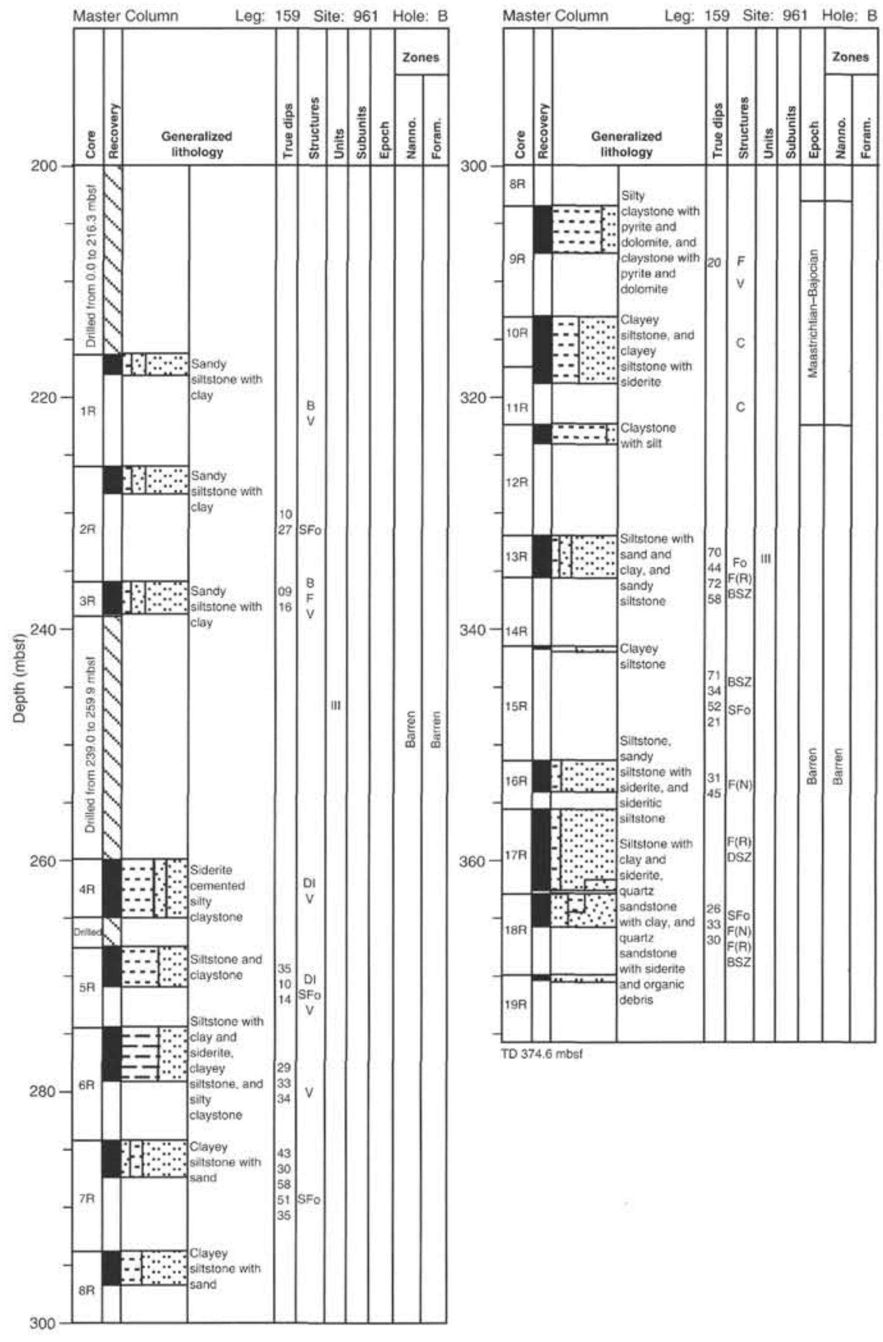

Figure 1 (continued).

10 wt% and below 0.2 wt%, respectively). Intermediate organic carbon content (about 0.4 wt%) but low carbonate content characterize the underlying sandstone and siltstone below 220 mbsf. The few maxima in organic carbon (up to 0.7 wt%) within these lithologies were probably caused by an enhanced supply of terrigenous organic matter. A vertical offset of about 10 m is proposed for Hole 961A and 961B deposits according to the matching of both carbonate and organic carbon records. In Hole 961A, very low headspace methane concentrations were recorded. A maximum methane content of 991 ppm was observed in Core 159-961A-34R (303.5 mbsf). No ethane was recorded. In Hole 961B, slightly higher readings of methane were seen. A maximum concentration of 7310 ppm was recorded in Core 159-961B-13R (333.6 mbsf), but no ethane was detected.

General correlation between different sets of physical properties data at Site 961 is good, but the low density of measurements does not permit more detailed studies. All physical properties data collected at Site 961 show a distinctive change in trend at the boundary between lithologic Units II and III at 188 mbsf, attributable to significant lithologic differences.

BACKGROUND AND OBJECTIVES

Site 961 is located in 3303 m water depth on the last significant morphologic expression of the Côte d'Ivoire-Ghana Marginal Ridge (CIGMR) just before its burial, toward the west, beneath the thick sedimentary cover of the Deep Ivorian Basin (Fig. 2). In this area, a multichannel seismic (MCS) line recorded along strike of the CIGMR shows that the progressively deepening pre- and synrift

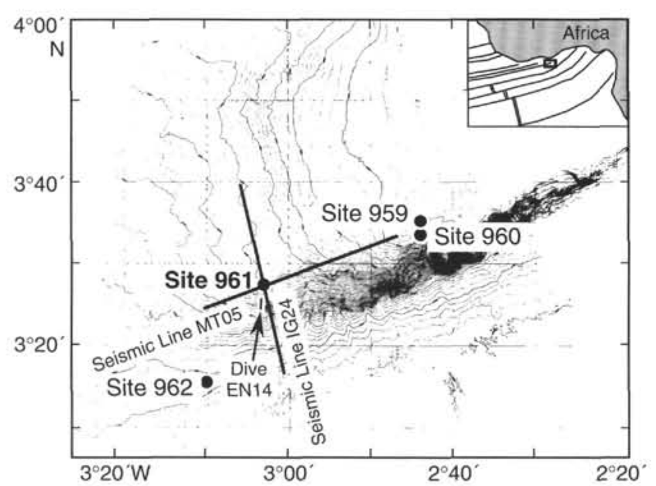

Figure 2. Location of Site 961 on a swath bathymetric map of the CIGMR and surrounding area (*Equamarge II* survey, 1988). Bathymetric contours are in meters (contour interval 50 m): MCS migrated seismic Line MT05 (*Equasis* survey, 1990) and single-channel Line IG24 (*Equamarge II* survey, 1988) on which the site is located, are also indicated. Location of dive EN 14 (*Equanaute* survey, 1992), 3 miles downslope of Site 961, is also shown.

basement consists of a series of rotated structural blocks and bordering half-grabens (Fig. 3), each about 5 km across. Detailed structural mapping (see Basile et al., this volume, Fig. 7) clearly indicates that these extensional structures are bounded by north–south-trending fault zones and are rather similar, in trend and size, to second-order extensional blocks detected to the north within the adjacent rifted Deep Ivorian Basin (see Basile et al., this volume, Fig. 8). The regional structural similarities between both extensional and transform domains led Basile et al. (1993) to propose that the CIGMR is a part of the deep extensional basin. The CIGMR was first uplifted by active wrench tectonism between equatorial Africa and northeast Brazil in Early Cretaceous times, and then, later, during the Late Cretaceous, by thermal exchange between adjacent hot oceanic lithosphere and colder stretched continental crust (Mascle and Blarez, 1987). As an alternative hypothesis, the fossil structural ridge may consist of a series of continental slivers (and Early Cretaceous sediment cover) left-laterally displaced from the eastern Ghanaian slope during the wrench tectonic stage (Lamarche et al., in press). A comparable mechanism has been proposed to explain the recovery of continental-derived metasediments exposed some 400 km farther west, within the deep oceanic abyssal plain, along the fossil Romanche Fracture Zone (Honnorez et al., 1994).

Site 961 is located on the summit of a fault-rotated block. The western margin of this block appears to be bounded by an important, north–south-trending fault zone that easily can be correlated with a similarly trending normal fault system that cuts across the pre-rift Deep Ivorian Basin acoustic basement (Basile et at., this volume). Moreover, crustal sections, deduced from wide-angle seismic data across this part of the CIGMR domain, show a similar thickness (on the order of 15–16 km) to the crust beneath the nearby northern extensional basin (Sage, 1994; Mascle et al., 1995). We believe that this asymmetric basement block, like other tilted basement features detected at depth beneath the CIGMR (Fig. 3), resulted first from an early extensional tectonic stage and has, only later, been rotated slightly during the margin transform phase (Basile et al., 1993).

At Site 961, MCS Line MT05 (Fig. 3) shows a relatively thin (approximately 300 m according to computed interval velocities), well-layered, sedimentary cover that includes only parts of seismic Units D to F as defined at Site 959 (see "Introduction" chapter, this volume). A single-channel seismic line (Line IG24; Fig. 4), almost perpendicular to the MCS MT05 line (Fig. 2), indicates that sediment thickness reduction is chiefly due to the pinching-out of seismic Units C and D against the block's northern slope. Drilling at Site 961 was expected to reach the top of a thick wedge of strong, almost parallel, reflectors, after penetrating about 100 m of contorted and discontinuous reflectors. Inspection of a migrated MCS section (96 channels) of Line MT05 (Fig. 5) reveals that this thin sequence correlates toward the east with an eastward-thickening sequence, where prograding figures can be detected. We infer this prograding wedge to be an equivalent, in a proximal depositional environment, of Unit B as defined at Site 959. The underlying reflectors may then represent Unit A, which is the synrift infilling of a half graben (Subunits A1 and A2 of Basile et al., 1993), or even potentially indicative of a pre-rift setting, judging by the subparallel arrangement of the deepest reflectors. If true, this interpretation may indicate strong erosive events during different stages of ridge uplift.

Equanaute dive EN 14, just 3 miles downslope of Site 961, retrieved barren, thinly laminated and burrowed siltstones and semi-indurated claystones that may belong to seismic Units A and B, respectively. The dive has also documented evidence of strong present-day bottom-current activities (Mascle et al., 1994).

Objectives

Transform Margin Evolution

As at Sites 959 and 960, the primary goals at Site 961 were to document the stratigraphically deepest seismic Units A and B, which are respectively inferred to be coeval with the extensional and transform phases of CIGMR tectonism. Unit A is expected to have recorded both tectonic regimes and should consequently be strongly deformed, while Unit B should have chiefly been affected by strike-slip deformation only. We also anticipated differences in sedimentary depositional environment between the two units. According to deep dive samples, Unit A was thought to be made of deltaic clastic sediments (Mascle et al., 1993), and Unit B of a prograding wedge of shallow marine sediments, as suggested by the internal seismic arrangement (G. Lamarche et al., unpubl. data). Continuous coring in both units was expected to help determine the relative and absolute timing of the successive events that prevailed during margin formation: (1) the onset of rifting by dating the deepest (pre-rift?) formations; (2) the end of rifting and the onset of ocean spreading by dating the Unit A/B boundary unconformity; (3) the end of transform tectonism by dating Unit B and its unconformable contact with Unit C. As for Sites 959 and 960, continuous coring was also required to better assess post-tectonic relative vertical motions of the CIGMR and their relationship to sea-level fluctuations. This can be achieved through dating the post-tectonic sediments and by determining their depositional environment. The comparison of sedimentary and stratigraphic data from Sites 959 and 960 with those gathered at Site 961 (40 km apart) will allow the hypothesis of a progressively westward moving and thermally induced uplift to be tested, through a subsidence reconstruction at each site.

As indicated above, two distinct mechanisms have been proposed to explain the presence of a series of asymmetric blocks beneath the main transform ridge. Are these blocks slivers of continental crust displaced along the main shear zone? Could these basement features be extensional horsts created during the rifting stage and subsequently uplifted and slightly rotated? We have relied on complementary detailed paleomagnetic and microstructural measurements and continuous Formation MicroScanner logging to provide true coordinate orientation data to help answer these questions.

Finally, the anticipated recovery of coarse-grained sandstones, such as the ones discontinuously sampled during deep dives on the southern slope of the CIGMR (Bouillin et al., 1994) should help to determine the past thermal, erosional, and subsidence histories of the transform margin. Analysis of the sandstones using fission-track techniques will provide a model of the thermal evolution of the

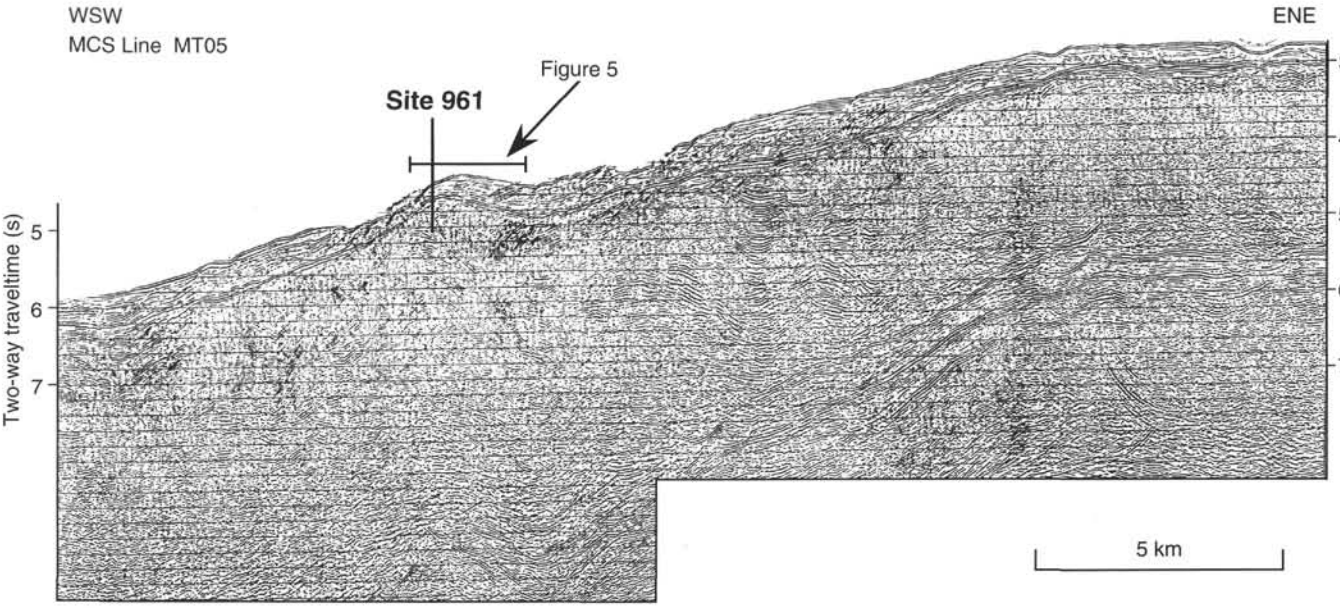

Figure 3. Migrated section of MCS seismic Line MT05 (*Equasis* survey, 1990) along strike of the western segment of the CIGMR (see Fig. 2). Location of Site 961 is shown. The site is located almost on the summit of a rotated basement block, chiefly to document the synrift stage (Unit A) and possibly the pre-rift A0 sequence; Unit B, inferred to be post-rift in the extensional basin and syntransform across the CIGMR, is also well expressed on this line.

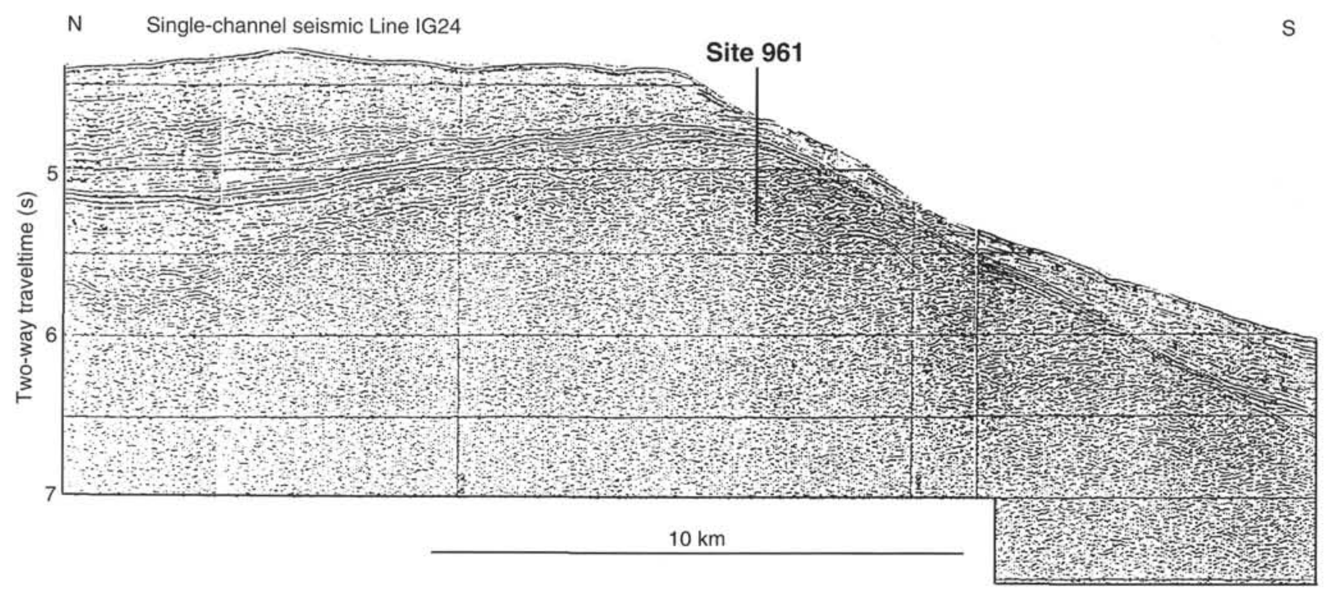

Figure 4. Single-channel seismic Line IG24 (*Equamarge II* survey, 1988) across the CIGMR, which is expressed in this area as an acoustic basement high. This consists of a rotated horst as demonstrated by MCS Line MT05. Units C through F, as defined at Site 959, progressively thin out toward the basement block.

CIGMR. Special emphasis will be placed on lateral differences in the thermal evolution between drill sites through time.

OPERATIONS

After the bit cleared the seafloor at Site 960, the vessel moved to Site 961 in dynamic positioning (DP) mode while continuing to trip the drill string. Once the bottom-hole assembly (BHA) components had been racked back into the derrick, the rotary table was available for use in the disposal of 2520 m of sandline from the aft core winch. This cut was required to get beyond a portion of the line that had broken. Approximately 15 m of line on either side of the damaged section was retained for evaluation by the sandline manufacturer. A rotary core barrel (RCB) polycrystalline diamond compact (PDC) anti-whirl bit was made up to a mechanical bit release and the RCB core barrels were spaced out in the outer core barrel. The remainder of the RCB BHA was then made up, and the rig crew began tripping the drill string to the seafloor. Before the drill string reached bottom at 0920 hr on 4 February, the signal from the pre-deployed positioning beacon was acquired, and by 1015 hr the vessel was within 20 m of the site coordinates. A summary of coring at Site 961 is given in Table 1, and drilling operations at Holes 961A and 961B are reviewed below.

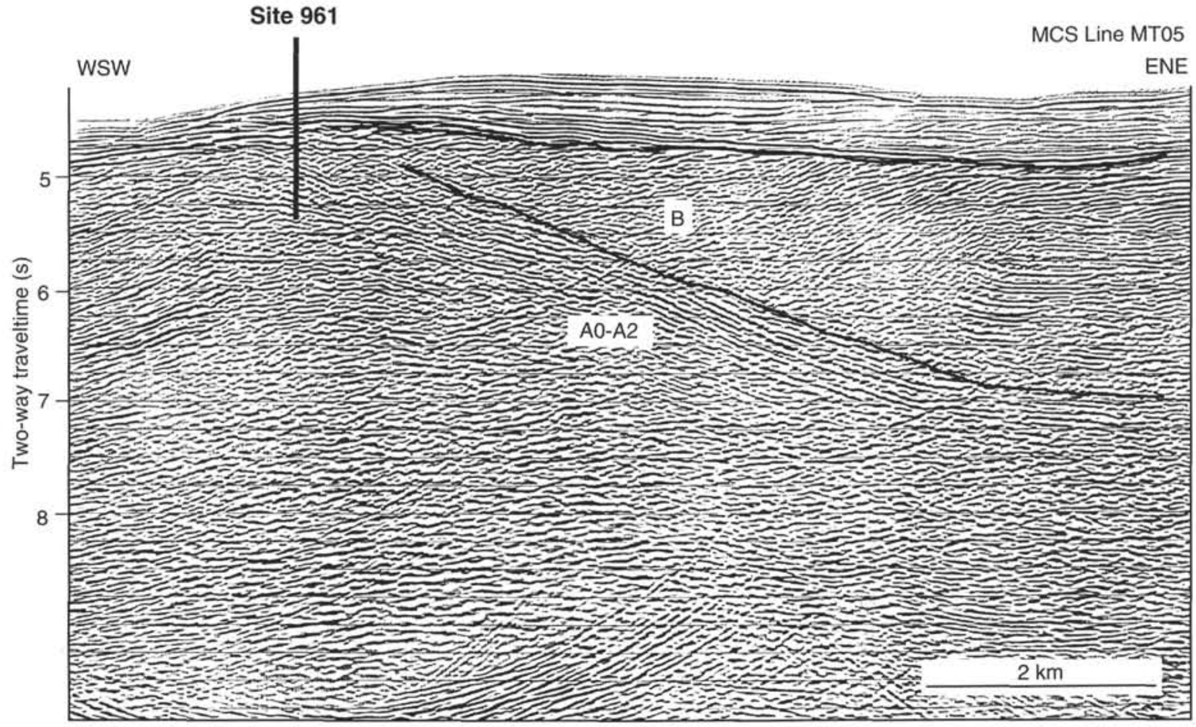

Figure 5. Detail of migrated MCS (96 channels) Line MT05 at Site 961 location. The seismic section shows successive seismic Units A (Subunits A0, A1, and A2, according to Basile et al., 1993), which are characterized by distinct acoustic facies. Subunit A0 appears to be bounded by prominent subparallel reflectors, which may potentially indicate a pre-rift arrangement. Unit B thickens considerably eastward, where it shows characteristic prograding internal reflectors.

Site 961

Hole 961A

After the drill pipe was run into the hole and the top drive was picked up, Hole 961A was spudded at 1230 hr on 4 February. Mud line was established at 3303.6 m by direct pipe measurement (DPM). The corrected precision depth recorder (PDR) reading normalized to driller's datum was 3302.4 m. RCB coring continued for the next 2-1/2 days (35 cores) at which point a depth of 3612.3 mbrf or 308.7 mbsf was achieved. Recovery was extremely erratic, ranging from as little as 0 to as much as 56%. Overall the recovery was a relatively poor 19.7%. The rate of penetration (ROP) with the RCB PDC anti-whirl bit was initially better than that achieved in similar formations with the CC-3 and CC-4 TCI core bits. ROP from 0 to 126 mbsf on the first day averaged 39.7 m/hr. By the second day the sediment became noticeably stiffer and extremely sticky. The clay appeared to be water sensitive becoming very slippery when wet yet retaining a hard, plastic property when compacted and dried by the drilling operation. The result was a severe problem with bit balling and bit jet plugging. ROP on the second day had slowed to an average of 10.1 m/hr. Circulation flow rates were continually increased in an attempt to keep the bit from balling and the jets open, but to little or no avail. The ROP further deteriorated to an average of 4.1 m/hr on the third day, and the recovered core began to exhibit evidence of core erosion, probably due to a failed bit seal. Pump pressures indicated that at least half of the six bit jets were plugged, and the poor ROP confirmed a continued balling problem.

As a result of the deterioration of core quality and poor ROP, it was decided that the bit should be pulled and inspected. A free fall funnel (FFF) was deployed followed by the vibration-isolated television (VIT) frame. The mini-cone appeared to be in proper position on the seafloor as the bit came clear of the hole and was tripped to the surface. At 0930 hr on 7 February the bit was at the rig floor. Upon inspection it was found to be severely balled, three of six jets were plugged, and three external PDC gauge cutters were missing. All of the remaining PDC cutters appeared to be in excellent condition. Approximately one quarter of the bit body was worn in a 90° quadrant where the outside diameter (OD) gauge cutters were missing. The missing cutters were probably broken during the course of drilling through chert layers in the upper part of the hole. The ROP achieved with this bit was 2–4 times that achieved with the TCI bits, but because the bit was not re-runable, it was decided that a cheaper CC-3 bit would be used next, to avoid leaving an expensive new PDC bit in the hole. This bit would have to be dropped in the hole to allow logging, even though it would then have only drilled 300 m.

The BHA was made up, the core barrels were spaced out, and the drill pipe was tripped back to bottom. At 1615 hr, after 15 min of vessel maneuvering, the FFF was reentered, and the pipe was run into the hole to 3568 m (264.4 mbsf), at which time the top drive was picked up. During preparations for the resumption of coring, the VIT frame was being recovered. However, at 1715 hr on 7 February the coax cable parted with the VIT frame at 752 mbrf. The winch operator reported that he did not have the VIT frame weight after being informed by the DP operator that cable continuity had been lost and the breaker had tripped twice in succession. The top drive was then set back again and the drill string was tripped back to the ship in the hope that the small diameter sleeve on the VIT frame survived the impact and the unit would come back riding on the bit body. The bit cleared the seafloor at 1830 hr, and at 2330 hr the VIT frame and 750 m of coax cable arrived in the moon pool. During this trip discussions were held to consider various drilling options were discussed. It was decided to spud a new hole rather than wait on the status report and subsequent repairs to the TV reentry system. The remaining coax cable had been inspected to a depth of 4700 m and was found to be of questionable integrity due to extremely corroded and brittle armor wires. Re-heading the cable was considered imprudent and would take up to 24 hr. To set up and spool on the spare coax cable, stored in the riser hold, was estimated to take about an additional 12 hr. It was unknown what

Table 1. Coring summary for Site 961.

Core	Date (1995)	Time (UTC)	Depth (mbsf)	Length cored (m)	Length recovered (m)	Recovery (%)
159-961A-						
1R	Feb 4	1330	0.0–3.4	3.4	3.38	99.4
2R	Feb 4	1415	3.4–13.1	9.7	0.04	0.4
3R	Feb 4	1500	13.1–22.7	9.6	4.64	48.3
4R	Feb 4	1545	22.7–32.3	9.6	2.40	25.0
5R	Feb 4	1630	32.3–41.9	9.6	2.25	23.4
6R	Feb 4	1700	41.9–51.5	9.6	0.17	1.8
7R	Feb 4	1740	51.5–61.2	9.7	0.21	2.2
8R	Feb 4	1830	61.2–71.0	9.8	1.07	10.9
9R	Feb 4	1910	71.0–80.6	9.6	2.65	27.6
10R	Feb 4	2000	80.6–90.3	9.7	0.00	0.0
11R	Feb 4	2045	90.3–99.9	9.6	0.00	0.0
12R	Feb 4	2135	99.9–109.6	9.7	2.27	23.4
13R	Feb 4	2235	109.6–119.3	9.7	0.00	0.0
14R	Feb 4	2335	119.3–128.9	9.6	2.21	23.0
15R	Feb 5	0030	128.9–138.5	9.6	0.78	8.1
16R	Feb 5	0130	138.5–148.1	9.6	1.64	17.1
17R	Feb 5	0250	148.1–157.8	9.7	0.51	5.3
18R	Feb 5	0430	157.8–167.4	9.6	0.12	1.3
19R	Feb 5	0540	167.4–177.0	9.6	0.78	8.1
20R	Feb 5	0630	177.0–186.7	9.7	2.88	29.7
21R	Feb 5	0730	186.7–196.4	9.7	3.18	32.8
22R	Feb 5	1000	196.4–206.1	9.7	1.93	19.9
23R	Feb 5	1300	206.1–215.7	9.6	0.87	9.1
24R	Feb 5	1515	215.7–225.5	9.8	2.05	20.9
25R	Feb 5	1900	225.5–235.6	10.1	2.82	27.9
26R	Feb 5	2215	235.6–245.7	10.1	2.25	22.3
27R	Feb 6	0005	245.7–255.3	9.6	0.70	7.3
28R	Feb 6	0200	255.3–264.9	9.6	4.72	49.1
29R	Feb 6	0400	264.9–274.5	9.6	2.33	24.3
30R	Feb 6	0615	274.5–284.2	9.7	3.66	37.7
31R	Feb 6	1030	284.2–293.8	9.6	1.46	15.2
32R	Feb 6	1430	293.8–299.5	5.7	2.05	35.9
33R	Feb 6	1730	299.5–303.5	4.0	1.29	32.2
34R	Feb 6	2130	303.5–308.2	4.7	2.65	56.4
35R	Feb 6	2330	308.2–308.7	0.5	0.46	92.0
Coring totals:				308.7	60.42	19.6
159-961B-						
		*** Drilled from 0.0 to 216.3 mbsf ***				
1R	Feb 8	2210	216.3–226.0	9.7	1.64	16.9
2R	Feb 9	0030	226.0–236.0	10.0	2.28	22.8
3R	Feb 9	0330	236.0–239.0	3.0	2.85	95.0
		*** Drilled from 239.0 to 259.9 mbsf ***				
4R	Feb 9	1330	259.9–264.9	5.0	6.48	129.0
		*** Drilled from 264.9 to 267.5 mbsf ***				
5R	Feb 9	1820	267.5–274.5	7.0	3.39	48.4
6R	Feb 9	2050	274.5–284.2	9.7	4.63	47.7
7R	Feb 9	2355	284.2–293.8	9.6	3.22	33.5
8R	Feb 10	0240	293.8–303.5	9.7	2.88	29.7
9R	Feb 10	0510	303.5–313.2	9.7	3.99	41.1
10R	Feb 10	0845	313.2–317.4	4.2	6.06	144.0
11R	Feb 10	1330	317.4–322.4	5.0	1.25	25.0
12R	Feb 10	1650	322.4–332.1	9.7	1.54	15.9
13R	Feb 10	2005	332.1–341.7	9.6	3.29	34.3
14R	Feb 10	2310	341.7–351.4	9.7	0.17	1.8
15R	Feb 11	0145	351.4–355.7	4.3	2.73	63.5
16R	Feb 11	0400	355.7–360.7	5.0	5.43	108.0
17R	Feb 11	0900	360.7–362.9	2.2	1.99	90.4
18R	Feb 11	1245	362.9–369.9	7.0	2.65	37.8
19R	Feb 11	2330	369.9–374.6	4.7	0.27	5.7
Coring totals:				134.8	56.74	42.1
Drilled:				239.8		
Total:				374.6		

damage may have been sustained by the VIT frame itself or the TV/sonar electronics mounted on it. Hole 961A was officially terminated at 2330 hr on 7 February, the time at which the bit/VIT frame arrived at the moon pool.

Hole 961B

Two hours were expended cutting away, and untangling, the 750 m of failed coax cable piled on top of, and beneath, the VIT frame. The failed wire was disposed of and the ship was offset 100 m west in preparation for spudding the next hole, assuming that the sediment layer would be thinner as we moved up dip, up the slope of the Marginal Ridge. Once the VIT frame was cleared and removed, the same drill pipe and RCB BHA from Hole 961A was tripped back to the seafloor. Hole 961B was spudded at 0800 hr on 8 February. As the PDR depth was virtually the same as at the previous hole, the same water depth of 3303.6 m (DPM) was used. RCB coring was initiated at a depth of 3519.9 m (216.3 mbsf) after drilling down with a center bit at an average ROP of 23.0 m/hr. Four spot cores were taken alternating with occasional center bit drilling to a depth of 3571.1 m or 267.5 mbsf. The cores were taken periodically because, surprisingly, the net ROP with a core barrel in place seemed to be better than that achieved with the center bit, even with allowances for the additional wireline time required.

Continuous RCB coring was initiated with Core 159-961B-5R and continued to a depth of 3673.5 m (369.9 mbsf) before deteriorating hole conditions prompted remedial action. Recovery over this interval was quite erratic due to the alternating hard and soft interbedded sediments and occasional chert layers. The average daily recovery ranged from 20% to 60%. Likewise, the ROP varied greatly, ranging from 1.5 to 10.5 m/hr. Bit balling probably contributed to the poor drilling rate. Drilling parameters were varied extensively, all with little or no effect on recovery and/or ROP. Coring was terminated at 369.9 mbsf when high pump pressures and torquing indicated hole instability. The pipe was worked off bottom, and the hole was back-reamed to a depth of 206.7 mbsf. At that point a 20-barrel high-viscosity mud pill was circulated, and the pipe was advanced back to bottom with normal pressure and torque parameters. Seven m of fill, found on bottom, was washed and reamed out of the hole, and another mud pill was circulated downhole. After the core barrel was recovered, hole conditions remained favorable, and coring resumed at 2030 hr on 11 February. Coring continued with Core 159-962B-19R to 3678.2 m (374.6 mbsf). However, hole instability again became a problem and continued attempts to deepen the hole were futile. Coring was abandoned at midnight. The drill pipe was pulled clear of the seafloor at 0130 hr on 12 February. The top drive was racked back and the pipe trip continued. The remaining drill string was recovered. The positioning beacon was released and recovered, and the vessel began moving in DP mode to Site 962 (proposed site IG-3). At 0715 hr on 12 February 1995 the bit cleared the rig floor ending Hole 961B.

SITE GEOPHYSICS

Site Survey

Two single-channel seismic reflection lines were recorded over Site 961, which corresponds to proposed Site IG2, during the seismic survey shot at the beginning of Leg 159 (full details of the acquisition of these data are given in the "Underway Geophysics" chapter, this volume). The two lines are arranged so as to form a figure-eight centered on the site (Fig. 6). Line IG2-1 runs west-southwest–east-northeast and is coincident with multichannel seismic Line MT05, acquired during the *Equasis* survey of 1990. The second line, IG2-2, has a north-south trend and is positioned between *Equamarge II* (1988) single-channel Lines IG23 and IG24. Shooting the new data close to, or coincident with, previously acquired data allowed us to verify the exact site location.

Although the single-channel data collected during Leg 159 have a low signal to noise ratio (i.e., the data are noisy), the acoustic basement can still be determined along the two lines crossing Site 961, where the overlying undeformed sediment cover is relatively thin.

Integration of Seismic Profiles with Observations from the Site

Due to poor hole conditions no downhole measurements were made at Site 961. Therefore the conversion from two-way traveltime to depth for this site is based on discrete velocity measurements taken

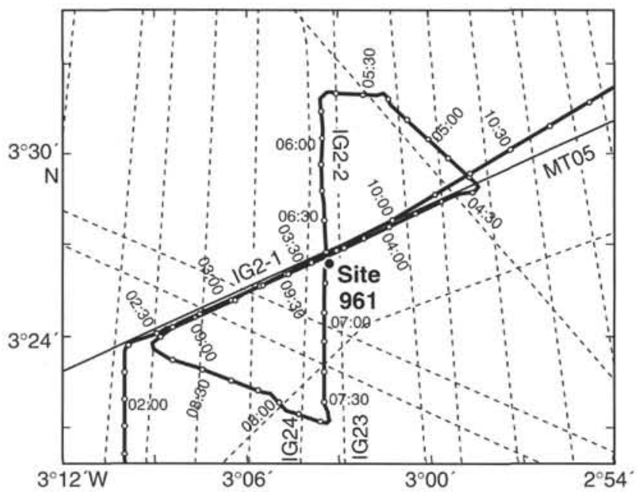

Figure 6. Track chart showing the location of Site 961 and the seismic data available in the area. Thick lines correspond to the single-channel data collected at the beginning of Leg 159, thin lines denote multichannel data acquired during the *Equasis* program of 1990, and dashed lines show the single-channel data from the *Equamarge II* survey of 1988.

Table 2. Depth of reflectors at Site 961.

Reflector	Time (s TWT)	Depth (mbsf)	Origin of reflector*
R1	0.20	160	Chert; top of lithologic Subunit IIB
R2	0.30	300	? Increase in cementation by siderite in lithologic Unit III

Note: *See "Lithostratigraphy" section, this chapter.

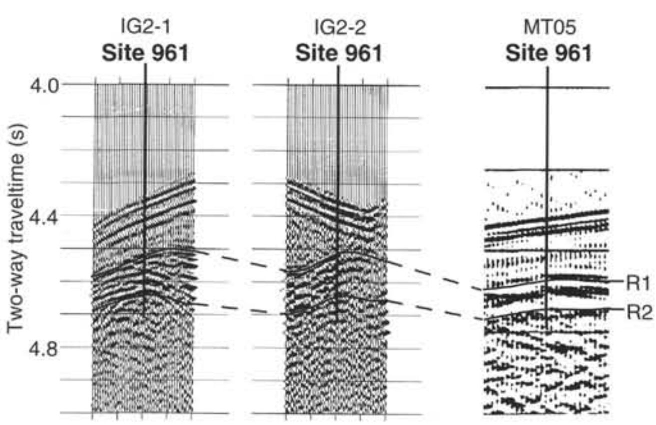

Figure 7. Ties of the principal reflectors observed on single-channel Lines IG2-1 and IG2-2 and multichannel Line MT05 to the lithologies at Site 961.

with the Digital Sound Velocimeter or the Hamilton Frame Velocimeter (see "Physical Properties" section, this chapter). The depth estimates of the major reflectors observed at Site 961 are summarized in Table 2, and the tie of the site to the two seismic lines collected at the beginning of Leg 159 (IG2-1 and IG2-2) and multichannel Line MT05 is shown in Figure 7.

Reflector R1: 0.20 s TWT Below Seafloor

Reflector R1 is a strong, laterally continuous reflector that marks the base of an acoustically transparent unit below the seafloor (Fig. 7). Assuming a velocity of 1.60 km/s in the upper part of the sedimentary column (determined from the average of the discrete velocity measurements taken over this region), Reflector R1 corresponds to a depth of 160 mbsf. This reflector therefore represents the top of lithologic Unit IIB, consisting of early Eocene to late Paleocene cherts, palygorskite/zeolite claystones, and porcellanite at 148 mbsf (see "Lithostratigraphy" section, this chapter). At the resolution of the seismic wavelet, where the wavelength equals 40 m at 1.6 km/s velocity and 40 Hz frequency, this small misfit between the computed and observed depths is perfectly acceptable.

Reflector R1 is equivalent to Reflector R1 at Site 960, farther east along the Côte d'Ivoire-Ghana Marginal Ridge and corresponding to the same Eocene chert layer (see "Site Geophysics" section in the "Site 960" chapter). The transparent seismic facies above Reflector R1 therefore can be correlated to seismic Units E and F; Units D and C can be seen to pinch-out against the northern slope of the ridge (see "Background and Objectives" section, this chapter).

Reflector R2: 0.30 s TWT Below Seafloor

Reflector R2 corresponds to a change in acoustic facies at 0.30 s TWT below the seafloor (Fig. 7). Here the continuous reflectors and transparent packages of the upper section are replaced by an apparent acoustic basement of discontinuous and dipping reflectors. Using an average velocity of 2.77 km/s for the section below the top of lithologic Subunit IIB, the computed depth of Reflector R2 is 300 m. From the lithology, index properties, and velocimetry (see "Lithostratigraphy" and "Physical Properties" sections, this chapter), the cause of this reflection is not immediately apparent. The best explanation is the increase in cementation by siderite below 250 mbsf.

From these results it becomes apparent that the top of lithologic Unit III is not seen as a clear reflection on the seismic profiles. This can be explained by the thinness of overlying lithologic Subunit IIB, which has a thickness of just 40 m. At a velocity of 2.7 km/s the wavelength of the seismic source is on the order of 70 m, and therefore the base of a thin layer cannot be differentiated from its top. Between Reflectors R1 and R2 a thin package of fairly continuous reflectors with a thickness of approximately 0.5 s TWT can be seen at Site 961 (Fig. 7). This thin sequence can be determined at Site 961 on multichannel seismic Line MT05 but is masked by interference with the R1 Reflector on the single-channel lines (IG2-1 and IG2-2) because these data were acquired with a less ideal seismic source with a longer signal duration. This sediment package corresponds to the top of lithologic Unit III. Although the age of lithologic Unit III could not be determined, we can correlate this unit to seismic Unit A, from the lithology and, particularly, the structures observed within the unit, as observed at Site 960. Seismic Unit B, seen at Sites 959 and 960 as limestones of Turonian through Coniacian age, appears to be absent at Site 961, although the uppermost part of lithologic Unit III may be equivalent to seismic Unit B at this site, as the age of this unit could not be determined.

The bottom of Hole 961B corresponds to a two-way traveltime of 0.36 s below seafloor.

LITHOSTRATIGRAPHY

In Hole 961A, 308.7 m of stratigraphic section was penetrated and cored. Hole 961B was not continuously cored: the top 216.3 m and the intervals 239.0–259.9 and 264.9–267.5 mbsf were drilled without coring, followed by coring to a total depth of 374.6 mbsf. RCB coring at this site yielded less than 20% recovery of most drilled intervals, and many of the recovered cores were highly disturbed by drilling.

Three lithologic units were identified at Site 961 (Fig. 8; Table 3). Described downsection, lithologic Unit I comprises calcareous, pelagic nannofossil ooze, which grades downhole into chalk and clay-

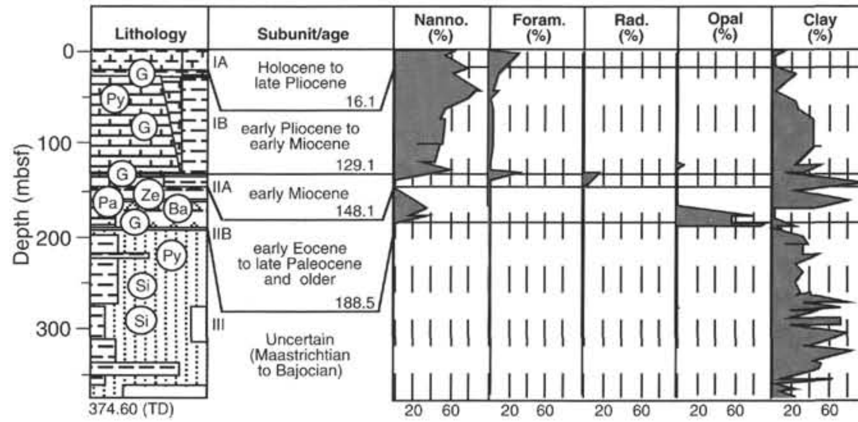

Figure 8. Stratigraphic column for Site 961.

Table 3. Lithologic units for Site 961.

Unit	Subunit	Cored interval	Depth interval (mbsf)	Thickness (m)	Lithology	Age (epoch)
I	A	159-961A-1R, 0 cm, to 61A-3R-2, 150 cm	0–16.1	16.1	Nannofossil ooze with foraminifers and foraminifer nannofossil ooze with micrite	Holocene to late Pliocene
	B	159-961A-3R-2, 150 cm, to 15R-1, 59 cm	16.1–129.5	113.4	Nannofossil ooze/chalk with foraminifers and nannofossil claystone with micrite (glauconitic)	early Pliocene to early Miocene
II	A	159-961A-15R-CC, 0 cm, to 16R-CC, 18 cm	129.5–148.1	18.6	Nannofossil chalk with radiolarians, and claystone (glauconitic)	early Miocene
	B	159-961A-17R-1, 0 cm, to 21R-2, 34 cm	148.1–188.5	40.4	Chert, palygorskite/zeolite claystones, and glauconite-rich porcellanite with nannofossils and clay	early Eocene to late Paleocene and older
III		159-961A-21R-2, 34 cm, to 35R-CC, 45 cm (TD)	188.5–308.7	120.2	Sandstone, silty sandstone, sandy siltstone, clayey siltstone, and silty claystone	Uncertain (Maastrichtian to Bajocian)
		159-961B-1R-1, 0 cm, to 19R-CC, 26 cm (TD)	216.3–374.6	158.3		

Note: TD = total depth

stone. It was divided into two subunits: Subunit IA (Holocene to upper Pliocene), which has a darker color because of higher pyrite and organic matter contents, and Subunit IB (lower Pliocene to lower Miocene). Lithologic Unit I at this site can be correlated with lithologic Unit I at Sites 959 and 960. The top boundary of lithologic Unit II is marked by the first significant appearance of siliceous microfossils in the sediments. It was also divided into two subunits. Lithologic Subunit IIA comprises lower Miocene nannofossil chalk with radiolarians and glauconite, and claystone with glauconite. Subunit IIB consists of chert interbedded with clayey porcellanite with micrite and zeolite, palygorskite/zeolite claystone, and glauconite-rich porcellanite, which are early Eocene to late Paleocene and older. Lithologic Unit II correlates with lithologic Unit II at Site 959 and with Units II and III at Site 960. Lithologic Unit III, of uncertain age (Maastrichtian to Bajocian), is entirely siliciclastic. It consists of dark gray to black silty sandstone, sandy siltstone, clayey siltstone, and silty claystone, with several intervals locally enriched in pyrite and siderite. This unit is characterized by tectonic deformation fabrics and appears to be correlative with the top of lithologic Unit V at Sites 959 and 960, although biostratigraphic control is poor.

Description of Lithologic Units

Unit I

Description: Nannofossil ooze with foraminifers, foraminifer nannofossil ooze with micrite, nannofossil chalk with clay, clayey nannofossil chalk, and nannofossil mudstone with micrite
Interval: Sections 159-961A-1R-1, 0 cm, through 159-961A-15R-1, 59 cm
Depth: 0–129.5 mbsf
Age: Holocene to early Miocene

Lithologic Unit I is similar in composition to lithologic Unit I at Sites 959 and 960 (see "Lithostratigraphy" sections, "Site 959" and "Site 960" chapters). Because of RCB coring at this site, recovery of this unit was very poor and the sediment highly disturbed by drilling. There was no recovery in several cored intervals. Lithologic Unit I comprises dark to light greenish gray, structureless or laminated, calcareous nannofossil ooze and chalk, with varying amounts of clay. The variation in color has been used to divide the unit into two subunits. Lithologic Subunit IA is darker as a result of higher contents of organic matter and pyrite, and is Pleistocene to late Pliocene in age. Lithologic Subunit IB is lighter, glauconite-rich, and early Pliocene to early Miocene in age. The top 8 m of this subunit comprises calcareous nannofossil ooze with foraminifers, which grades downhole into nannofossil chalk with clay and claystone. Lithologic Subunit IB is more micritic toward its boundary with the underlying lithologic Unit II. At Site 961, lithologic Unit I is 129.5 m thick, compared with 185 and 100 m at Sites 959 and 960, respectively.

Subunit IA

Description: Nannofossil ooze with foraminifers and foraminifer nannofossil ooze with micrite
Interval: Sections 159-961A-1R-1, 0 cm, through 3R-2, 150 cm
Depth: 0–16.1 mbsf
Age: Holocene to late Pliocene

Lithologic Subunit IA comprises dominantly dark greenish gray nannofossil ooze with foraminifers, although foraminifer nannofossil ooze with micrite occurs at Section 159-961A-1R-2, 70–120 cm. The formation of micrite is probably a result of the dissolution of calcareous shells. The increase in foraminifer content commonly results in a slightly lighter color of several intervals of the subunit. Some disseminated foraminifer tests are stained slightly green by glauconite. The subunit is mainly structureless, with little or no visible evidence of bioturbation, in comparison with Sites 959 and 960; this observation, however, may be an artifact of RCB drilling. Disseminated pyrite occurs throughout, and smear slides reveal that organic matter content is higher in this subunit than the underlying lithologic Subunit IB.

Subunit IB

Description: Nannofossil ooze/chalk with foraminifers, clayey nannofossil chalk, micrite nannofossil chalk, and nannofossil claystone with micrite
Interval: Sections 159-961A-3R-2, 150 cm, through 15R-1, 59 cm
Depth: 16.1–129.5 mbsf
Age: early Pliocene to early Miocene

The boundary between Subunits IA and IB is marked by a change of color from a dark greenish gray to a light greenish gray color within a nannofossil ooze with foraminifers. This color change is accompanied by a decrease in the pyrite content, a decrease in total organic carbon content (see "Organic Geochemistry" section, this chapter), and a change in magnetic properties (see "Paleomagnetism" section, this chapter). Lithologic Subunit IB contains more glauconite than Subunit IA. Nannofossil chalk becomes more clayey with depth, and thin interbeds of nannofossil claystone are present. Generally, the lithotypes of this subunit are interbedded with one another and are characteristically color banded and laminated. Greenish color bands are formed by the concentration of glauconite pellets, mainly along subhorizontal burrows and millimeter-thick laminae, whereas brownish laminae result from an increase in siderite, clay, and/or pyrite. The lighter intervals in the subunit are slightly richer in foraminifers. Color bands have diffuse boundaries because of bioturbation, which is slight to moderate at most intervals. The principal burrow type is *Chondrites*.

The transition from ooze to chalk is gradual and occurs at a much shallower depth at Site 961 than at Sites 959 and 960: 22.7 mbsf compared with 75 mbsf and 49.1 mbsf, respectively. The sediments at these depths are late Miocene in age at Sites 959 and 961 and early Pliocene at Site 960. Because of poor recovery and drilling disturbance at Site 961, there are no physical properties data for this depth interval (see "Physical Properties" section, this chapter). Poor recovery in this interval may reflect a change in rock properties because of a diagenetic front, as suggested by the pore-water composition (see "Inorganic Geochemistry" section, this chapter), and a marked decrease in calcium carbonate content (see "Organic Geochemistry" section, this chapter). Dissolution of calcitic shells results in the increased content of micrite (up to 30%) in Core 159-961A-14R (119.3–128.9 mbsf). Remnants of brown bioturbated porcellanite (burrow fills) in this core contain pyritized radiolarians and diatoms. Their presence suggests that porcellanite is interbedded with nannofossil chalk and claystone, which contain minor amounts (5%) of radiolarians and sponge spicules. However, the base of lithologic Subunit IB was placed at the first significant appearance (15%) of siliceous microfossils, in brownish foraminifer nannofossil chalk at 129.5 mbsf. This boundary is coincident with a change in magnetic properties (see "Paleomagnetism" section, this chapter).

Unit II

Description: Nannofossil chalk with radiolarians and glauconite, claystone with glauconite, chert, palygorskite and zeolite claystones, and porcellanite with nannofossils
Interval: Sections 159-961A-15R-CC, 0 cm, through 21R-2, 34 cm
Depth: 129.5–188.5 mbsf
Age: early Miocene to late Paleocene and unknown

Lithologic Unit II was cored only in Hole 961A, where poor recovery and severe drilling disturbance were caused by RCB drilling and the presence of chert. Lithologic Unit II comprises a variety of silica-rich, glauconite-bearing lithofacies over a 60-m interval. Siliceous components include radiolarians, opal-CT, microquartz, and zeolite. Lithologic Unit II was divided into two subunits. Lithologic Subunit IIA, early Miocene in age, consists of foraminifer nannofossil chalk with radiolarians and glauconite, and claystone with glauconite. Lithologic Subunit IIB comprises chert, with thin interbeds of clayey porcellanite with micrite and zeolite, which overlie palygorskite and zeolite claystones, and porcellanite with nannofossils and/or clay. Its age is early Eocene to late Paleocene and older.

Lithologic Unit II at this site can be correlated with lithologic Unit II at Site 959 and with Lithologic Units II and III at Site 960, but there are differences in the style and timing of lithologic successions. At Site 959, calcite content decreases with depth, whereas there is no clear overall trend at Site 961. Calcite content decreases with depth in lithologic Subunit IIA, but reappears at several intervals in lithologic Subunit IIB before decreasing again toward the base of the subunit. At all three sites, siliceous microfossils have been diagenetically altered to form opal-CT, microquartz, and zeolite downsection. Whereas lithologic Unit II at Site 959 consists of diatomite, chert, and porcellanite, at Site 960 lithologic Unit II comprises radiolarian nannofossils/micrite chalks, claystone, porcellanite, and chert and lithologic Unit III is defined by palygorskite claystone (see "Lithostratigraphy" sections of "Site 959" and "Site 960" chapters). Furthermore, late Paleocene and older porcellanites preceded the early Eocene palygorskite claystone and chert at Site 961. In contrast, at Site 960, siliceous sediment followed but did not precede palygorskite deposition. Palygorskite claystone was not detected at Site 959, where chert is middle to early Oligocene and early Eocene in age instead of all early Eocene.

Subunit IIA

Description: Nannofossil chalk with radiolarians, and claystone
Interval: Sections 159-961A-15R-CC, 0 cm, through 16R-CC
Depth: 129.5–148.1 mbsf
Age: early Miocene

The upper boundary of lithologic Subunit IIA was placed at the first significant appearance (15%) of radiolarians in brownish gray (7.5GY 4/1) foraminifer nannofossil chalk at 129.5 mbsf. Overall, this brownish color is related to the presence of siliceous microfossils. Downsection (in Core 159-961A-16R), this lithology is replaced by greenish gray (5G 2.5/3) to brownish gray (7.5GY 4/1) claystone, which also contains siliceous microfossils, dominantly radiolarians. This heavily bioturbated subunit has *Chondrites* burrows. Glauconite grains and faint color bands are present.

Subunit IIB

Description: Chert, palygorskite and zeolite claystones, and porcellanite with nannofossils and clay
Interval: Sections 159-961A-17R-1, 0 cm, through 21R-2, 34 cm
Depth: 148.1–188.5 mbsf
Age: early Eocene to late Paleocene and unknown

The upper boundary of lithologic Subunit IIB was placed at the first occurrence of chert in Core 159-961A-17R. Thin layers of light greenish gray clayey porcellanite with micrite and zeolite are intercalated with the dark greenish gray (5BG 4/1) chert (Fig. 9). XRD analysis of this clay shows strong reflections for palygorskite and opal-CT and weaker reflections for quartz and zeolite (probably clinoptilolite). Recovery drops to only 12 cm of light greenish gray (2.5BG 5/1) palygorskite claystone with nannofossils in Core 159-961A-18R, which might be caused by a chert/claystone alternation above or be-

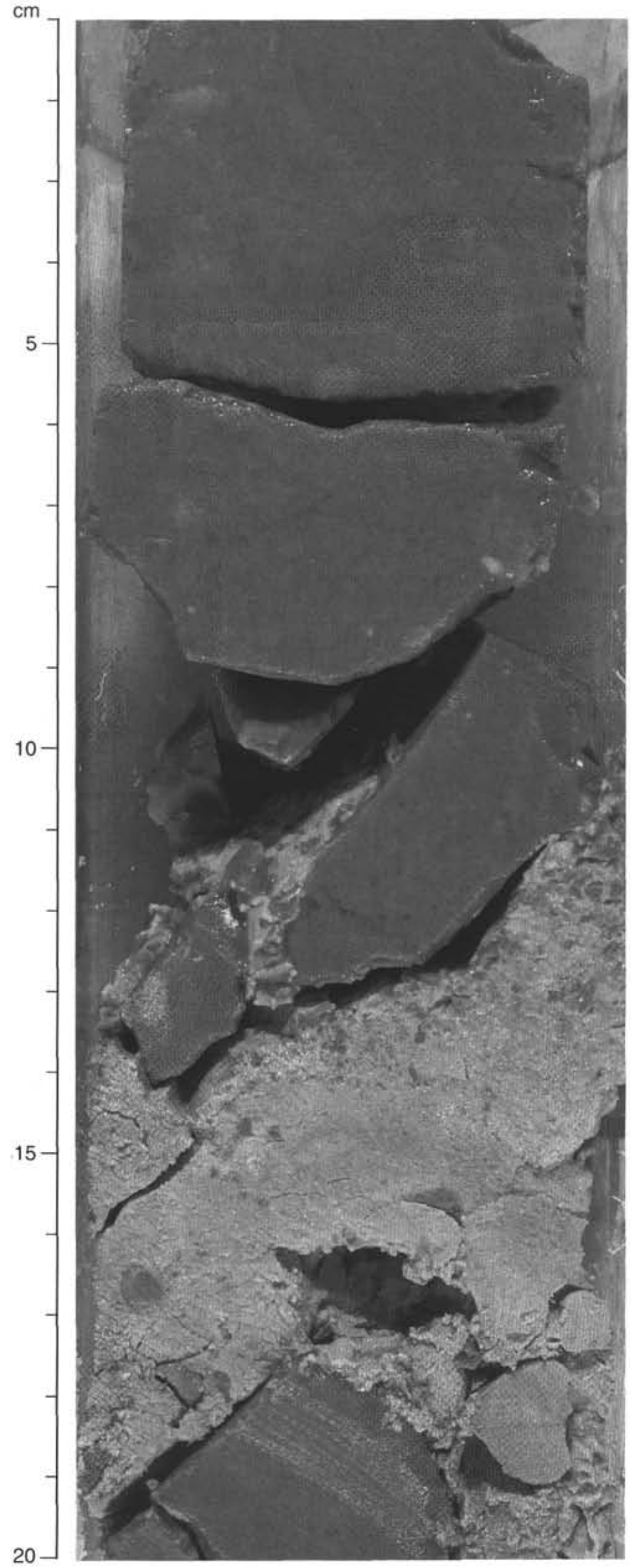

Figure 9. Section 159-961A-17R-CC, 1–20 cm. Greenish gray chert interbedded with clayey porcellanite with zeolite and micrite.

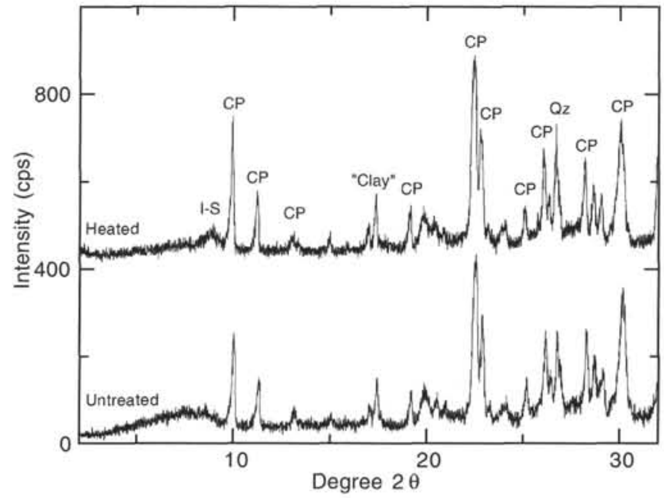

Figure 10. X-ray diffractogram traces of zeolite claystone from Section 159-961A-19R-1, 20–25 cm. The lower trace shows a typical clinoptilolite/heulandite (CP) pattern; the upper trace was measured after heating the sample at 450°C for 15 hr. The unchanged pattern of the peak positions after heating is evidence that this zeolite is a clinoptilolite (Mumpton, 1960). Quartz (Qz) and mixed-layer minerals with a very broad peak between 10 and 15 Å also occur. The shift of this peak toward 10 Å on heating suggests that the mixed-layer minerals are of illite/smectite type (I-S).

low the recovered claystone. Core 159-961A-19R is characterized by light greenish gray zeolite claystone in the top 25 cm (Fig. 10), followed by greenish gray palygorskite claystone with zeolite and nannofossils at Section 159-961A-19R-1, 25–55 cm, and light greenish gray micritic limestone at Sections 159-961A-19R-1, 55 cm, through 19R-CC, 11 cm. A piece of this micritic limestone at Section 159-961A-19R-1, 55–68 cm, contains lath-shaped crystals of barite that reach 1 cm in length (Fig. 11). *Chondrites* burrows are present.

The lower part of lithologic Subunit IIB encompasses Sections 159-961A-20R-1, 3 cm, through 21R-2, 34 cm. It consists of bioturbated, light olive gray nannofossil porcellanite, and greenish gray porcellanite with an overall trend of decreasing amounts of nannofossils downhole. The principal burrows are *Chondrites* and *Zoophycos*. In Sections 159-961A-21R-1, 0 cm, through 21R-2, 34 cm, porcellanite and porcellanite with clay are enriched in pyrite and glauconite pellets (Fig. 12). The lower boundary of lithologic Subunit IIB was placed at 188.5 mbsf, which corresponds to the first appearance of pyrite-bearing siliciclastic sediments.

Unit III

Description: Sandstone, silty sandstone, sandy siltstone, clayey siltstone, and silty claystone
Intervals: Sections 159-961A-21R-2, 34 cm, through 35R-CC, 45 cm (TD) and Sections 159-961B-1R-1, 0 cm, through 20R-CC, 26 cm (TD)
Depth: 188.5–308.7 mbsf, Hole 961A; 216.3–374.6 mbsf, Hole 961B
Age: Uncertain (Maastrichtian to Bajocian)

Lithologic Unit III comprises dark gray to dark brownish gray siliciclastic sediments ranging from silty sandstones to sandy siltstones, clayey siltstones, and silty claystones. The upper boundary of this unit was defined as the last downhole occurrence of glauconite and porcellanite, which are characteristic of the lower part of lithologic Subunit IIB, and the first occurrence of detrital quartz-, chlorite-, and feldspar-rich siliciclastic sediments. This boundary is quite sharp in Section 159-961A-21R-2, 34 cm (Fig. 13), where the lithol-

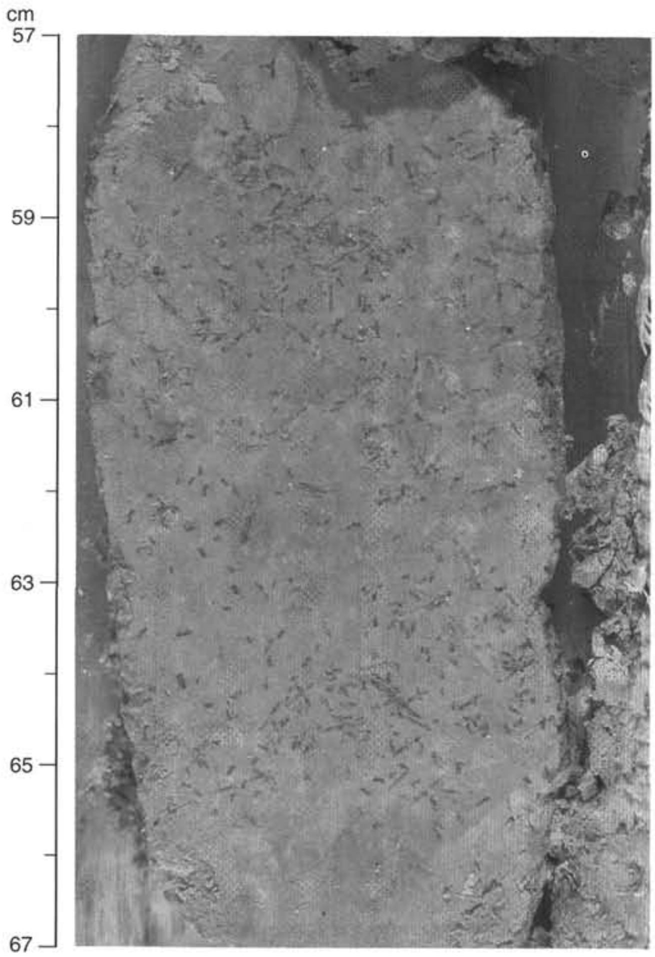

Figure 11. Section 159-961A-19R-1, 57–67 cm. Light greenish gray micritic limestone with lath-shaped crystals of barite is overlain by bluish green palygorskite claystone.

ogy above and below this contact is highly brecciated into 1- to 2-cm-sized fragments. This coincides with an equally abrupt change observed in the physical properties (see "Physical Properties" section, this chapter) and magnetic properties (see "Paleomagnetism" section, this chapter). In the lowermost part of Hole 961B (Cores 195-961B-18R and 19R), a slight increase in grain size, from clayey siltstone to silty sandstones and sandstones, was observed. Drilling terminated within lithologic Unit III, and there are no criteria related to sediment composition, fabric, or sedimentary structures that warrant further subdivision of this interval into subunits. Variations in bed forms, mineralogic composition, or tectonic fabrics observed in lithologic Unit III do not change systematically with depth, except for an increase in siderite content below 250 mbsf.

Claystones and silty claystones are poorly represented because of poor recovery associated with RCB coring methods. Where present, claystones exhibit hydroshear slickensides on claystone fragments. These claystones occur as intervals of dark gray to black drilling breccia. They are dominated by chlorite and highly illitic mixed-layer clays (Fig. 14A, B), which first occur at Section 159-961A-21R-2, 62 cm, in Hole 961A and at Section 159-961B-1R-1, 66 cm, in Hole 961B. In contrast, chlorite is absent from lithotypes of Subunit IIB that contain smectite, zeolite, and opal (Section 159-961A-21R-1, 9 cm). A highly expandable (>90%) smectite comprises the glauconitic material (Fig. 14C). The chlorite beneath it is interpreted as an authigenic phase produced by thermal alteration during burial and/or tec-

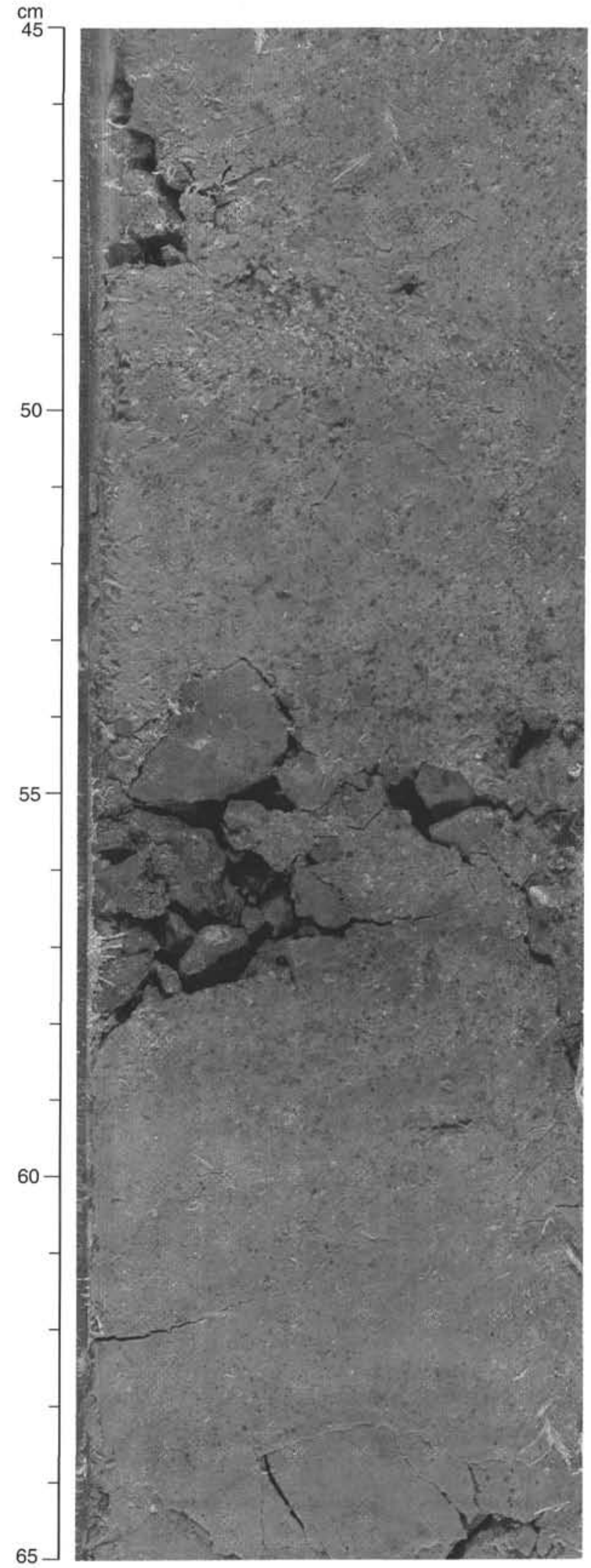

Figure 12. Section 159-961A-21R-1, 45–65 cm. Glauconite pellets and pyrite are common associated minerals in porcellanite.

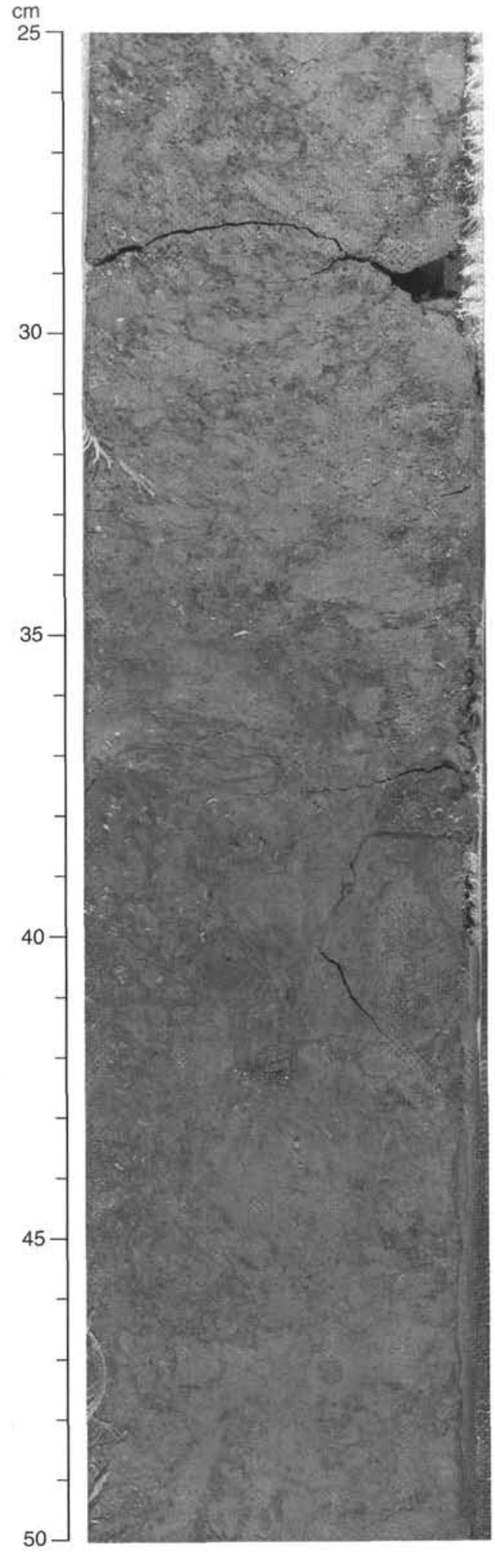

Figure 13. Section 159-961A-21R-2, 25–50 cm. The upper boundary of lithologic Unit III occurs at Section 159-961A-21R-2, 34 cm. The quartz siltstones of lithologic Unit III, which contain chloritic clays, are highly brecciated at this contact. This lithology is abruptly overlain by porcellanites of lithologic Subunit IIB, which contain disseminated glauconite peloids distributed throughout the matrix.

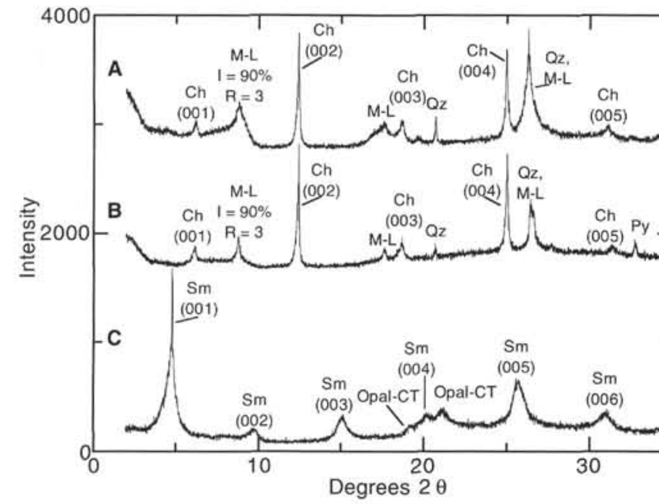

Figure 14. X-ray diffractograms of samples from Site 961 illustrating the thermal maturation of lithologic Unit III compared to Unit II. All samples are clay separates, and were treated with ethylene glycol prior to scanning. **A.** Sample 159-961A-22R-1, 23–25 cm. **B.** Sample 159-961B-1R-1, 66–68 cm. These two samples are from approximately the same stratigraphic interval, at the top of lithologic Unit III. Both have iron-rich chlorite, as indicated by the reduced size of odd-order reflections [(001), (003), and (005)]. A 10/17 Å mineral (labeled M–L) developed a low-angle shoulder upon glycolation, indicating it is mostly the 10 Å mineral (probably illite), with a high degree of ordering of the expandable layers (R = 3): some 90% of the layers are illitic. **C.** Sample 159-961A-21R-1, 9–11 cm. Only 10 m above the sample in Figure 14A, this sample from the base of lithologic Unit II comprises a highly expandable (>90%) 10/17 Å mineral and opal-CT. The former mineral could not have survived the temperatures required to form chlorite and R = 3, 10/17 Å mineral of the other two samples, indicating that an unconformity exists between the two lithologic units. Ch = chlorite; M–L = 10/17 Å, "mixed-layer" clay; I = percent illitic clays; R = Reichweite (Moore and Reynolds, 1989) ordering of the 10-17-10-10 Å type (ISII); Qz = quartz; Py = pyrite; Sm = highly expandable 17 Å mineral (smectite group). Numbers in parentheses refer to Miller indices of lattice responsible for the peak.

tonism because of the unlikelihood of its survival during weathering in this equatorial area (e.g., Chamley, 1989). As such, its presence may be used for the discrimination of older, tectonically deformed sediments from younger sediments observed at shallower levels at this and other sites. For example, chlorite is also present in lithologic Subunit VA at Site 960, which comprises tectonically deformed strata of Albian and older age. Importantly, chlorite is not present in the Paleocene to Coniacian black claystones of lithologic Unit III at Hole 959D, which passively filled the intra-shelf Deep Ivorian Basin.

Despite the thickness of this lithologic unit (120 to 158 m), the mineralogical and textural composition does not vary systematically over its stratigraphic range. The variation that is present reflects alternating and interbedded lithotypes that differ primarily in their relative abundance of sand, silt, and clay. Quartz is the dominant mineral in lithologic Unit III, and it includes grains derived from both metamorphic (undulose extinction and composite grains) and igneous (rutilated quartz, unstrained quartz) source terrains. A dominant igneous provenance is indicated by the abundance of plagioclase feldspars and trace amounts of tourmaline and zircon. Locally, plagioclase feldspar is quite common in the coarse size fractions, comprising as much as 20% of the bulk sediment (Sections 159-961B-4R-1, 23 cm, and 18R-2, 86 cm). Throughout this unit, well-rounded quartz grains are common, although intermixed with subrounded to subangular quartz and feldspar (e.g., Section 159-961B-15R-1, 123 cm). The rounded quartz grains suggest that some sediment was derived from shallow shoreface settings and intermixed with less mature feldspar and angular quartz sands before transport to the depositional site. Pyrite is present throughout this interval, occurring both as cubic silt-sized crystals and as framboids. Locally, pyrite is a significant mineral component of the bulk sediment.

In general, lithologic Unit III contains little primary carbonate, with biogenic shell material either dissolved or replaced by secondary carbonate minerals, such as siderite and dolomite. Of these, siderite is abundant at numerous intervals below 250 mbsf, occurring as a replacement of primary carbonate bioclasts and nannofossils (Section 159-961B-9R-1, 33 cm) or as concretions and nodules (Cores 159-961A-29R through 31R and 159-961B-4R through 10R). In these cases, siderite forms as fine silt-sized crystallites localized around and in burrows, as septarian nodules, or as a disseminated mineral intermixed within the claystone. Dolomite (or ankerite) is also present locally (Section 159-961B-15R-1) as silt- and sand-sized rhombs. What controls the distribution of these phases within the core is not known. Biogenic calcite is relatively rare within this unit except in Core 159-961B-9R, where some long-ranging nannofossils (Bajocian to Maastrichtian age) were recovered. Calcite cement is relatively common where tectonic veins and breccias have been filled by late-stage calcite (Fig. 15). These vein-fill calcite cements contain abundant fluid-filled inclusions, which impart a cloudy, white appearance in hand samples.

Bedding characteristics of the clayey siltstones and sandy siltstones provide some constraints on the depositional setting of the lithology. For example, siltstones locally occur as massive beds, with few primary sedimentary structures present or preserved. These intervals are extensively burrowed, with only thin and faint parallel laminations (e.g., Section 159-961B-1R-1). Elsewhere, siltstones are finely laminated, with coarser grained, light gray layers and finer grained, dark gray layers (Fig. 16). Much of this lamination is lenticular and is formed by small isolated ripples draped by finer grained silt and clay (Fig. 17). In general, the lack of graded beds or other features characteristic of density or turbidity current deposition suggests that these lithotypes were deposited in settings where the sediment, comprising a mixture of clay-, silt-, and sand-sized material, was periodically winnowed by storm-generated waves or bottom currents on the shelf.

Bioturbation of this unit is highly variable, with 0.5-cm-sized burrows, commonly compacted, and disrupting horizontal bedding (Fig. 15). These burrows are relatively free of coarser sediment grains and are typically altered to siderite. The burrows are not sufficiently distinct to identify different trace fossil types.

The presence of tectonic fractures and associated fracture-vein mineralization is also used as a criterion for the identification of lithologic Unit III at Site 961. Tectonic fabrics include shear-related slickensides within claystones, brecciation, and brittle fracturing of the more competent siltstone beds. The breccia is marked by both calcite-filled fractures and brecciated intervals, where fragments are floating in a silty claystone matrix. Evidence for multiple events of fracturing is present in Section 159-961B-1R-1, 109–122 cm, where fragments, partially coated by calcite cement, have subsequently undergone a second phase of brecciation. Here, angular clasts occur within a matrix of clayey siltstone (Fig. 18).

Tectonic breccia and veining are particularly abundant within the interval of 200 to 240 mbsf in Holes 961A and 961B. Throughout this unit, evidence of extensional and compressional deformation is present as slickensided fractures, breccias, and brittle fracturing of layers (see "Structural Geology" section, this chapter). In Section 159-961B-3R-2, 25–26 cm, fractures filled with calcite do not show appreciable offset, suggesting that the fracture mechanism may not have been related to differential shear stresses (Fig. 15). An alternative mechanism would be the hydrofracturing of this interval during the compression of the sequence, but without appreciable shear-related movement. The occurrence of brecciation at similar depths in Holes 961A and 961B, a distance of 100 m, argues against brecciation along a single fault plane with appreciable dip. An alternative mechanism may be slump-related deformation with failure parallel to the bedding plane. The coherence of the sediment, however, argues against an early origin related to synsedimentary deformation.

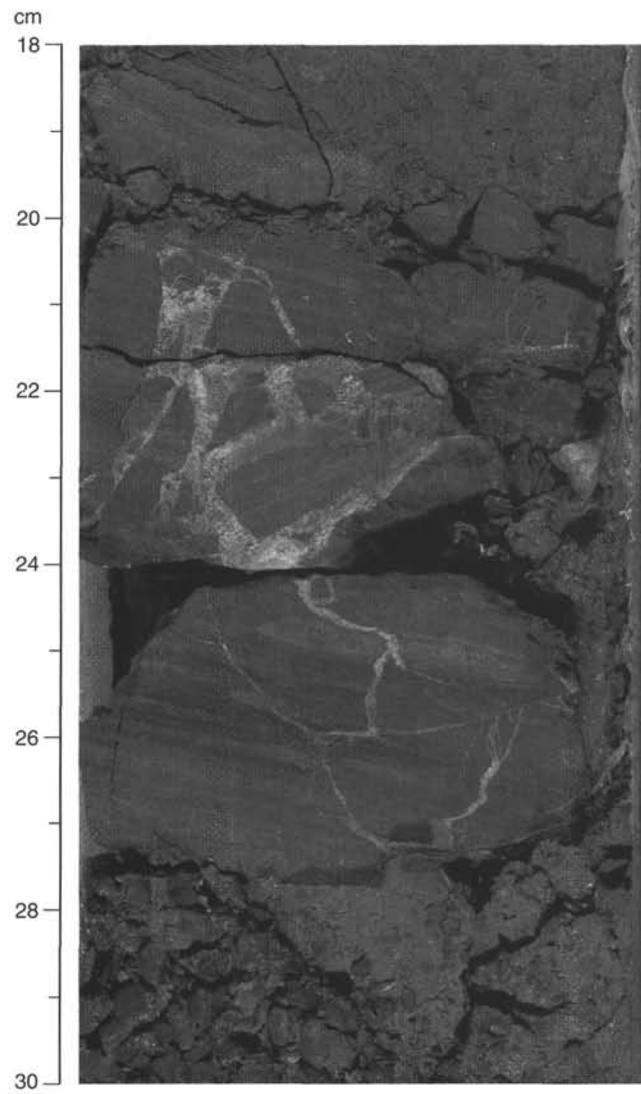

Figure 15. Section 159-961B-3R-2, 18–30 cm. Tectonic fractures in lenticular to laminated clayey siltstones and silty sandstones of lithologic Unit III are commonly filled by cloudy calcite cement and exhibit little offset of sedimentary layering.

As noted earlier, little systematic variation in lithology was observed in this unit. However, there is some suggestion that at the base of the unit, the sediment becomes slightly coarser with the development of silty sandstone. These beds exhibit possible truncation surfaces and draping sand laminations that are suggestive of hummocky cross-stratification, a sedimentary bed form produced by periodic reworking during storms. Overall, the lithologic features suggest that this unit formed in an outer shelf, lower energy setting. Moreover, the similarity in sediment grain size and bedding characteristics over the thick interval represented by this unit suggests that the water depth remained relatively constant throughout its deposition. Given the thick sequence present at this site, therefore, such vertical stacking of facies requires a setting where depositional rates are closely matched to the rates of basinal subsidence.

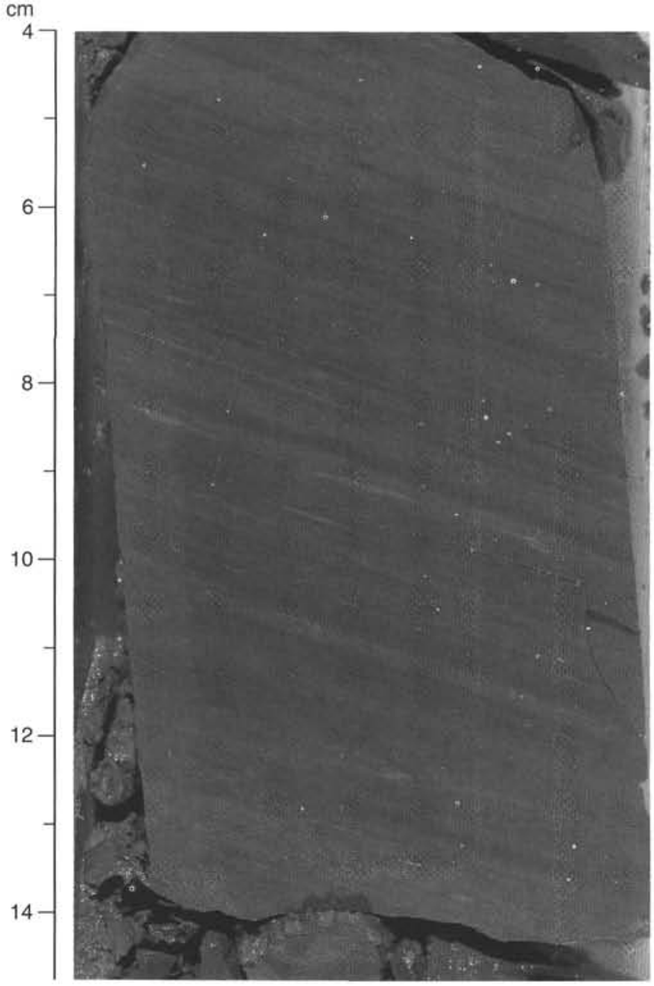

Figure 16. Section 159-961B-6R-3, 4–15 cm. Finely laminated siltstone and fine sandstone exhibit indistinct boundaries between the lighter coarse-grained and darker fine-grained layers. Bioturbation locally cuts these laminations, producing a mottled fabric.

Discussion

At Site 961, we recognized three depositional sequences:

1. marine (shelf) deposition below wave base, comprising siliciclastic sediments (lithologic Unit III);
2. open-marine biosiliceous deposition, represented by glauconite-rich porcellanite grading upward into palygorskite and zeolite claystones and by chert (lithologic Subunit IIB was deposited unconformably above lithologic Unit III); and, finally,
3. deposition along a subsiding passive margin of calcareous pelagic sediments, comprising nannofossil chalk and claystone with radiolarians and glauconite (lithologic Subunit IIA), which grade upward into nannofossil chalk and ooze with foraminifers (lithologic Unit I).

Marine (Shelf) Deposition

The siliciclastic succession of lithologic Unit III probably represents deposition under marine water conditions. This is indicated by the abundance of pyrite throughout this interval and by the periodic occurrence of nannofossil-rich layers, which require open-marine salinities. Because the occurrence of sedimentary, framboidal pyrite re-

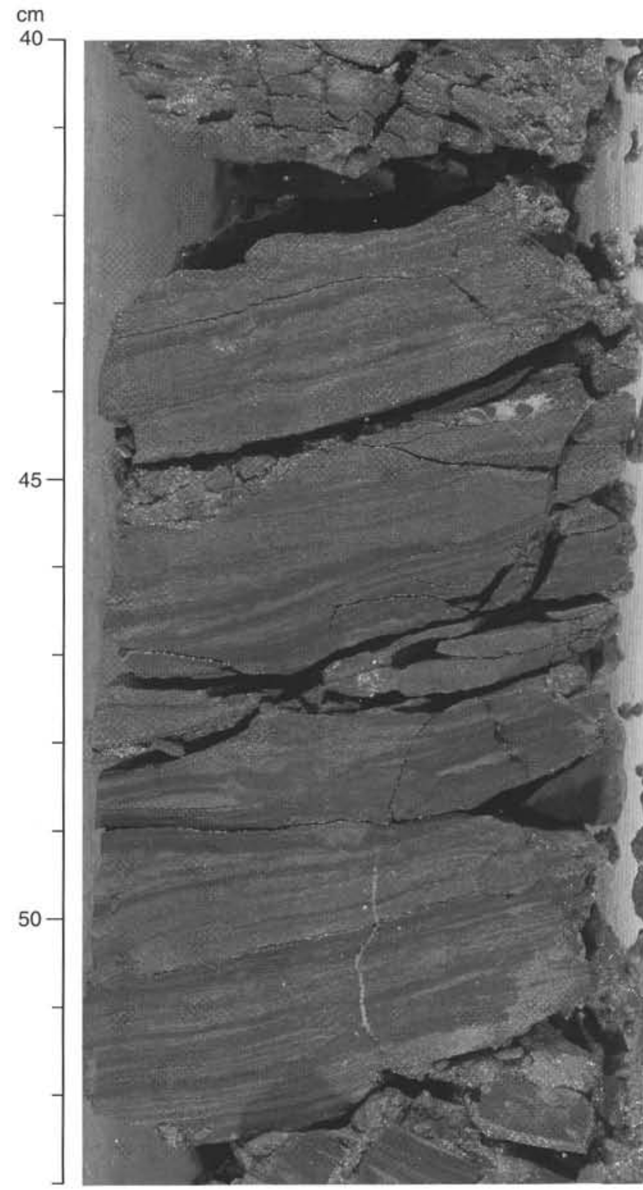

Figure 17. Section 159-961A-23R-1, 40–53 cm. This lithology, comprising alternating sandy siltstones and clayey siltstones, exhibits irregular fine laminations. Lenticular bedding may reflect the development of small ripples overlain by the finer grained sediment that drapes the bedforms.

quires a source of reducible sulfate, diffusion of marine waters into an organic-rich sediment could easily account for the pyrite observed in lithologic Unit III. Other than in intervals where nannofossils occur, it is not possible to determine the extent to which open-marine salinities were maintained. For example, the presence of abundant siderite throughout this unit, as cement and concretions, implies a setting where sulfate reduction is limited either by initially low concentrations or by its complete reduction in the pore-water system by reaction with organic material. Siderite could have precipitated from brackish waters (low initial sulfate concentrations) associated with a marginal marine environment. Alternatively, given the abundance of pyrite, if sulfate were depleted within the pore waters and reducible iron were still available, siderite can form from marine connate fluids. Without elemental and isotopic analysis of these siderites, it is not possible to exclude either setting.

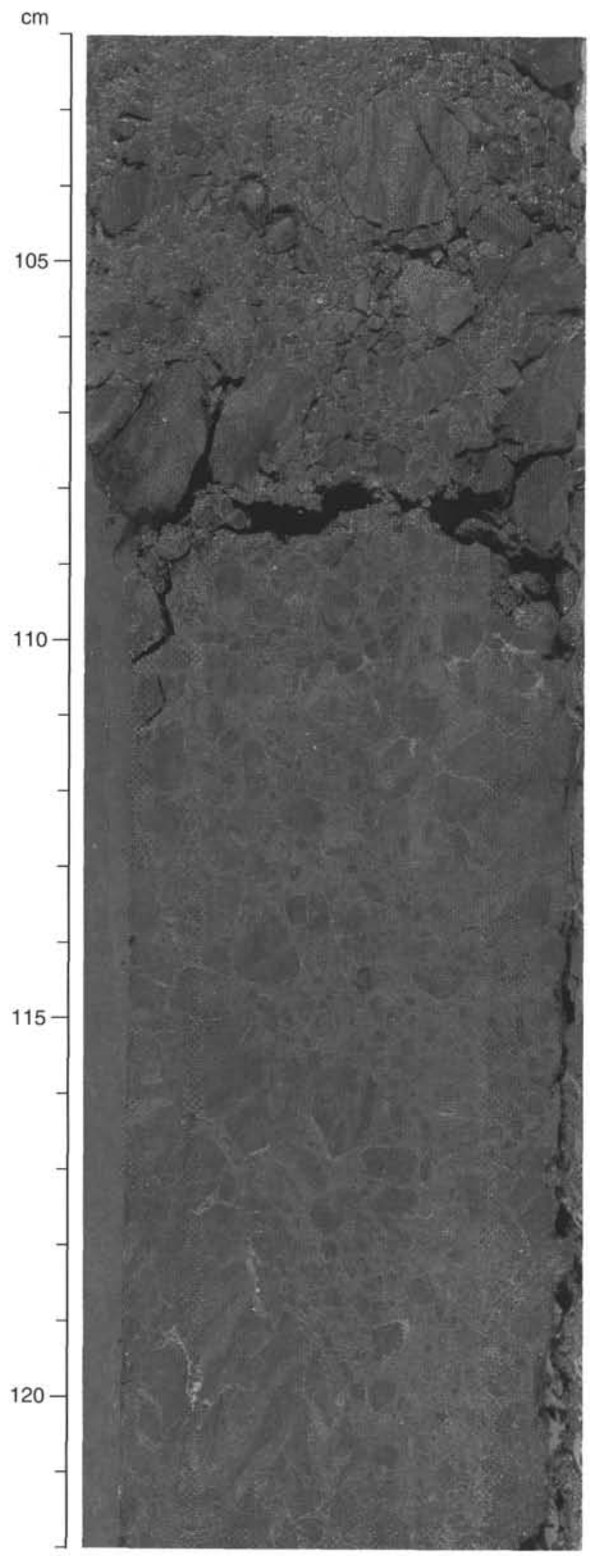

Figure 18. Section 159-961B-1R-1, 102–122 cm. This interval of brecciated siltstones of lithologic Unit III suggests multiple events of deformation and fracturing. Clasts, presently floating within a silty claystone matrix, have fractures that were filled by calcite before brecciation. Unlike the material illustrated in the interval from 101 to 108 cm, which has undergone extensive drilling-induced brecciation, the interval from 108 to 123 cm is lithified and massive.

Some constraints can be placed on the depositional energies of the environment that formed lithologic Unit III. The absence of coarse sands and the lack of medium- to large-scale cross-stratification preclude a shoreface to shallow-water setting. One might envision a setting where periodic winnowing of the seafloor produced local, "starved" ripples, or winnowed laminations. This type of reworking would allow for the interbedding and interlamination of lenticular, coarser and laminated, clay-rich lithologies. In contrast, the occurrence of rounded to subrounded quartz sands requires a provenance of well-worked shoreface sediments. However, the occurrence of subangular quartz grains and plagioclase feldspars together with the rounded grains suggests that this sediment represents a mixture from mature and immature sediment sources. One possible setting that could provide such a mixture is a delta. This is not to imply that the sedimentary structures observed in lithologic Unit III were formed within a delta system. Rather, sediments delivered to the ocean by a fluvial deltaic complex could be locally reworked at the shoreface, variably intermixed with texturally immature grains, and periodically transported into the deeper shelf by stronger currents, such as might be generated by storms.

Based upon the sediment characteristics (and its depositional setting), tectonic deformation features, and clay mineralogy, we suggest that lithologic Unit III at Site 961 is broadly correlative with lithologic Unit V at Site 959 and with lithologic Subunit VA at Site 960, which represents a transitional marine sequence overlying lacustrine siltstones and claystones. The fact that a thicker marine sequence was recovered at Site 961, and the failure to penetrate an underlying lacustrine facies, may reflect differential uplift between these two sites or disconnected basins. For example, if Site 960 were uplifted higher, erosion could have removed most of the upper sediments recording the transition to marine conditions.

The co-occurrence of chlorite and the highly illitic mixed-layer clay, and the absence of the highly expandable smectite, may be used to constrain, somewhat, the maximum temperatures these sediments reached during their heating. For example, chlorite first appears as a diagenetic product in Gulf of Mexico shales only at the greatest depths reached by drilling, where the ambient temperature is near 150°C (Hower et al., 1976). In a shale/slate transition in the southern Appalachians of the U.S., chlorite occurs with incipient slaty cleavage where the temperatures reached 250°–330°C (Weaver et al., 1984). R = 3-type mixed-layer illite-smectite clays apparently may lose the last expandable layers only at temperatures of 360°C or greater (Weaver and Broekstra, 1984), but above this temperature the phase should appear as a mica (Srodon and Eberl, 1984), with a peak width of less than 0.2° 2θ (Reynolds, 1980). The temperature effecting this transformation varies depending on particle size. The maximum temperature may be further constrained by determination of the polytype. More detailed work is needed before a temperature range can be better constrained, but at present it is reasonable to infer that this sediment was heated above 150°C, but not above 330°C.

Independent of the succession of depositional environments observed at each site, both lithologic Unit III at Site 961 and lithologic Subunit VA at Site 960 have undergone tectonic deformation and associated thermal metamorphism, which are recorded by mineralized tectonic fractures and the formation of chloritic clays. Such features have not been observed in any lithologic units at Sites 959 or 960 that are above the unconformable, upper contact of lithologic Unit V. On this basis, we interpret lithologic Unit III of Site 961 to represent a succession that was formed during the "synrift" depositional stage (see "Lithostratigraphy" section, "Site 960" chapter, this volume).

Pelagic Biosiliceous Deposition

The boundary between lithologic Units II and III marks a sharp break from siliciclastic deposition to open-marine, biogenic deposition. From its base, lithologic Unit II is characterized by a silica-rich lithology related to the diagenetic alteration of biogenic, opaline silica. The accumulation of biogenic silica indicates enhanced productivity from upwelling or increased continental runoff conditions, which were also inferred at Sites 959 and 960 (see "Lithostratigraphy" sections, "Site 959" and "Site 960" chapters, this volume). These sediments are glauconite-rich, such as the porcellanite that occurs in Sections 159-961-21R-1, 0 cm, through 21R-2, 34 cm, toward the base of lithologic Subunit IIB. Enrichment in glauconite is generally related to depositional hiatuses, but in a basinal setting such as that proposed here, oxidizing conditions at the sediment/water interface and local reducing conditions within the sediment may account for the formation of glauconite (Odin and Matter, 1981; see discussion in "Lithostratigraphy" section, "Site 960" chapter, this volume).

In Cores 159-961A-17R through 20R, the presence of moderately to poorly preserved radiolarians suggests that siliceous microfossils supplied the silica for the formation of opal-CT and the zeolite of the clinoptilolite group (cf. Mumpton, 1960; Bohrmann and Stein, 1989; Stein and Faugères, 1989). Sediments of lithologic Subunit IIB are similar in many respects to Eocene siliceous deposits, including zeolite clays, that have been described from Site 661 of ODP Leg 108 on the Sierra Leone Rise (Stein and Faugères, 1989). These deposits have been attributed to a period of high oceanic productivity. This interpretation is supported by the presence of barite in lithologic Subunit IIB, which also points to an increased flux of organic matter or its components to the seabed. The presence of calcareous nannoplankton, calcareous benthic foraminifers (see "Biostratigraphy" section, this chapter), and micritic limestones in lithologic Subunit IIB indicates deposition above the carbonate compensation depth (CCD).

As at Site 960, the palygorskite claystones in Sections 159-961A-17R–CC, 12 cm, through 19R-1, 3 cm, are early Eocene (CP10) in age. Their coeval occurrence over a distance of 32 km suggests that palygorskite clay formation and deposition was a regional phenomenon. The interpretation of the palygorskite claystone in terms of paleo-water depth is difficult. We suggest three working hypotheses:

1. Palygorskite clay formed in situ at Site 961, as a shallow-water deposit (as proposed for Site 960). The presence of open-marine calcareous nannoplankton within the palygorskite claystone may be related to intense mixing caused by drilling.
2. Palygorskite clay formed in situ below 1000 m water depth as suggested by the presence of benthic foraminifers that indicate bathyal to abyssal water depths (see "Biostratigraphy" section, this chapter) in Cores 159-961A-16R and 20R, which bracket the occurrence of palygorskite clay.
3. Palygorskite clay was eroded from its original depositional environment, which was probably similar to the one envisaged for Site 960. It was then transported to Site 961 in a more open-marine setting that allowed depositional mixing of palygorskite clay with marine nannoplankton. Without electron microscopic studies, however, these hypotheses cannot be tested.

Continued deposition in an open-marine setting resulted in the formation of chert at this site. Chert formation was probably periodic because it is interbedded with clayey porcellanite with micrite and zeolite. This chert unit can be correlated with lithologic Subunit IIB at Site 960, and its stratigraphic position is consistent with the formation of chert during the early to middle Eocene in the Atlantic, Indian, and northwest Pacific Oceans (Pisciotto, 1981; see "Lithostratigraphy" section, "Site 960" chapter, this volume).

Passive Margin Subsidence—Pelagic and Hemipelagic Deposition

At Site 961, there is a hiatus between the lower Eocene chert of lithologic Subunit IIB, and the lower Miocene sediments of lithologic Subunit IIA, which were deposited in a subsiding, normal pelagic to hemipelagic marine setting. The presence of claystone and clayey nannofossil chalk in Subunit IIA indicates some terrigenous clastic input into the basin. Because these glauconite-bearing sediments contain siliceous microfossils more resistant to dissolution (predominantly radiolarians and sponge spicules), it appears that the amount of biogenic silica decreased as the environment became more calcareous, and nannofossil and foraminifer oozes were deposited.

The structures of the sediments of lithologic Unit I (nannofossil oozes and chalks with foraminifers, clayey nannofossil chalks, and nannofossil claystones) suggest that the environment was subjected to alternating periods of oxygenation and anoxia of bottom waters. Bioturbation of the sediment by the infauna was enhanced during increases in oxygen levels. Anoxia probably favored the preservation of laminated layers by inhibiting the infauna. The abundance of clay in this lithologic unit shows some variation with depth. As at Site 959, the clay content of lithologic Unit I decreased steadily since the early Miocene, accompanied by an increase in the calcareous component. The transition from ooze to chalk at a shallower depth than at Sites 959 and 960, but of a comparable age, suggests that sedimentation was more condensed at this site during the late Miocene to Holocene.

BIOSTRATIGRAPHY

Introduction

Rotary drilling severely disturbed the cores throughout the recovered section, so biostratigraphic work was confined to the study of core-catcher samples in all but a few intervals. Biostratigraphic control was provided by shipboard analyses of calcareous nannoplankton, planktonic foraminifers, and radiolarians. Benthic foraminifers were studied to provide approximate paleodepth estimates.

A discontinuous sequence from Pleistocene to upper Paleocene was identified at Site 961. Bathymetric ranges of benthic foraminifers suggest that much of the Cenozoic sequence was deposited at lower bathyal to abyssal depths. Pleistocene sediments were recovered in Hole 961A within Core 159-961A-1R (0.0–3.4 mbsf). A Pliocene section extends from Core 159-961A-2R to the Miocene/Pliocene boundary within Core 159-961A-4R (13.1–32.3 mbsf). Below a Miocene interval that extends to Core 159-961A-16R, an unconformity has removed most or all of the Oligocene and middle to upper Eocene sequences. There also may be an unconformity or condensed interval in the upper middle Miocene within Cores 159-961A-10R and 11R (81–100 mbsf). The lower Eocene is present in Cores 159-961A-17R through 18R (157.8 to 167.4 mbsf) and the upper Paleocene in Cores 159-961A-19R through 20R (177.0 to 186.7 mbsf). Below this, the section is barren of calcareous and siliceous microfossils. Hole 961B is barren of planktonic foraminifers. Only one species of calcareous nannofossil has been identified in Cores 159-961B-9R and 11R (313.2–322.4 mbsf). This taxon, *Watznaueria barnesae,* ranges from the Bajocian through the Cretaceous.

Calcareous Nannofossils

Zones spanning the upper Paleocene (Zone CP6) to the uppermost Quaternary (Zone CN15) were identified in Hole 961A. Although rotary drilling caused poor recovery, nearly all zones of the uppermost Quaternary through the upper Miocene were recognized. The zonal assignment of Site 961 is illustrated in Figure 19.

Sample 159-961A-1R-1, 3–5 cm (0.05 mbsf), is assigned to the uppermost part of Quaternary Zone CN15 by the abundant occurrence of *Emiliania huxleyi.* This sample is dominated by well-preserved *Gephyrocapsa caribbeanica* and *G. oceanica.* Sample 159-961A-1R-CC (3.7 mbsf) contains abundant *Pseudoemiliana lacunosa* but lacks *Gephyrocapsa caribbeanica, G. oceanica,* and *Discoaster* spp., indicating the early Quaternary Subzone CN13a. This sample also contains common *Helicosphaera kamptneri* and *Florisphaera profunda* and few to rare *Helicosphaera sellii, Calcidiscus macintyrei, C. leptoporus, Coccolithus pelagicus, Syracosphaera*

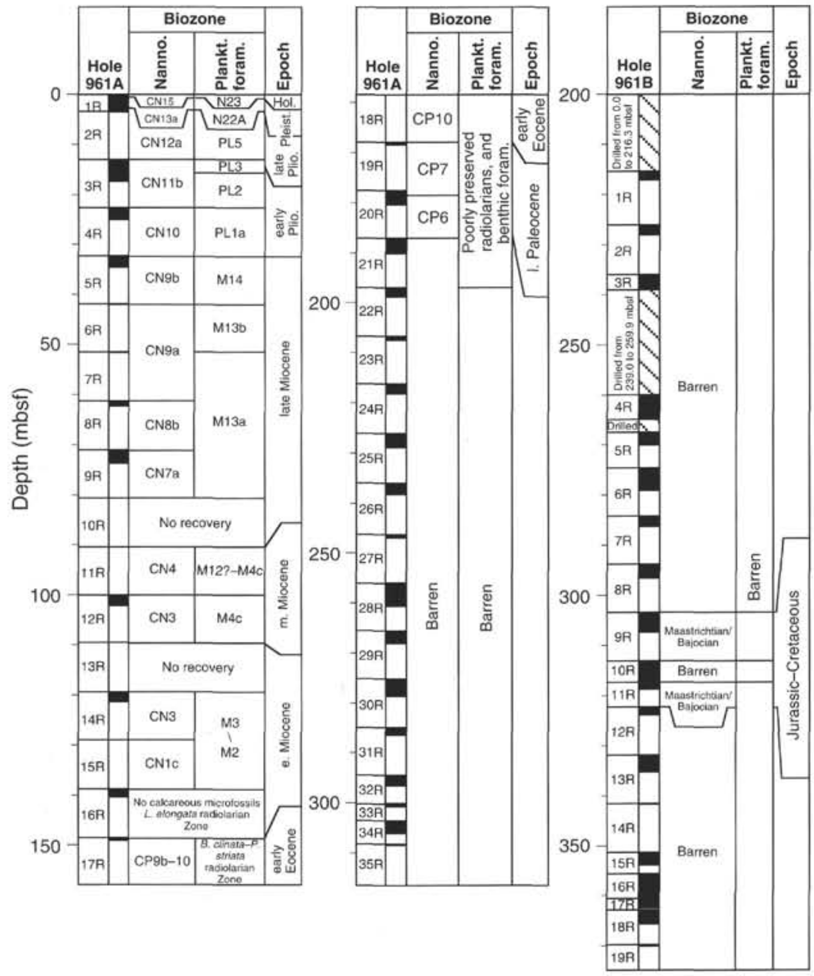

Figure 19. Sequence of biostratigraphic zones in Holes 961A and 961B.

pulchra, Umbilicosphaera sibogae, Reticulofenestra minutula, and *Rhabdosphaera claviger.*

Samples 159-961A-2R-CC through 3R-1, 34–35 cm (13.1–13.45 mbsf), contain *Discoaster brouweri, D. pentaradiatus, D. surculus, D. tamalis, D. quadramus, D. asymmetricus, Pontosphaera japonica, Ceratolithus cristatus,* and *Calcidiscus leptoporus.* This assemblage, in the absence of *Reticulofenestra pseudoumbilica,* indicates late Pliocene Subzone CN12a.

Sample 159-961A-3R-CC (22.7 mbsf) contains *D. asymmetricus* (few), *Pseudoemiliania lacunosa* (common), and *Reticulofenestra pseudoumbilica* (common to few), which indicates the top of early Pliocene Subzone CN11b. Other species in this sample include *Discoaster pentaradiatus, D. brouweri, D. surculus, D. variabilis, D. tamalis, Coccolithus pelagicus, Calcidiscus leptoporus, C. macintyrei, Ceratolithus separatus, Sphenolithus abies, S. neoabies, Florisphaera profunda,* and *Helicosphaera kamptneri.* Samples 159-961A-3R-2, 34-35 cm, and 3R-3, 34–35 cm (13.75–17.95 mbsf), also belong to early Pliocene Subzone CN11b, as indicated by the presence of *Pseudoemiliania lacunosa* and *R. pseudoumbilica.*

Evidence of minor reworking occurs in both Cores 159-961A-2R and 3R. For example, *Triquetrorhabdulus rugosus* in Sample 159-961A-2R-CC is reworked from Subzones CN9b to CN10c, and *Discoaster hamatus* in Sample 159-961A-3R-2, 34–35 cm is reworked from Zone CN7 sediments.

The early Pliocene Zone CN10 occurs in Sample 159-961A-4R-CC (32.3 mbsf). The assemblage includes *Discoaster pentaradiatus, D. surculus, D. challengeri, D. asymmetricus, D. variabilis, D. pansus, D. brouweri, Sphenolithus abies, S. neoabies, Helicosphaera kamptneri,* and *Reticulofenestra pseudoumbilica.* This sample includes species indicative of Subzone CN10b through Subzone CN10d, such as rare specimens of *Ceratolithus acutus, C. rugosus,* and *Discoaster asymmetricus.* Low abundance and poor preservation of these species prevent an accurate subdivision of Zone CN10. Generally, the Pliocene calcareous nannofossil assemblages are abundant and show good preservation except for some discoasters. For example, Sample 159-961A-2R-CC shows common occurrences of isolated rays or ray fragments of discoasters.

Samples 159-961A-5R-1, 64–66 cm, through 5R-CC (34.5–41.9 mbsf) contain abundant *Discoaster quinqueramus* and rare *Amaurolithus primus,* indicating latest Miocene Subzone CN9b. This interval also contains common occurrences of *D. pentaradiatus* and *D. berggrenii* as well as rare occurrences of *D. surculus, D. challengeri, A. delicatus,* and *Triquetrorhabdulus rugosus.*

Well-preserved latest Miocene assemblages (Subzone CN9a) in Samples 159-961A-6R-CC through 7R-CC (51.5–61.2 mbsf) contain occasional specimens of reworked *Cyclicargolithus floridanus* (late Eocene to early Miocene). The indigenous assemblage includes *Discoaster quinqueramus, D. berggrenii, D. surculus, D. pentaradiatus, D. challengeri, D. brouweri, Reticulofenestra pseudoumbilica, Coccolithus pelagicus, Sphenolithus abies,* and *Calcidiscus macintyrei.* No *Amaurolithus* species, including *A. primus,* were observed from this interval, indicating Subzone CN9a.

A middle late Miocene assemblage in Samples 159-961A-8R-1, 90–92 cm, through 8R-CC (63.6–71.0 mbsf) contains abundant *Discoaster prepentaradiatus, D. neohamatus, Sphenolithus abies, S. neoabies, Helicosphaera kamptneri,* and common *D. pentaradiatus, D. challengeri, D. brouweri, D. loeblichii,* and *Reticulofenestra pseudoumbilica.* The presence of rare specimens transitional to *Discoaster berggrenii* and the absence of *D. quinqueramus* place this sample in the uppermost part of Subzone CN8b, in the middle late Miocene.

Samples 159-961A-9R-1, 100–102 cm, through 9R-CC (73.52–80.6 mbsf) belong to the early late Miocene Subzone CN7a, based on the presence of *Discoaster hamatus* and *Catinaster coalitus* and the absence of *Catinaster calyculus.* The assemblage from this sample includes abundant *Reticulofenestra pseudoumbilica* and common to rare *Discoaster challengeri, D. pseudovariabilis, D. bellus, D. brouweri, D. variabilis, D. braarudii, D. calcaris, Calcidiscus macintyrei,* and *Sphenolithus* spp. Late to middle Miocene calcareous nannofossils are abundant and show good preservation.

Rare, moderately preserved nannofossils in Sample 159-961A-11R-CC (99.9 mbsf) include *Sphenolithus heteromorphus,* without the association of *Helicosphaera ampliaperta,* indicating early middle Miocene Zone CN4.

Samples 159-961A-12R-CC (109.6 mbsf) and 14R-CC (128.9 mbsf) are assigned to early Miocene Zone CN3, based on the presence of both *Sphenolithus heteromorphus* and *Helicosphaera ampliaperta.* Co-occurring species include *Reticulofenestra pseudoumbilica, Cyclicargolithus floridanus, Discoaster druggii, D. variabilis, D. deflandrei,* and *C. pelagicus.*

The presence of *Discoaster druggii* and *Orthorhabdus serratus,* without *Sphenolithus belemnos,* in Sample 159-961A-15R-CC (138.5 mbsf) indicates early Miocene Subzone CN1c. This sample also contains *Coronocyclus nitescens, Reticulofenestra pseudoumbilica, R. minuta, Coccolithus miopelagicus, Helicosphaera rhomba, H. granulata, H. obliqua, H. mediterranea, Sphenolithus compactus, S. moriformis, Discoaster deflandrei,* and *D. adamanteus.*

Sample 159-961A-16R-CC (148.1 mbsf) is barren of calcareous nannofossils. Sample 159-961A-17R-CC (157.8 mbsf) is assigned Zone CP9b-CP10 by the absence of *Discoaster lodoensis.* However, the presence of *Chiphragmalithus acanthodes, C. calathus,* and *Discoaster kuepperi* are indicative of Zone CP10. Sample 159-961A-18R-CC (167.4 mbsf) contains *Discoaster kuepperi, D. lodoensis,* and *Tribrachiatus orthostylus,* also suggesting early Eocene Zone CP10. Moderately to poorly preserved nannofossil assemblages from Samples 159-961A-17R-CC and 18R-CC include *D. robustus, D. diastypus, D. sublodoensis, D. binodosus, D. septemradiatus, D. barbadiensis, Sphenolithus primus, S. moriformis, Chiasmolithus solitus, Coccolithus pelagicus, Cyclicargolithus gammation, Ellipsolithus lajollaensis, Ericsonia ovalis,* and *E. robusta.* The nannofossil abundance ranges from few to common and preservation is poor to moderate.

Sample 159-961A-19R-1, 33–35 cm (169.25 mbsf), contains very poorly preserved, rare specimens of *Discoaster multiradiatus,* which ranges from Zone CP8 to Zone CP9. Sample 159-961A-19R-CC (177.0 mbsf) is assigned to late Paleocene Zone CP7 by the presence of the *Heliolithus riedelii* and the absence of *Discoaster multiradiatus.* This sample includes *Chiasmolithus consuetus, Sphenolithus primus, Toweius pertusus, Fasciculithus clinatus, Discoaster splendidus, D. delicatus, D. megastypus, Ericsonia ovalis, E. robusta,* and *Neochiastozygus junctus.* The nannofossil abundance is low and preservation is moderate.

Zone CP6 of late Paleocene age is recognized in Sample 159-961A-20R-CC (186.7 mbsf) by the presence of *Discoaster mohleri* and the absence of *D. nobilis* and *H. riedelii.* The assemblage includes *Fasciculithus tympaniformis, Placozygus sigmoides, Ericsona ovalis, E. cava, Toweius eminens, Cruciplacolithus tenuis, S. primus, Ellipsolithus distichus, E. macellus, Discoaster mohleri,* and *Neochiastozygus digitosus.* Nannofossils are common and moderately preserved. Samples below Core 159-961A-20R-CC (186.7 mbsf; middle middle Paleocene) are barren of calcareous nannofossils.

Eleven cores were retrieved from Hole 961B. All core-catcher samples are barren of calcareous nannofossils except 159-961B-9R-CC (313.2 mbsf) and 11R-CC (322.4 mbsf). These two samples only contain very rare and very poorly preserved specimens of the dissolution-resistant species *Watznaueria barnesae. Watznaueria barnesae* has a long stratigraphic range from the Bajocian to the Maastrichtian and indicates that Samples 159-961B-9R-CC and 11R-CC are of late Mesozoic age.

Planktonic Foraminifers

Fifty-four samples from Site 961 were studied aboard ship. Zonal assignments are summarized in Figure 19. Preservation is good to moderate throughout the Miocene to Holocene sections (down to Sample 159-961A-15R-CC; 138.5 mbsf), but samples deeper than this are barren. A long sequence from Sample 159-961A-22R-CC (196.4 mbsf) through 35R-CC (308.7 mbsf), and from Sample 159-961B-1R-CC (226.0 mbsf) through 19R-CC (374.6 mbsf) contains no calcareous or siliceous microfossils, except in Samples 159-961B-9R-CC (313.2 mbsf) through 11R-CC (322.4 mbsf), where calcareous nannofossils were found.

Sample 159-961A-1R, 3–5 cm, contains a moderately preserved assemblage including *Globorotalia tumida,* and *Pulleniatina obliquiloculata* without *Globorotalia tosaensis* or *Globigerinoides fistulosus.* Nannoplankton from this sample indicate latest Pleistocene or Holocene age. The foraminifer assemblage is typical of Zones N22b to N23 and represents an interglacial assemblage, as both *G. tumida* and *P. obliquiloculata* are present in the equatorial and North Atlantic only during the interglacial stages of the late Pleistocene (Ericson and Wolin, 1968; Ericson et al., 1961). The combination of the nannoplankton evidence for latest Pleistocene-Holocene age and the interglacial foraminifer assemblage suggests that the youngest sediments in Hole 961A may be from the Holocene.

Sample 159-961A-1R-CC (3.4 mbsf) yielded an abundant and well-preserved microfauna. Taxa include common *G. tumida, G. scitula, Pulleniatina obliquiloculata, Globigerinoides ruber, G. sacculifer, Orbulina universa, Neogloboquadrina dutertrei, N. pachyderma, G. bulloides, Sphaeroidinella dehiscens,* rare *Globorotalia menardii, G. crassaformis,* as well as a few specimens of well-preserved *Globorotalia pseudomiocenica* and *Globorotalia pertenuis.* The presence of *G. pseudomiocenica* and *G. pertenuis* suggests a Pliocene age for the assemblage, but the sample may also belong to Pleistocene Zone N22, if *G. pseudomiocenica* and *G. pertenuis* are reworked. Markers for the top of the Pliocene such as *Globorotalia tosaensis* and *Globigerinoides fistulosus* have not been found and support the inference that Sample 159-961A-1R-CC is of Pleistocene age.

The Pliocene is very condensed, as it is present only between Cores 159-961A-2R and 4R (3.5–32.5 mbsf). Zones PL6 and PL4 have not been identified, and neither have Subzones PL1b and PL1c.

The assemblage of Sample 159-961A-2R-CC (13.1 mbsf) identifies Zone PL5, with the presence of abundant *Globorotalia miocenica, N. dutertrei,* common *G. pertenuis, G. sacculifer, G. ruber, G. glutinata,* and *G. pseudomiocenica. Globigerina bulloides, Globigerinoides fistulosus,* and *Globorotalia tumida* are also present. Preservation is good; foraminifers are preserved with glassy walls. Unfortunately, the vertical distribution of Zone PL5 cannot be determined as this assemblage was found only in the core-catcher, and the core barrel itself was empty.

Zone PL3 is present in Samples 159-961A-3R-1, 34–36 cm, and 3R-2, 34–36 cm (14.9–16.4 mbsf). Foraminifers are common to abundant, and include well-preserved *Globorotalia multicamerata* and *Sphaeroidinellopsis seminulina.* Samples from Zone PL3 are dominated by common to abundant *Orbulina universa, G. sacculifer,* and *N. dutertrei. Globorotalia multicamerata* has its earliest occurrence in Zone PL3 and the extinction of *Sphaeroidinellopsis* spp. marks the top of the zone.

The highest occurrence of *Globorotalia margaritae* in the absence of *Globigerina nepenthes* identifies Zone PL2 in Sample 159-961A-3R-CC (22.7 mbsf). Other foraminifers include abundant and well-preserved *Neogloboquadrina dutertrei*, common *G. tumida, G. sacculifer, Globigerinoides extremus,* few *G. crassaformis,* and *Sphaeroidinella kochi,* as well as rare *G. pertenuis.*

Foraminifers of Samples 159-961A-4R-1, 89–90 cm, and 4R-CC (23.6–32.3 mbsf) belong to Subzone PL1a. Species include the markers for the subzone: *G. nepenthes, Globorotalia cibaoensis,* and *G. tumida,* as well as common to abundant specimens of *G. menardii, N. dutertrei,* and *G. venezuelana. Sphaeroidinella dehiscens, G. margaritae,* and *Globorotalia plesiotumida* are also present, although rare. As is the case throughout the Pliocene intervals at Site 961, foraminifers are well preserved.

The Miocene/Pliocene boundary is thought to occur between Samples 159-961A-4R-CC and 5R-1, 64–66 cm (32.3–32.9 mbsf), if we use the convention that recovered sediment is shifted to the top of the core barrel. Dissolution has produced extensive fragmentation in Samples 159-961A-5R-1, 64–66 cm, and 5R-2, 8–10 cm, and preservation is only marginally better in Sample 159-961A-5R-CC. All these samples contain *Globorotalia plesiotumida, G. cibaoensis, G. margaritae,* and *N. nepenthes,* but lack *G. tumida.* In as much as *G. tumida* is usually more resistant to dissolution than either *G. margaritae* or *G. plesiotumida,* its absence suggests that the samples were taken from below its first appearance and are of late Miocene age. In addition, intense dissolution is common in other eastern equatorial Atlantic sites during the latest Miocene, whereas early Pliocene assemblages (when defined on the first occurrence of *G. tumida*) are usually well preserved (Weaver and Raymo, 1989).

Zone M14 was assigned to Samples 159-961A-5R-1, 64–66 cm (32.9 mbsf), and 159-961A-5R-CC (41.9 mbsf) because of the presence of *G. margaritae, G. cibaoensis,* and *G. plesiotumida* in the absence of *G. lenguaensis.* Common species include *D. altispira, G. menardii, G. sacculifer, Globigerinoides extremus, N. dutertrei,* and *N. acostaensis. Globigerina nepenthes, S. seminulina,* and *G. bulloides* are present, as well.

Zone M13 extends from Samples 159-961A-6R-CC through 9R-CC (51.5–80.6 mbsf). Sporadic specimens of *G. plesiotumida,* together with *G. lenguaensis,* in Sample 159-961A-6R-CC indicate Subzone M13b. This sample contains common *G. obliquus, G. sacculifer,* and *G. nepenthes,* with common to rare specimens of *Globorotalia cibaoensis, S. seminulina, D. altispira, G. venezuelana, S. dehiscens, Neogloboquadrina acostaensis, Globigerina woodi,* and *Globorotalia juanai. Globorotalia margaritae* is not present, in accordance with its reported first appearance above the last occurrence of *G. lenguaensis* (Bolli and Saunders, 1985). In Samples 159-961A-7R-CC through 9R-CC, *G. plesiotumida* is absent, and the samples are assigned to Subzone M13a. Samples 159-961A-7R-CC (61.2 mbsf) and 159-961A-8R-CC (71.0 mbsf) contain most of the precedent taxa and common, well-preserved *Globigerinoides seigliei, O. universa,* and *Dentogloboquadrina altispira,* as well as sporadic specimens of *G. merotumida* and *G. lenguaensis.* Only dissolution-resistant taxa are left in Sample 159-961A-9R-CC (80.6 mbsf), which contains abundant *S. kochi, S. seminulina, Globoquadrina venezuelana,* and *G. sacculifer.* However, *G. merotumida* and *N. acostaensis* are still present and indicate Subzone M13a.

Both Cores 159-961A-10R (80.6–90.3 mbsf) and 11R (90.3–100 mbsf) were empty but may have cored through an unconformity separating upper Miocene sediments from lower Miocene deposits. A small sample of mud in Sample 159-961A-11R-CC (99.9 mbsf) yielded only one benthic foraminifer and single specimens of *G. sacculifer* and *Globigerina druryi.* The latter ranges from Subzone M4c to Zone M12. The earlier planktonic foraminifer zone is suggested by the presence of nannofossil Zone CN3 in the same sample.

The occurrence of *Praeorbulina sicana* in Sample 159-961A-12R-CC (109.6 mbsf), in the absence of *Praeorbulina glomerosa,* indicates Subzone M4c. The assemblage consists of abundant *G. sacculifer,* common *Globorotalia peripheroronda, G. venezuelana, Globigerinoides subquadratus, Globigerinella praesiphonifera,* and a few specimens of *P. sicana, G. dehiscens, Globorotalia mayeri, Globorotalia birnageae,* and *Globigerina praebulloides.* Foraminifers are rare but are well preserved. Sample 159-961A-13R-CC (119.3 mbsf) was not recovered.

In Samples 159-961A-14R-CC (128 mbsf) and 15R-CC (138.5 mbsf) radiolarians appear. Planktonic foraminifers are rare and moderately preserved. The foraminifer microfauna consists of *Catapsydrax dissimilis, D. altispira, G. subquadratus, G. venezuelana, G. dehiscens,* and members of the *G. mayeri* plexus in the first core catcher; in the second core catcher are found *C. dissimilis, D. altispira, G. trilobus.* These samples probably belong to Subzone M1b to Zone M3 based on the last occurrence of *C. dissimilis* (marker for the top of Zone M3) and the lowest occurrence of *G. dehiscens* at the base of Subzone M1b.

Core-catcher Samples 159-961A-22R-CC (206.1 mbsf) to 35R-CC (308.7 mbsf) are barren of calcareous and siliceous microfossils. Samples from core catchers in Hole 961B are barren of planktonic foraminifers.

Benthic Foraminifers

Benthic foraminifers were not examined in detail, but a few samples were studied to provide approximate paleodepth estimates. The ratio of planktonic to benthic foraminifers is probably an unreliable depth recorder for the pre-upper Miocene section at this site due to the considerable dissolution of the planktonic foraminifers below ~80 mbsf in Hole 961A.

Sample 159-961A-1R-1, 3–5 cm, contains a rich assemblage of Pleistocene abyssal species including *Uvigerina peregrina, Sphaeroidina bulloides, Hoeglundina elegans, Eponides polius, Pyrgo murrhina, Pullenia quinqueloba,* and *Gyroidina zelandicus.* Some of these species, such as *Hoeglundina elegans,* have wide bathymetric occurrences, whereas others, like *Eponides polius,* have been reported mostly from deep water facies such as the lower slope and abyssal floor in the Gulf of Mexico (Poag, 1981).

The upper Miocene assemblage in Sample 159-961A-5R-1, 64–66 cm, includes *Laticarinina pauperata, Matazia* sp. cf. *M. bermudezi, Stilostomella spp., Gyroidina zelandicus,* and *Pullenia quinqueloba.* A similar assemblage was found in Sample 159-961A-8R-CC from planktonic foraminifer Biozone M13a that contains *Uvigerina peregrina, Anomalinoides globulosus, Rectuvigerina striata, Vulvulina spinosa,* and *Bulimina spp.* These species suggest middle bathyal to abyssal depths based on bathymetric ranges reported by van Morkhoven et al. (1986).

Lower Miocene benthic foraminifers are generally abundant and diverse, particularly because much of the planktonic foraminifer assemblage is highly dissolved. Sample 159-961A-12R-CC, from planktonic foraminifer Subzone M4c, contains a rich assemblage that includes the bathyal to abyssal species, *Pullenia bulloides, P. quinqueloba, Pyrgo spp., Stilostomella spp., Anomalinoides semicribratus, Cibicides wuellerstorfi, Cibicidoides bradyi, C. havanensis,* and *Laticarinina pauperata.* Buliminids are also common constituents of this microfauna.

Samples 159-961A-16R-CC and 20R-CC contain Paleocene and Eocene species such as *Spiroplectammina spectabilis* and *Nuttallides truempyi,* suggestive of lower bathyal to abyssal depths. The presence of these species suggests that much of the Paleocene and Eocene sequence in Hole 961A was deposited at water depths of 1000 m or more, based on bathymetric ranges suggested by van Morkhoven et al. (1986). Foraminifers are uncommon and are moderately preserved in both samples. Sample 159-961A-20R-CC also includes species reported by van Morkhoven et al. (1986) to have bathyal to abyssal depth ranges, such as *Quadratobuliminella pyramidalis, Aragonia velascoensis, Stensioina beccariiformis, Nonion havanensie*, and *Gyroidinoides globosa.*

Core-catcher samples taken below Core 159-961A-21R (187.0 mbsf) are barren of benthic foraminifers. Likewise, no calcareous or agglutinated foraminifers were found in any part of Hole 961B.

Radiolarians

Core-catcher Samples 159-961A-16R-CC to 21R-CC (148.1–196.4 mbsf) are barren of planktonic foraminifers; they contain only rare benthic foraminifers and moderately to well-preserved radiolarians. Sample 159-961A-16R-CC yielded well-preserved lower Miocene radiolarians (*Lychnocanoma elongata* Zone), with *Calocycletta serrata, Theocyrtis annosa, Lychnocanoma elongata, Dorcadospyris papilio,* and *Tholospyris mammallaris.* Radiolarians in Sample 159-961A-17R-CC (157.8 mbsf) are moderately preserved with *Spongatractus balbis, Thyrsocyrtis hirsuta, Sethochytris babylonis,* and *Lithochytris archaea* that indicate an early Eocene age.

PALEOMAGNETISM

Investigations of magnetic properties at Site 961 included measurements of bulk susceptibility on whole cores and natural remanent magnetization (NRM) on archive-half sections and selected discrete samples. Coring with the rotary core barrel (RCB) was employed at this site, and drilling disturbance was particularly pronounced. Hence, whole-core directional measurements are of limited value, and we have confined ourselves to a discussion of bulk susceptibility and NRM intensity. The cores at this site were not demagnetized by alternating field (AF) techniques.

Bulk Susceptibility

Magnetic susceptibility measurements were made on whole cores from Holes 961A and 961D. These data are included in Site 961 Appendix A on the CD-ROM. Poor recovery means that the susceptibility record with depth is discontinuous (Fig. 20A, B), and that the depth and nature of transitions in magnetic properties cannot be determined with a high degree of precision.

The first 50 cm of Hole 961A has susceptibilities of $\sim 20 \times 10^{-5}$ SI units. Below this depth, susceptibility drops abruptly to $<10 \times 10^{-5}$ SI units; it then increases progressively to a maximum of 50×10^{-5} SI units between 71 and 73 mbsf. Below 73 mbsf, bulk susceptibility drops to values of $<10 \times 10^{-5}$ SI units at about 120 mbsf, at the boundary between lithologic Units I and II. Susceptibility remains low in the interval from 120 to 188 mbsf, falling to values of $<5 \times 10^{-5}$ SI units at the base of this interval. Below 188 mbsf, susceptibility increases to about 15×10^{-5} SI units. This change in susceptibility coincides with the boundary between lithologic Units II and III. In the upper part of Unit III, to a depth of 260 mbsf, susceptibility values generally range from 10 to 20×10^{-5} SI units, except for the interval between 226 and 227 mbsf, where values up to 30×10^{-5} SI units were encountered. Below 260 mbsf, to the base of both Holes 961A and 961D, susceptibility increases to values from 20 to 30×10^{-5} SI units, which may correspond to an increase in siderite content in cores beneath this depth.

Remanent Magnetization

Measurements of remanent magnetization were made on core sections and discrete cubes from Holes 961A and 961B (Fig. 20C, D; Site 961 Appendixes B and C on CD-ROM). Variations in NRM intensity with depth follow similar patterns to those seen at Sites 959 and 960. In Core 159-961A-1R, the NRM intensity is generally <10 mA/m. In Core 159-961A-3R (13.1–22.7 mbsf), intensities increase up to 50 mA/m (N.B.: only 4 cm was recovered in Core 159-961A-2R). As observed at previous sites, this increase in intensity also corresponds to the upper/lower Pliocene boundary (planktonic foraminifer Biozones PL3/PL2). This interval, with NRM intensities that range from 30 to 120 mA/m, extends to a depth of 73.65 mbsf (base of recovered portion of Core 159-961A-9R). Core 159-961A-12R has NRM intensities between 10 and 30 mA/m. The decrease in the magnetization between these cores corresponds to a change in age from Zone M4 in Core 159-961A-12R to Zone M13 in Core 159-961A-9R, consistent with observations at Sites 959 and 960.

A marked reduction in NRM intensity (to <1 mA/m) occurs in Core 159-961A-16R at a depth of about 139 mbsf, the first full core of lithologic Unit II. The majority of the cores in lithologic Unit II exhibit a low NRM intensity (<1 mA/m); however, in the last two cores in this unit (Cores 159-961A-20R and 21R), NRM intensities increase to values up to 10 mA/m. NRM values remain at this level through the transition to lithologic Unit III at 188.5 mbsf, to the bases of Holes 961A and 961B. The high values of NRM intensity and bulk susceptibility encountered in lithologic Unit III at this site are similar to those of lithologic Unit V at Site 959.

Where possible, one discrete cube sample was taken per core from Holes 961A and 961B. The NRMs of discrete samples were measured on the WCC magnetometer. These data show similar variations to the trend observed in the NRM record of the archive-half sections of this hole (Site 961 Appendix C).

STRUCTURAL GEOLOGY

Most of the structures measured at this site are restricted to the base of Hole 961B. Bedding dips and fault attitudes will be reoriented after the cruise, once the paleomagnetic data have been fully processed. Unfortunately, technical problems with Hole 961A and a collapse in Hole 961B prevented the use of the Formation MicroScanner logging tool.

The few structures observed and measured at Site 961 include bedding planes, soft-sediment structures, rare veins and breccias, shears, faults, and microfolds. Most of the tectonic features of Site 961 were observed in lithologic Unit III, in Cores 159-961B-13R and 18R (332.1–341.7 and 362.9–369.9 mbsf, respectively). Core 159-961B-13R in particular shows well-developed shearing and roughly crenulated bedding.

Bedding

Recovery in Hole 961A was generally poor and, as a result, only a few bedding planes could be measured. Bedding measurements made on Cores 159-961A-8R, 9R, and 12R from lithologic Unit I display dip values ranging from 5° to 18° (Fig. 21A). Drilling disturbance in these soft sediments accounts for the range in dips. Few measurable bedding planes were observed in the remainder of Hole 961A. The only possible measurement of a bedding plane in lithologic Subunit II was made in the porcellanites of lithologic Subunit IIB. The dip of the bed is 14°, but as the bed is adjacent to a normal fault the measurement may not reflect the general dip of the unit as a whole. Only two bedding measurements were made in the siltstones in the deepest part of Hole 961A (Section 159-961A-33R-1). Bedding is defined by fine laminations that are slightly disrupted by bioturbation. The measurements were made in adjacent loose blocks that had rotated within the core liner. The two blocks were obviously part of the same laminated sequence, and, although the beds are clearly dipping, the two dips of 16° and 31° do not reflect a true change in dip.

The first core from Hole 961B was recovered from a depth of 216 mbsf. Thus, this entire hole is within lithologic Unit III. The cores from this hole are less disrupted than those from Hole 961A and more

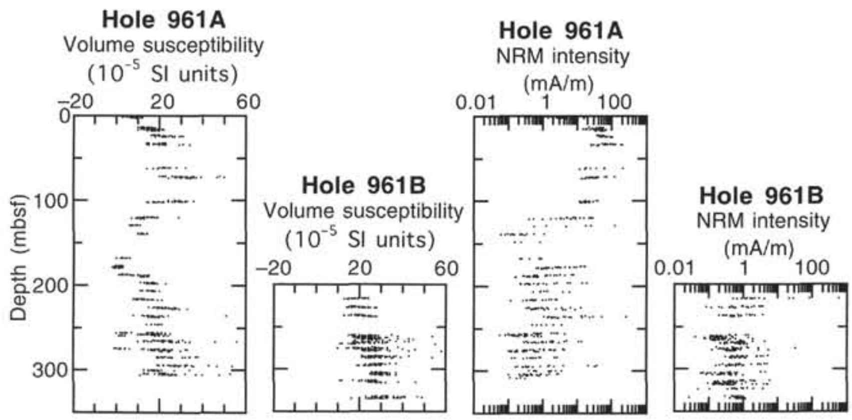

Figure 20. Variations in bulk susceptibility and NRM intensity vs. depth, Holes 961A and 961B.

bedding measurements were possible. As shown in Figure 21B, bedding dips display a wide range of values. Bedding dips in the upper part of Hole 961B (220–240 mbsf) lie between 9° and 27°. A sharp increase in dip occurs in the laminated gray siltstones of Core 159-961B-7R (284.2–293.8 mbsf). Dips ranging from 30° to 58° were measured in this core. The presence of synsedimentary deformation features (including faults, convolute bedding, and slump folds) in Core 159-961B-7R suggests that slumping may have caused the wide variation of dip values. Dip values are scattered and widely varied through the remainder of Hole 961B. Bedding dips in the gray siltstones and claystones of Cores 159-961B-13R and 15R include particularly high dip values, ranging from 39° to 72° (Core 159-961B-13R) and from 21° to 71° (Core 159-961B-15R). The high degree of deformation in Core 159-961B-13R implies that the high dips are a tectonic rather than a slump feature. Dips in Cores 159-961B-16R and 18R are lower on average than those of Cores 159-961B-13R and 15R. Dips range between 26° and 45°, clustering at about 30°.

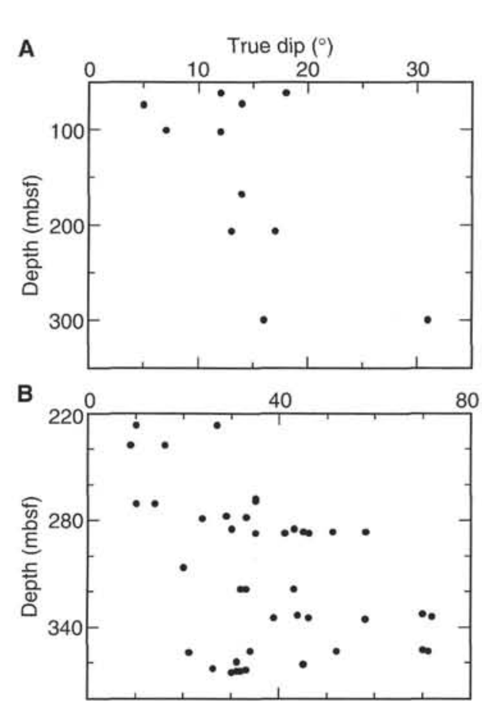

Figure 21. Variation of bedding dip with depth in (**A**) Hole 961A and (**B**) Hole 961B. Dip values are calculated from two apparent dips.

Faults and Shears

Faults were rarely observed in Hole 961A, mostly because of poor recovery and the disrupted nature of the cores. Normal microfaults were observed in Sections 159-961A-19R-1 and 31R-CC (lithologic Subunit IIB and Unit III, respectively). The faults in both cases have offsets of 1 cm or less. In Section 159-961A-31R-CC, the normal microfaults define a series of tilted blocks and horst and graben structures. Steeply dipping curved faults marked by thin seams of fine-grained material (up to 0.5 mm wide) were observed in Section 159-961A-33R-1. The sense of motion was not determined. Loose blocks within Section 159-961A-33R-1 display minor normal faults with 1 mm of offset.

Structural features are more abundant in Hole 961B, because core recovery was better. Core 159-961B-13R (332.1–341.7 mbsf) is one of the most interesting cores of Hole 961B from a structural point of view. In Sections 159-961B-13R-1 and 13R-2, the bedding is well marked by alternating pale and dark laminae of 1 mm to several millimeters in thickness. The bedding dip is generally high and commonly close to vertical. In Section 159-961B-13R-1, 11–35 cm, bedding is subvertical and affected by microfolding. In Section 159-961B-13R-1, 61–65 cm, a microfold is sheared along its short limb by a fault. Throughout Core 159-961B-13R, the fine bedding is asymmetrically microfolded due to the occurrence of a series of parallel shear planes at high angles to the bedding. The best example is found in Section 159-961B-13R-3, where the bedding is cut by a series of closely spaced shears with 0.5–1-mm offsets. The shear zones impart a rough crenulation to the rock, which may be described as an incipient cleavage (Fig. 22). In thin section, it can be seen that the shears are discontinuous in extent and commonly characterized by seams of dark, clay-rich (and ?micaceous) material. A vertical shear band cuts Section 159-961B-13R-1 from 140 to 80 cm. The shear splays upward from a zone up to 2 cm wide into several thinner shears. In Section 159-961B-13R-1, 127–140 cm, at the base of the shear described above, two shear planes enclose a band of gray material and the walls bear slickensides pitching 90° (i.e., dip-slip motion) (Fig. 23). On the adjacent blocks, steeply dipping minor faults offset thin laminae that are affected by small-scale microfolding, resulting in a rough crenulated aspect. This crenulation may result either from effective or potential shear planes. On a horizontal section through the core in Section 159-961B-13R-1, 79 cm, asymmetric drag microfolds were observed. Evidence of shearing was also observed in Section 159-961B-13R-2. Shear zones, normal microfaults, and microfolding are closely associated in Section 159-961B-13R-2, 97–100 cm. The shear zones attenuate and deform laminae without cutting them. Re-

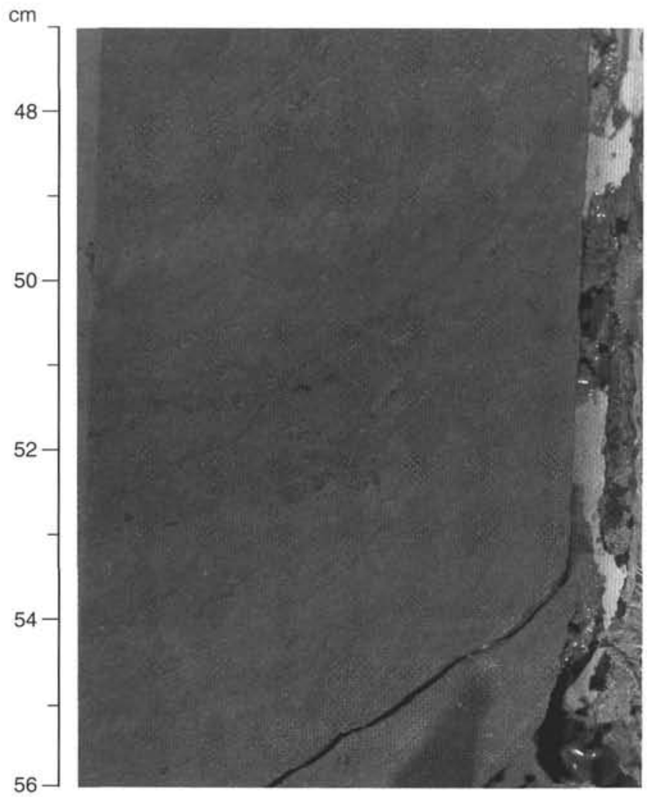

Figure 22. Rough crenulation in laminated siltstone due to closely spaced shear zones (Section 159-961B-13R-3, 47–56 cm).

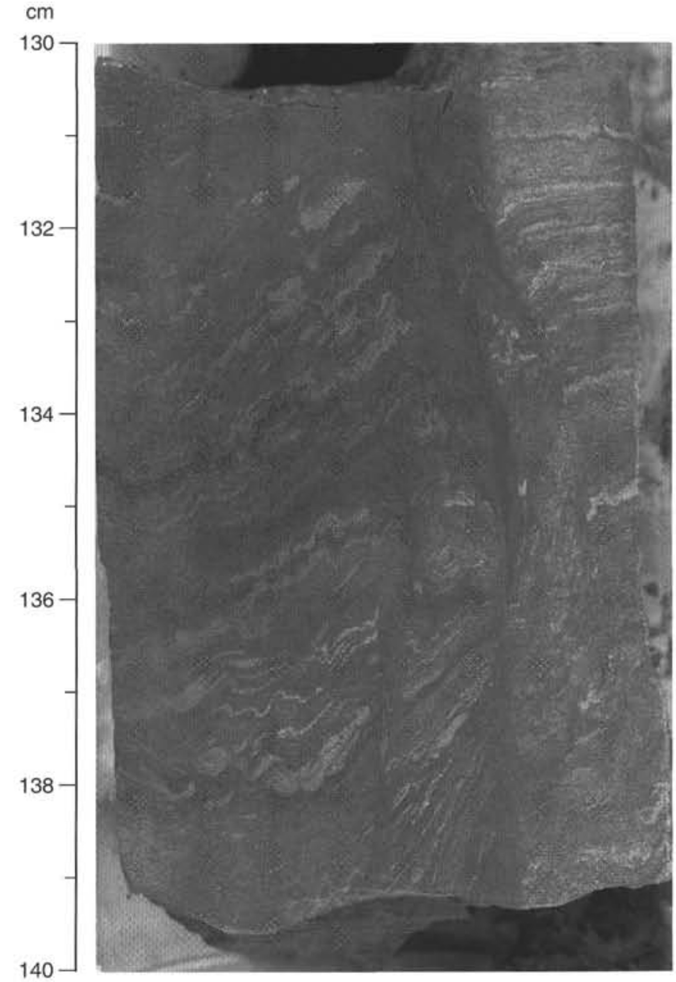

Figure 23. Steeply dipping shear bands. Minor faults offset thin laminae affected by a rough crenulation (Section 159-961B-13R-1, 130–140 cm).

verse faults were first observed in the silty claystones of Section 159-961B-17R-1. Steeply dipping thin beds are displaced by 2–3 mm by shallow reverse faults. The faults are thin shear zones 0.5 mm wide, rather than discrete fault planes. They appear to have been active when the sediment was not completely lithified.

Core 159-961B-18R (362.9–369.9 mbsf), near the base of Hole 961B, displays a beautifully preserved array of predominantly normal microfaults and shear zones (Fig. 24). In Section 159-961B-18R-1, a synsedimentary fold has a sheared lower limb (Fig. 25). A shallowly dipping shear zone below the fold is cut by a steeply dipping planar normal fault. Section 159-961B-18R-2 displays several fault/shear sets (Fig. 26). A set of conjugate faults up to 2 cm long forms a series of horst and graben structures and rotated fault blocks. Several of these faults extend to a greater length (up to 12 cm) and display fault splaying and pop-up structures. One set of these conjugate faults is steep while the other is shallow, implying that they were formed in flat-bedded sediments and subsequently tilted. Slickensides observed on a moderately dipping polished fault plane (Section 159-961B-18R-2, 74–81 cm; Fig. 26) pitch at 83°, indicating a predominantly normal dip-slip sense of motion. The footwall of this fault is characterized by intense normal microfaulting, whereas the hanging wall displays little deformation. Slickensides on a steeply dipping fault in the footwall pitch at 72°, again indicating a predominantly normal dip-slip sense of motion. Section 159-961B-18R-2, 40–46 cm, also displays a fault with a deformed footwall and a relatively undeformed hanging wall. A shallowly dipping minor reverse fault was observed in Section 159-961B-18R-2, 61–63 cm.

Veins

Calcite veining in gray claystone in Section 159-961A-26R-1 was the only veining observed in Hole 961A. The veining is intense in Sections 159-961A-26R-1, 0–10 cm, and 50–55 cm. The veining is associated with fracturing.

In Hole 961B veining is common in Cores 159-961B-2R and 3R. In Section 159-961B-2R-1, pyrite and calcite occur around a pale siltstone clast within gray siltstone. Pyrite also occurs within a fracture. Intense calcite veining was observed in the laminated gray siltstones of Core 159-961B-3R. In Section 159-961B-3R-1 calcite veining is associated with brecciation and fracturing. Sideritic veins were observed in the brown sideritic siltstones in Core 159-961B-4R. A white, probably kaolinite, vein was observed in Section 159-961B-5R-1. The deepest example of veining observed in Hole 961B was a patch of calcite mineralization in black claystone in Section 159-961B-9R-CC.

Soft-sediment Deformation

Examples of soft-sediment deformation were observed in both Holes 961A and 961B. In Hole 961A, a water escape structure and a sand pipe were observed in Section 159-961A-27R-1. Microslumps and convolute bedding were found in Section 159-961B-5R-2. Several examples of soft- sediment deformation were observed in Core 159-961B-7R. In Section 159-961-7R-1, synsedimentary faults and wavy to convolute bedding were observed. The beds are steeply dipping in Section 159-961B-7R-2 and may be part of a slumped sequence. A

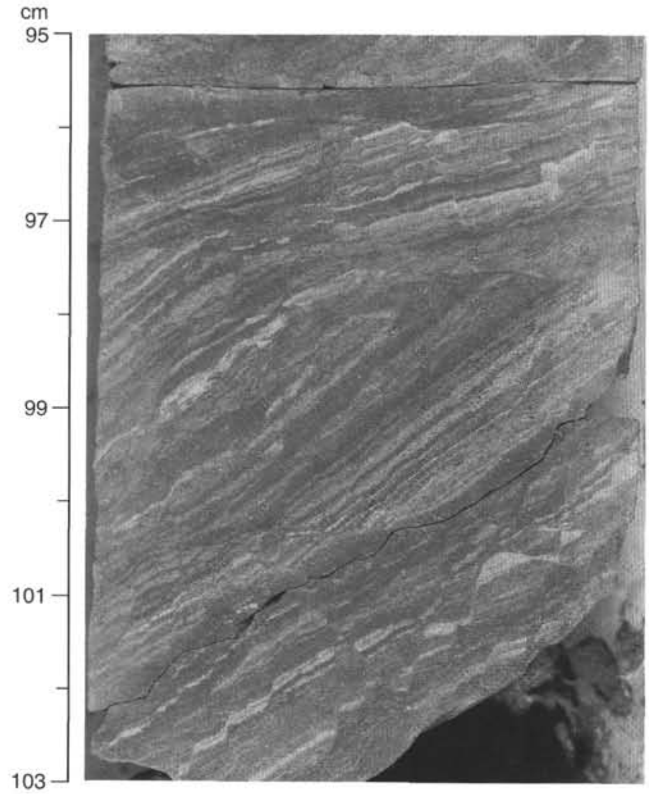

Figure 24. Microfaults and shear zones in finely laminated siltstones (Section 159-961B-18R-2, 95–103 cm).

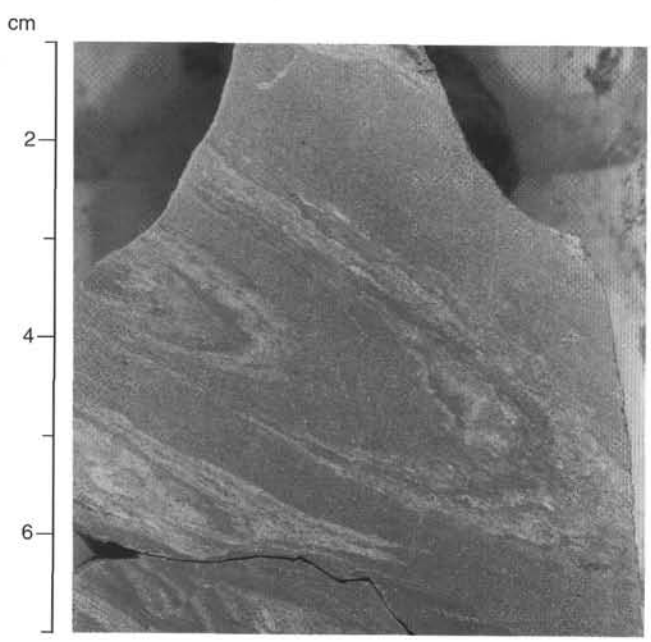

Figure 25. Soft-sediment fold with a sheared lower limb (Section 159-961B-18R-1, 1–7 cm). A bedding-parallel shear zone below the fold is cut by a steeply dipping planar normal fault.

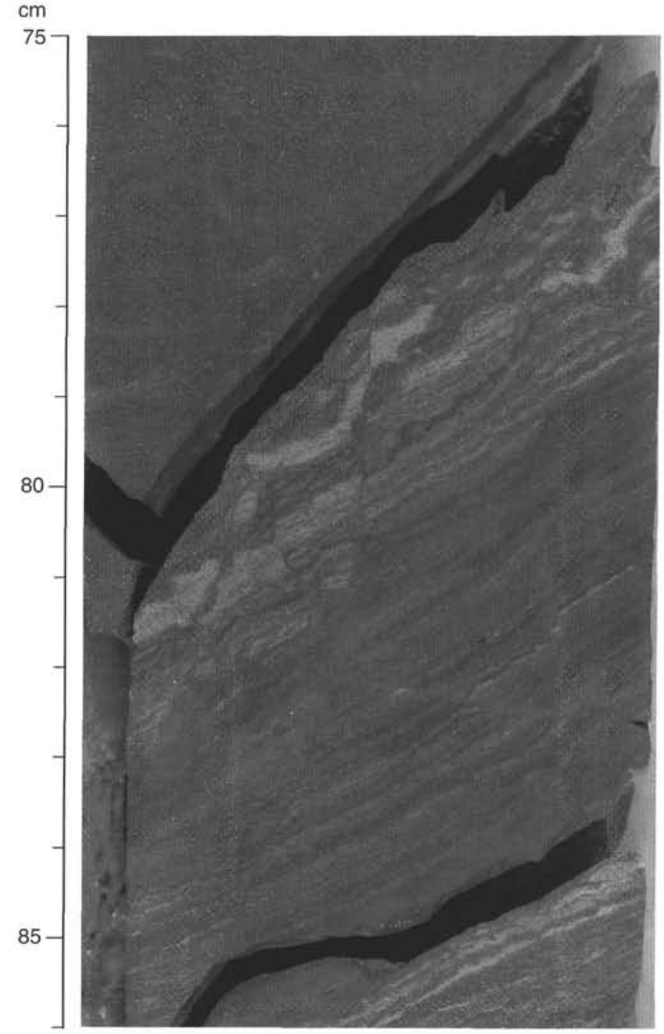

Figure 26. Conjugate set of microfaults form a series of horst and graben structures and rotated fault blocks. The faults are concentrated in the footwall of a shallower fault, which is marked by a break in the core (Section 159-961B-18R-2, 75–86 cm).

microslump fold in Section 159-961B-7R-2, 86–89 cm, confirms that slumping occurred during or soon after deposition of these sediments. In Section 159-961B-18R-1, 2–6 cm, a slump fold, several centimeters across, is oriented parallel to the bedding. Its lower limb is sheared and thinned relative to the upper one (Fig. 25). A characteristic synsedimentary fault was observed in Section 159-961B-9R-CC, 12–13 cm. Laminations change in thickness across the fault (from 1.5 to 3 mm) and the lamination above the fault is undistorted, thus confirming a synsedimentary origin for the faulting (Fig. 27).

Deformation that occurred under more lithified conditions was also observed. For example, an open fold with parasitic microfolds and sinuous slickensides in Section 159-961B-5R-CC may indicate synlithification deformation.

ORGANIC GEOCHEMISTRY

Introduction

At Site 961 real-time monitoring of volatile hydrocarbons, determination of inorganic carbon, total carbon, total nitrogen, and Rock-

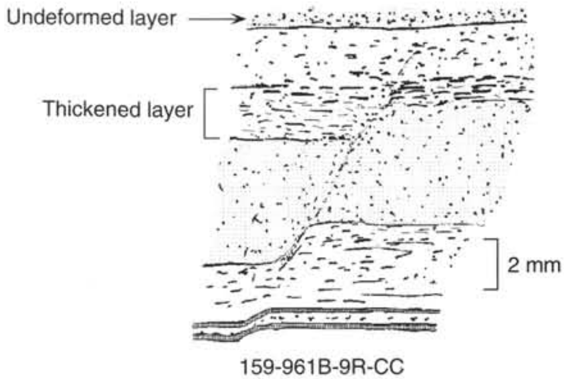

Figure 27. Sketch of a synsedimentary fault in laminated siltstone/fine-grained sandstone showing variation in thickness of the same layer across the fault (Section 159-961B-9R-CC, 12–13 cm).

Table 4. Summary of elemental analysis of sediments at Site 961.

Core, section, interval (cm)	Depth (mbsf)	Inorg-C (wt%)	$CaCO_3$ (wt%)	Tot-C (wt%)	Org-C (wt%)	TN (wt%)	C/N
159-961A-							
1R-1, 100–101	1.0	5.05	42.1	5.68	0.63	0.07	9.5
3R-1, 90–91	14.0	5.92	49.3	6.31	0.39	0.06	6.9
3R-3, 90–91	17.0	4.93	41.1	5.29	0.36	0.06	6.3
4R-1, 10–11	22.8	5.58	46.5	5.95	0.37	0.05	7.0
4R-2, 55–56	24.8	3.56	29.7	3.87	0.31	0.04	7.0
5R-2, 20–21	34.0	4.76	39.7	4.98	0.22	0.04	5.9
8R-1, 65–66	61.9	3.66	30.5	3.71	0.05	0.04	1.4
9R-1, 117–118	72.2	1.32	11.0	1.47	0.15	0.04	3.5
12R-1, 58–59	100.5	0.98	8.2	1.13	0.15	0.04	3.6
14R-1, 43–44	110.0	2.49	20.7	2.78	0.29	0.03	9.2
14R-2, 35–36	111.5	1.17	9.7	1.36	0.19	0.04	4.9
15R-1, 16–17	129.1	1.18	9.8	1.24	0.06	0.03	1.8
16R-1, 25–26	138.8	0.07	0.6	0.28	0.21	0.05	4.3
19R-1, 17–18	167.6	0.05	0.4	0.06	0.01	0.03	0.4
20R-2, 80–81	179.3	3.56	29.7	3.63	0.07	0.00	
22R-CC, 9–11	198.3	0.76	6.3	0.83	0.07	0.10	0.7
23R-1, 25–27	206.4	0.26	2.2	0.41	0.15	0.04	3.9
24R-1, 97–98	216.7	0.64	5.3	0.81	0.17	0.03	4.9
25R-1, 63–64	226.1	1.36	11.3	1.94	0.58	0.09	6.2
26R-1, 96–97	236.6	0.04	0.3	0.45	0.41	0.08	4.8
27R-1, 25–26	246.0	0.17	1.4	0.44	0.27	0.07	4.0
28R-1, 52–53	255.8	0.72	6.0	0.95	0.23	0.10	2.2
29R-1, 93–94	265.8	1.98	16.5	2.18	0.20	0.18	1.1
30R-2, 85–87	276.9	1.20	10.0	1.23	0.03	0.12	0.3
33R-1, 25–27	299.8	0.56	4.7	0.86	0.30	0.06	5.1
34R-1, 68–69	304.2	0.37	3.1	0.72	0.35	0.11	3.2
35R-1, 38–39	308.6	0.43	3.6	1.08	0.65	0.11	6.0
159-961B-							
1R-1, 110–112	217.4	1.61	13.4	1.92	0.31	0.21	1.5
2R-1, 43–44	226.4	0.08	0.7	0.40	0.32	0.08	4.0
3R-2, 43–44	237.9	0.17	1.4	0.58	0.41	0.06	6.3
4R-2, 11–12	261.5	3.55	29.6	3.86	0.31	0.07	4.3
5R-1, 97–98	268.5	0.44	3.7	0.81	0.37	0.11	3.3
5R-CC, 2–4	270.8	1.11	9.2	1.37	0.26	0.05	5.3
7R-1, 90–92	285.1	0.81	6.7	1.08	0.27	0.09	3.0
7R-2, 95–96	286.7	0.16	1.3	0.46	0.30	0.05	6.2
7R-3, 5–6	286.8	0.29	2.4	0.55	0.26	0.08	3.2
8R-2, 43–44	295.7	0.70	5.8	0.85	0.15	0.04	3.7
10R-1, 43–44	313.6	0.16	1.3	0.58	0.42	0.13	3.2
10R-4, 54–55	318.2	0.12	1.0	0.84	0.72	0.08	8.9
11R-1, 31–32	317.7	0.12	1.0	0.51	0.39	0.09	4.4
12R-1, 58–59	323.0	0.17	1.4	0.53	0.36	0.11	3.4
13R-1, 74–75	332.8	0.36	3.0	0.80	0.44	0.10	4.5
13R-3, 17–19	334.8	0.32	2.7	0.83	0.51	0.06	7.9
15R-1, 79–80	352.2	0.56	4.7	1.02	0.46	0.14	3.3
15R-2, 43–44	353.3	0.37	3.1	0.72	0.35	0.11	3.1
16R-1, 43–44	356.1	0.56	4.7	0.88	0.32	0.12	2.6
16R-2, 125–126	358.5	1.35	11.2	1.84	0.49	0.10	5.0
16R-3, 113–114	359.8	1.78	14.8	2.24	0.46	0.09	5.2
16R-CC, 4–5	361.0	2.60	21.7	3.09	0.49	0.06	7.6
17R-CC, 11–13	362.6	0.59	4.9	1.03	0.44	0.10	4.5
18R-2, 62–63	364.6	0.78	6.5	1.18	0.40	0.10	4.1
19R-CC, 4–5	369.9	0.57	4.7	1.03	0.46	0.13	3.5

Note: Inorg-C = inorganic carbon, $CaCO_3$ = carbonate, Tot-C = total carbon, Org-C = total organic carbon, TN = total nitrogen, and C/N = organic carbon/total nitrogen ratios.

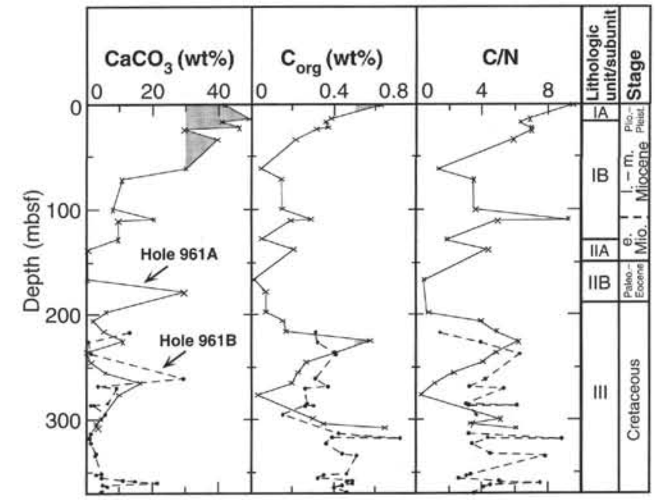

Figure 28. Carbonate content, total organic carbon content, and C/N ratios in sediments at Site 961. Lithologic units (see "Lithostratigraphy" section, this chapter) and preliminary stratigraphic stages are indicated.

Eval measurements were performed (for methods, see "Explanatory Notes" chapter, this volume). Results on volatile hydrocarbons are discussed in the "Source Rock Geochemistry" section (this chapter).

Carbonate and Organic Carbon Records

At Site 961 carbonate and organic carbon and total nitrogen contents were measured on 52 samples. Because of rotary drilling at Site 961, sediments were disturbed and core recovery was low throughout the entire core section from Holes 961A and 961B. Therefore average sampling frequency for organic geochemical studies was about one sample per core. Table 4 and Figure 28 summarize and present results obtained.

The highest carbonate and organic carbon contents in Holes 961A and 961B were measured in early Pliocene to Holocene nannofossil-foraminifer oozes. Carbonate contents fluctuate between 40 and 50 wt% in lower Pliocene deposits followed by a significant decrease below 30 wt% carbonate at the Miocene/Pliocene boundary (32 mbsf; Fig. 28). The similarity in carbonate patterns with those of Sites 960 and 959 (see "Organic Geochemistry" sections of "Site 959" and "Site 960" chapters, this volume) may suggest either terrigenous dilution in pelagic areas of the Deep Ivorian Basin, or changes in carbonate dissolution due to shifts in the position of the CCD, probably in response to glacial-interglacial cycles. Pleistocene high resolution carbonate records, obtained from various piston cores and ODP Sites 662 and 663 from the equatorial divergence zone farther east of Site 961, record distinctly higher carbonate contents (70–95 wt%) at similar water depths as Site 961 (deMenocal et al., 1993; Verardo and McIntyre, 1994; Ruddiman and Janecek, 1989); these values are characteristic for open marine depositional conditions in the eastern equatorial Atlantic. In contrast, variations in the deposition of organic matter throughout the Quaternary are not apparent in the organic carbon record of deep-sea Site 961 (Fig. 28). Organic carbon contents sharply decrease downcore from 0.6 wt% at 1 mbsf to 0.35 wt% at the Miocene/Pliocene boundary at 32 mbsf probably because of preferential degradation of labile organic matter. This trend continues down to 60 mbsf where organic carbon contents reach pelagic baseline levels below 0.15 wt%. The generally lower organic carbon contents of sediments at Site 961 compared to deposits from Sites 960 and 959 (see "Organic Geochemistry" sections of "Site 959" and "Site 960" chapters, this volume) probably reflect the more pelagic depositional conditions of Site 961, a setting that typically is characterized by very low accumulation of organic carbon (Emerson and Hedges, 1988).

Only a few samples of late Paleocene to late Miocene age were available for organic geochemical studies at Site 961. Carbonate contents in nannofossil chalks and nannofossil claystones (lithologic Subunit IB) display a steep downcore decrease. This carbonate trend correlates with the organic carbon pattern down to 60 mbsf, suggesting diagenetic dissolution of calcite. Farther downcore, carbonate contents do not reflect changes in lithology (glauconitic chalks, claystones, and porcellanites of lithologic Unit II) but persist at low levels (0–10 wt%). A single peak in carbonate (30 wt%) was identified at the base of the chert/porcellanite unit (lithologic Subunit IIB) at 180 mbsf (Fig. 28). Corresponding Tertiary organic carbon records below 0.2 wt% reach minimum values toward the base of late Paleocene porcellanites. In summary, carbonate and organic carbon patterns of this sedimentary section suggest extensive diagenetic modification.

Sandstones and siltstones of probable Cretaceous age were recovered in Holes 961A and 961B (Fig. 28). They are characterized by higher and more variable organic carbon content. Carbonate carbon, in contrast, consistently remains below 10 wt%. Peaks in carbonate were encountered at 260 and 360 mbsf (22–30 wt%), whereas deposits below and above these levels are nearly devoid of carbonate. Organic carbon content in lithologic Unit III varies between 0.7 and almost zero wt%. Intervals characterized by intermediate organic carbon content occur between 220 to 270 mbsf and from 310 mbsf down to the bottom of Hole 961B (Fig. 28). Few spikes in organic carbon with values exceeding 0.5 wt% were recognized at 215 and 310 mbsf in Hole 961A and at 320 mbsf in Hole 961B.

Composition of Organic Matter

Due to the generally low organic carbon content in Site 961 deposits, typing of sedimentary organic matter in terms of marine vs. terrigenous sources is problematic (see "Organic Geochemistry" sections and "Site 959" chapter, this volume). Results from few Rock-Eval measurements and C/N ratios were calculated and are summarized in Tables 4 and 5, and in Figure 28.

C/N ratios of Site 961 sediments vary from values <1 to almost 10. They consistently follow patterns in organic carbon contents except in lithologic Unit III (below 220 mbsf), which is characterized by a few insignificant fluctuations in C/N, ranging between 3 and 8. Changes in the composition of sedimentary organic matter in general cannot be deduced from variations in C/N ratios, considering the corresponding low organic carbon content (Müller, 1977). Rock-Eval data of one sample from the uppermost section of Hole 961A (Section 159-961A-1R), however, suggest elevated proportions of thermally immature marine organic matter close to the sediment/water interface (Table 5). Slightly elevated proportions of terrigenous organic matter, however, might be deduced from co-occurring spikes in organic carbon and C/N in Cretaceous deposits between 310 and 320 mbsf (Fig. 28). This interpretation is supported by relatively low hydrogen indices (between 50 and 110 mgHC/gTOC; Table 5) and smear slide analysis. They show elevated plant fragment content in late Pliocene through Pleistocene and Cretaceous sections (see "Lithostratigraphy" section, this chapter).

SOURCE ROCK GEOCHEMISTRY

Concentrations of headspace methane and ethane were measured in Holes 961A and 961B. In Hole 961A, very low methane concentrations were recorded. A maximum methane content of 1111 ppm was observed in Core 159-961A-28R at a depth of 256.8 mbsf. Very minor amounts of ethane ranging from 2 to 64 ppm were recorded in this hole.

In Hole 961B, slightly higher concentrations of methane were measured. A maximum concentration of 7310 ppm was recorded in Core 159-961B-13R at a depth of 333.6 mbsf. Ethane concentrations up to a maximum of 123 ppm were observed. There were also trace amounts of propane (C_3) detected in extremely low quantities of up to 18 ppm in Hole 961B.

It is not clear whether the hydrocarbon gases measured at Site 961 were generated in situ or had migrated from elsewhere. In either case, no safety or pollution problems were indicated at this location.

INORGANIC GEOCHEMISTRY

Eight interstitial water samples were taken during coring operations at Site 961. Holes 961A and 961B were rotary drilled from the outset. A combination of low core recovery and extensive drilling disturbance resulted in a sample set with discontinuous depth coverage. In the uppermost 16 mbsf of Hole 961A, two interstitial water samples were taken, one within lithologic Unit I, and the second at the lithologic Unit I/Unit II boundary (see "Lithostratigraphy" section, this chapter). No whole-round samples were cut between 16.05 mbsf and 256.75 mbsf. Below this depth six additional whole-round samples were taken. Two samples were taken from Hole 961A and four from Hole 961B, with the deepest sample occurring at 333.55 mbsf. All six of the deep samples are from lithologic Unit III (see "Lithostratigraphy" section, this chapter).

Drilling disturbance also necessitated extensive sample trimming to minimize the influence of contamination with drilling fluid. During most of the drilling, seawater was used as drilling fluid. However, when heavy mud was used to clear the hole, fresh water was used in drilling operations. Thus, there are two potential contaminating fluids with distinct compositions. In spite of efforts to minimize contamination, the possibility of sample contamination cannot be ruled out. In light of the discontinuous nature of the vertical profiles of interstitial water composition and the possibility of contamination, the discussion of Site 961 is focused on evaluating the integrity of the interstitial water data and comparing these data to samples from similar lithologic units from Sites 959 and 960. The complete data set resulting from interstitial water analyses at Site 961 is given in Table 6.

Although the data are scant, the major diagenetic processes occurring at Site 961 appear to be similar to those occurring at Sites 959 and 960. Chloride concentrations are similar to ambient seawater, but are slightly more variable than at Sites 959 and 960. Sulfate concentrations decrease with increasing depth (Fig. 29A). The concentration of methane in headspace samples increases above background levels at approximately 240 mbsf (Fig. 29B). Ammonium concentrations also increase with increasing depth (Fig. 29C). All of these trends are analogous to those observed at Sites 959 and 960 and reflect the influence of microbially mediated organic matter degradation on interstitial water chemistry. However, the absolute ammonium concentrations at Site 961 are lower than at Sites 959 and 960, which likely reflect the lower organic carbon content of the sediments at this site (see "Organic Geochemistry" section, this chapter). Because of the small volumes of extractable pore fluids obtained from the Site 961 samples, pH, alkalinity, and dissolved iron could be measured only in the two shallowest samples. Thus, although pH and alkalinity of interstitial water samples are also sensitive to the extent and mode of organic matter degradation in the sediment, we do not discuss them here. Similarly, the iron chemistry of the interstitial water at Site 961 cannot be considered in any detail. We simply note here that the relatively high dissolved iron concentration, 31 µM, at 16.05 mbsf, suggests the sediment dissolved oxygen in the pore water has been completely consumed above this depth.

The combined interstitial water and headspace gas data are somewhat enigmatic in that appreciable pore fluid sulfate concentrations,

Table 5. Summary of total organic carbon (Org-C), obtained from elemental analysis, and of T_{max}, S_1, S_2, S_3, hydrogen index (HI) values, and oxygen index (OI) values derived from Rock-Eval pyrolysis in sediments at Site 961.

Core, section, interval (cm)	Org-C (wt%)	T_{max} (°C)	S_1 (mgHC/gRock)	S_2 (mgHC/gRock)	S_3 (mgHC/gRock)	HI (mgHC/gTOC)	OI (mgHC/gTOC)
159-961A-							
1R-1, 100–101	0.63	355	0.07	0.81	0.73	211	189
25R-1, 63–64	0.58	381	0.05	0.26	3.02	63	740
35R-1, 38–39	0.65	427	0.01	0.16	0.45	53	146
159-961B-							
10R-1, 43–44	0.42	355	0.07	0.81	0.73	113	101

Table 6. Interstitial water analyses from Site 961.

Core, section, interval (cm)	Depth (mbsf)	IW vol (mL)	pH	Alkalinity (mM)	Salinity (g/kg)	Ca (mM)	Mg (mM)	Sr (µM)	Cl (mM)	SO_4 (mM)	NH_4 (µM)	K (mM)	SiO_2 (µM)	Fe (µM)	Mn (µM)
159-961A-															
1R-2, 145–150	2.95	42	7.44	2.01	37	10.51	50.84	94.00	554	24.6	95	12.4	327	2.1	1.5
3R-2, 145–150	16.05	40	7.36	3.28	36	10.48	49.29	111.00	555	25.4	145	12.3	182	30.8	1.4
28R-1, 140–150	256.75	11	—	—	—	16.25	33.12	374.00	557	8.0	699	8.0	227	—	1.1
30R-2, 140–150	277.45	8	—	—	—	16.47	33.65	406.00	559	7.5	750	7.4	200	—	0.7
159-961B-															
4R-2, 140–150	262.85	5	—	—	—	16.06	33.65	373.00	547	7.4	573	7.5	198	—	0.9
7R-1, 140–150	285.65	3	—	—	—	16.3	34.81	403.00	565	9.6	712	8.0	125	—	0.8
10R-4, 0–10	317.70	5	—	—	—	16.5	29.03	468.00	548	6.6	926	6.8	167	—	0.6
13R-1, 140–150	333.55	0.5	—	—	—	15.15	26.48	—	—	5.9	—	5.9	—	—	—

Note: All reported calcium concentrations were determined by titration except Sample 159-961B-13R-1. Because of the small volume of interstitial water extracted for this sample, Ca was determined by ion chromatograph. All magnesium analyses were made by ion chromatography. For a comparison of titration and ion chromatograph calcium and magnesium data see the "Inorganic Geochemistry" section of the "Explanatory Notes" chapter, this volume.

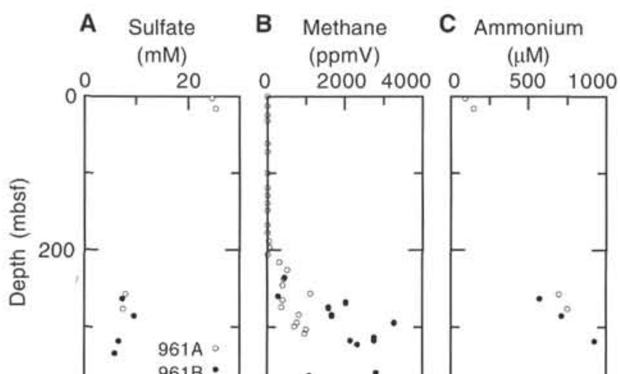

Figure 29. Interstitial water concentrations for (**A**) sulfate, (**B**) methane, and (**C**) ammonium plotted vs. depth below seafloor at Site 961.

approximately 6 mM, persist below the depth in the sediment where methane concentrations rise above background levels. This stands in marked contrast to results from previous Leg 159 sites and other DSDP and ODP legs drilled proximal to continental margins (Prell, Niitsuma, et al., 1989; Leg 117, Oman Margin). In general, the zone of microbially mediated sulfate reduction and bacterial methanogenesis occurs in distinct portions of the sediment pile (Gieskes, 1983). Nonzero sulfate concentrations within the zone of methane production may reflect contamination of the interstitial water samples with seawater. Given the drilling disturbance apparent in interstitial water samples and the extensive amount of trimming required to obtain relatively small drilling "biscuits," this interpretation is not unreasonable. If this is the case, it is surprising that scatter in the depth profiles of the concentrations of calcium, magnesium, silica, ammonium, and sulfate are not greater, as would be expected if the samples analyzed were composed of variable proportions of seawater and pore fluid. Alternatively, the increase in methane in headspace gases may be unrelated to bacterial methane production. Rather, the methane may reflect traces of relict thermogenic hydrocarbons. Although this is a speculative interpretation, methane/ethane ratios of 200 are unusually low for bacterially produced methane in sediments less than 400 mbsf (Myhre, Thiede, Firth, et al., 1995; Leg 151). Based on the available information, it is not possible to discount this hypothesis. However, the data from the deep interstitial water samples should be examined cautiously, because the possibility of contamination cannot be ruled out.

Dissolved calcium concentrations similar to those of seawater were measured in samples from lithologic Unit I (Fig. 30A). Concentrations of samples below 256.75 mbsf exhibit little variability, averaging 16.3 ± 0.18 mM, and are not significantly different from that of the one sample from the same lithologic unit at Site 960. Higher calcium concentrations of ~21 mM have only been measured from the Eocene-Oligocene porcellanite sediments of Site 959 (lithologic Subunits IIB and IIC) that are not well represented at either Site 960 or 961. Thus, in spite of the few data points and the discontinuous nature of the record at Site 961, this profile is comparable to that of the previous Site 960. The calcium enrichment at depth at Site 961 may result from the dissolution of calcite. The relative abundance of calcite averages ~5% in this part of the sequence (see "Organic Geochemistry" section, this chapter).

The dissolved magnesium profile shows a trend of decreasing concentrations with depth (Fig. 30B). The uppermost samples are slightly lower (5%) than seawater values, but have comparable concentrations to samples from the same depth interval at Site 960. At Site 961, magnesium concentrations are 50% to 60% lower than seawater concentration within the siltstone in lithologic Unit III. The formation of dolomite and/or ankerite rhombs observed in smear slides and XRD analysis of sediments throughout the entire section (see "Lithostratigraphy" section, this chapter) is a likely cause for the observed overall magnesium decrease with depth. Moreover, there is a

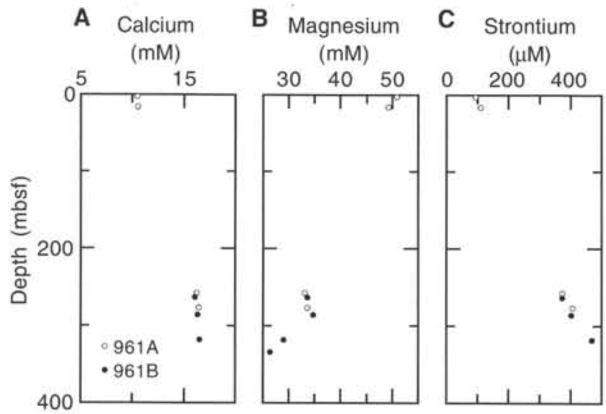

Figure 30. Interstitial water concentrations for (**A**) calcium, (**B**) magnesium, and (**C**) strontium plotted vs. depth in the sediment at Site 961. Calcium concentrations were titrated, whereas magnesium concentrations were obtained from ion chromatography. See "Explanatory Notes" chapter, this volume, for explanation of results using these approaches.

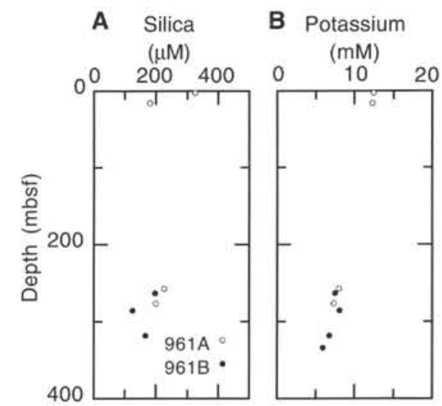

Figure 31. Interstitial water concentrations for (**A**) silica and (**B**) potassium plotted vs. depth at Site 961.

considerable decline in dissolved magnesium below ~290 mbsf relative to concentrations of samples above this level. This change in magnesium is not accompanied by any variation in dissolved calcium. It could be from magnesium uptake during clay mineral transformations. For example, XRD analyses demonstrate the presence of the clay mineral chlorite beginning at ~187 mbsf within these clay-rich sediments (see "Lithostratigraphy" section, this chapter).

Dissolved strontium concentrations increase with depth analogous to the pattern observed at Sites 959 and 960 and are attributed to calcite recrystallization (Fig. 30C). At depth within lithologic Unit III, concentrations between 374 and 468 μM are in the range of that measured in the deepest sample from Site 960, which also has comparable carbonate percentage abundance. At Site 959, slightly higher concentrations than these were measured toward the base of the younger porcellanite sediments.

In contrast to Sites 959 and 960, variations in dissolved manganese concentrations do not appear to be related to carbonate diagenesis. Rather than displaying a pronounced sub-seafloor maximum, as at Sites 959 and 960, manganese concentrations remain low and nearly constant in all Site 961 samples (Table 6). The reason for this difference is not immediately clear, but it is likely related to the supply of manganese oxides to the sediment, to the uptake of dissolved manganese within the sediment pile, or both.

Depth profiles of silica and potassium concentrations are given in Figures 31A and B. The highest measured silica concentration, 327 μM, is associated with the shallowest sample. Although Sites 959 and 960 exhibited local maxima in dissolved silica in the upper few tens of meters of the sediment, the highest silica concentrations, more than 1000 μM, were associated with deeper siliceous portions of the core. Lithologic Subunit IIB of Site 961 is composed of porcellanites (see "Lithostratigraphy" section, this chapter), but low recovery and drilling disturbance at Site 961 precluded interstitial water sampling of this unit. Therefore, we suspect that the low silica concentrations observed in Site 961 pore waters reflect sampling bias rather than dramatic differences in interstitial water silica chemistry of Site 961 relative to Sites 959 and 961. In this regard, it is noteworthy that the deep interstitial water samples from Site 961 occur in sandy siltstones to silty claystones designated as lithologic Unit III (see "Lithostratigraphy" section, this chapter). The silica concentration of pore fluid from a single sample from lithologic Unit III at Site 960 was similarly low. Potassium concentrations at Site 961 decrease with increasing depth in the sediment, as was observed at Sites 959 and 961. As before, we interpret this decrease to reflect potassium uptake in association with authigenic clay mineral formation. See the "Inorganic Geochemistry" section in the "Site 959" chapter (this volume) for additional discussion of this topic.

In summary, in spite of a discontinuous sample suite, and the possibility of seawater contamination of interstitial water samples at Site 961, the data are sufficient to demonstrate that a set of diagenetic reactions is occurring in Site 961 sediments that is analogous to those that have been more completely documented 0at Sites 959 and 960.

PHYSICAL PROPERTIES

The sediments cored at Site 961 had a very poor recovery and were highly disturbed by drilling. As a consequence, physical properties data collected at Site 961 are rather sparse. Hole 961A was cored to 308.7 mbsf, and Hole 961B was cored from 216.3 to 239 mbsf and from 259.9 to 374 mbsf. Data collected at Hole 961B show the same trends as data at Hole 961A below 216.3 mbsf.

MST measurements were made on whole cores using the gamma-ray attenuation porosity evaluator (GRAPE), Natural Gamma Radiation (NGR) tool, and magnetic susceptibility meter. The *P*-Wave Logger was not used at Site 961, as rotary drilled (RCB) sediments are not of appropriate quality. Generally, the diameter of the sediments in the liner was nonuniformly smaller than the diameter of the liner, which results in poor-quality MST data. Because of drilling disturbances and low recovery, only a few thermal conductivity, index properties, velocimetry, and undrained shear strength measurements were made, whereas no resistivity measurements could be made at Site 961. Descriptions of the experimental methods are provided in the "Physical Properties" section of the "Explanatory Notes" chapter (this volume). All tables presented and all MST data are available on CD (this volume).

Multisensor Track

The magnetic susceptibility data are presented in the "Paleomagnetism" section (this chapter).

The quality of the GRAPE density data was deteriorated because the liner was not completely filled with sediments, which results in a high error in the data. GRAPE density values were edited and Boyce-corrected, and only the maximum bulk densities were taken into consideration. At Hole 961A, within the depth interval from 0 to 190 mbsf, the density values are not higher than 1.6 g/cm^3. Higher values (≤2.3 g/cm^3) were measured below 196 mbsf at Hole 961A and at the

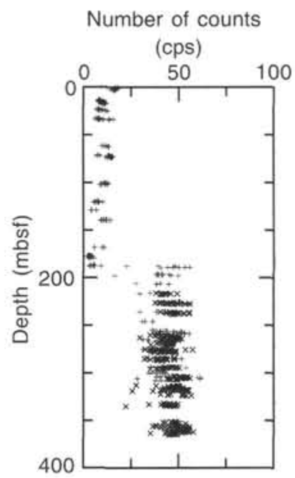

Figure 32. Total number of counts vs. depth at Site 961; results from NGR. Plus signs = Hole 961A, "x" symbols = Hole 961B.

entire Hole 961B. This shift in magnitude occurs near the boundary between lithologic Units II and III (188.5 mbsf) at Hole 961A.

NGR data were collected within a 30-s counting period, and the background radiation of 8.74 cps was subtracted (Fig. 32). The total number of counts were less than 15 cps to the depth of about 190 mbsf at Hole 961A. Below 190 mbsf, there is a significant increase to much higher values ranging from 35 to 55 cps. This change corresponds to the boundary between lithologic Units II and III (at 188.5 mbsf). Both units contain a high composition of clay minerals, but of different types. Lithologic Unit II comprises mainly smectite and kaolinite, whereas in the lithologic Unit III there are chlorite, illite/mica, and feldspar that contain potassium. Thus, the higher amount of potassium in the lithologic Unit III is probably responsible for the distinct increase in natural gamma radiation.

Thermal Conductivity Measurements

Only nine thermal conductivity measurements could be collected at Hole 961A in full-space geometry. At Hole 961B, as sediments were more compacted, the full-space method could not be used. Poor recovery did not allow half-space measurements at Hole 961B.

Thermal conductivity values range from 0.86 to 1.50 $Wm^{-1}C^{-1}$ at Hole 961A (Table 7). Two maximum values (1.44 and 1.50 $Wm^{-1}C^{-1}$) were measured in lithologic Unit III, which has a high siliciclastic content, and they compared to the more carbonate-rich lithologic Unit II.

Index Properties

Index properties were determined from measurement of wet and dry masses and volumes between 34 and 308 mbsf at Hole 961A, and between 217 and 369 mbsf at Hole 961B.

Index property measurements at Hole 961A are sparse, but two general trends can be distinguished (Table 8; Fig. 33). From 34 to 179 mbsf bulk density is generally lower than 1.70 g/cm^3 and porosity higher than 62%, and below 190 mbsf there is a shift to higher bulk density values (2.11 to 2.72 g/cm^3) and lower porosity values (<42%) oscillating at about 25%. This change corresponds to the boundary between lithologic Units II and III (at 188.5 mbsf). The local peak at 148.4 mbsf, with a porosity of 14% and bulk density of 2.15 g/cm^3, was recorded for a sample cut from the chert layer of lithologic Subunit IIB. Water content and void ratio approximately follow the trend of porosity, and dry density follows that of bulk density. Solids-grain density is rather constant (2.69–2.86 g/cm^3) with four lower values within lithologic Units II and III. At Hole 960B, the data show the same trends as at Hole 960A.

Table 7. Thermal conductivity data at Hole 961A.

Core, section, interval (cm)	Depth (mbsf)	Lithologic unit	Thermal conductivity ($Wm^{-1}C^{-1}$)
159-961A-			
8R-1, 50	61.70	IB	1.15
9R-1, 75	71.75	IB	1.20
14R-, 85	120.15	IB	0.86
15R-1, 50	129.40	IB	0.93
16R-1, 75	139.25	IIA	0.93
20R-1, 70	177.70	IIB	0.97
21R-1, 112	187.82	IIB	1.08
26R-1, 90	236.50	III	1.44
28R-3, 75	259.05	III	1.50

Velocimetry

Discrete measurements of *P*-wave velocity at Hole 961A were collected close to the location of samples for index properties in softer sediments and, below 187 mbsf, in more lithified sediments, measurements were collected on the same cube samples. At Hole 961B, as sediments were compacted, only cubes were cut for measurements.

In the upper part of Hole 961A (34–187 mbsf), velocities are low and range between 1.51 and 1.76 km/s (Table 9; Fig. 34). The highest value of vertical (4.34 km/s) and horizontal (4.17 km/s) velocity was measured on the chert cube at 174 mbsf from lithologic Subunit IIB. A significant shift to much higher velocities occurs across the boundary between lithologic Units II and III (at 188 mbsf). The range of both horizontal and vertical velocities is between 2.37 and 3.50 km/s.

The anisotropy of velocity calculated from discrete velocity measurements in the vertical and horizontal directions ranges from –0.10 to 0.19 (Table 9; Fig. 34C). The anisotropy is mainly positive from 198 to 286 mbsf and below 360 mbsf, whereas negative values of anisotropy were calculated between 295 and 353 mbsf. The measurements of negative anisotropy (i.e., with higher vertical than horizontal velocity) were made in recrystallized sediments (with calcite, dolomite, or siderite) and sediments with steeply dipping beds (cf. "Lithostratigraphy" section, this chapter).

Table 9 further shows *P*-wave velocities corrected to in situ conditions. The corrected velocity is calculated from the in situ seawater velocity, sediment porosity, seawater velocity in the laboratory, and sediment velocity (cf. "Physical Properties" section of the "Explanatory Notes" chapter, this volume). The downhole variation of in situ seawater velocity and porosity was determined from regression analysis. The linear and the power regression models in KaleidaGraph 3.0.4 were used to generate curve-fit equations for in situ seawater velocity and porosity. The curve fit between the equations and data is good (>0.96) for in situ seawater velocity at Holes 961A and 961B and for porosity in the upper part of Holes 961A and 961B. The curve fit between the equations and data for porosity at the lower part of Holes 961A and 961B is not as good (0.73).

Undrained Shear Strength

Eight undrained shear strength measurements were made between 34 and 189 mbsf in Hole 961A. Below 190 mbsf the sediments of lithologic Unit III were too consolidated for vane shear or penetrometer measurements. Values above 189 mbsf range from 20 to 72 kPa (Table 10). The highest shear strength (176 kPa) was measured at 189 mbsf in pyritized siltstone of lithologic Unit III.

Summary

The general correlation between different sets of physical properties data at Site 961 is rather good, but the low density of measurements does not permit more detailed studies. All physical properties data collected at Site 961 show distinctive changes in trend at the boundary between lithologic Units II and III at 188.5 mbsf (Tables 7–10; Figs. 32–34). Sediments in these units are significantly different because lithologic Unit II is composed mainly of carbonate-rich hemipelagic to pelagic sediments, whereas Unit III consists mainly of lithified siliciclastic sediments.

REFERENCES

Basile, C., Mascle, J., Popoff, M., Bouillin, J.P., and Mascle, G., 1993. The Côte d'Ivoire-Ghana transform margin: a marginal ridge structure deduced from seismic data. *Tectonophysics,* 222:1–19.

Bohrmann, G., and Stein, R., 1989. Biogenic silica at ODP Site 647 in the southern Labrador Sea: occurrence, diagenesis, and paleoceanographic implications. *In* Srivastava, S.P., Arthur, M.A., Clement, B., et al., *Proc. ODP, Sci. Results,* 105: College Station, TX (Ocean Drilling Program), 155–170.

Bolli, H.M., and Saunders, J.B., 1985. Oligocene to Holocene low latitude planktonic foraminifera. *In* Bolli, H.M., Saunders, J.B., and Perch-Nielsen, K. (Eds.), *Plankton Stratigraphy:* Cambridge (Cambridge Univ. Press), 155–262.

Bouillin, J.P., Poupeau, G., Riou, L., Sabil, N., Basile, C., Mascle, J., Mascle, G., and the *Equanaute* Scientific Party, 1994. La marge transformante de Côte d'Ivoire-Ghana: premières données thermo-chronologiques (campagne Equanaute, 1992). *C. R. Acad. Sci. Ser. 2,* 318:1365–1370.

Chamley, H., 1989. *Clay Sedimentology:* Berlin (Springer-Verlag).

deMenocal, P.B., Ruddiman, W.F., and Pokras, E.M., 1993. Influence of high- and low-latitude on African terrestrial climate: Pleistocene eolian records from equatorial Atlantic Ocean Drilling Program Site 663. *Paleoceanography,* 8:209–242.

Emerson, S., and Hedges, J.I., 1988. Processes controlling the organic carbon content of open ocean sediments. *Paleoceanography,* 3:621–634.

Ericson, D.B., Ewing, M., Wollin, G., and Heezen, B.C., 1961. Atlantic deep-sea sediment cores. *Geol. Soc. Am. Bull.,* 72:193–286.

Ericson, D.B., and Wollin, G., 1968. Pleistocene climates and chronology in deep-sea sediments. *Science,* 162:1227–1234.

Gieskes, J.M., 1983. The chemistry of interstitial waters of deep-sea sediments: interpretation of deep-sea drilling data. *In* Riley, J.P., and Chester, R. (Eds.), *Chemical Oceanography* (Vol. 8): London (Academic), 222–269.

Honnorez, J., Villeneuve, M., and Mascle, J. 1994. Old continent-derived metasedimentary rocks in the Equatorial Atlantic: an acoustic basement outcrop along the fossil trace of the Romanche transform fault at 6°30′W. *Mar. Geol.,* 117:237–251.

Hower, J., Eslinger, E.V., Hower, M.E., and Perry, E.A., 1976. Mechanism of burial metamorphism of argillaceous sediment. 1. Mineralogical and chemical evidence. *Geol. Soc. Am. Bull.,* 87:725–737.

Lamarche, G., Basile, C., Mascle, J., and Sage, F., in press. The Côte d'Ivoire-Ghana transform margin: sedimentary and tectonic structure from multichannel seismic data. *Geo-Mar. Lett.*

Mascle, J., Basile, C., Pontoise, B., and Sage, F., 1995. The Côte d'Ivoire-Ghana Transform Margin: an example of an ocean-continent transform boundary. *In* Banda, E., Talwani, M., and Thorne, M. (Eds.), *Rifted Ocean-Continent Boundaries,* NATO ASI Ser.: Dordrecht (Kluwer), 327–339.

Mascle, J., and Blarez, E., 1987. Evidence for transform margin evolution from the Côte d'Ivoire-Ghana continental margin. *Nature,* 326:378–381.

Mascle, J., Guiraud, M., Basile, C., Benkhelil, J., Bouillin, J.P., Cousin, M., and Mascle, G., 1993. La marge transformante de Côte d'Ivoire-Ghana: premiers résultats de la campagne Equanaute (Juin 1992). *C. R. Acad. Sci. Ser. 2,* 316:1255–1261.

Mascle, J., and the Scientific Party, 1994. Les marges continentales transformantes ouest-africaines—Côte d'Ivoire, Ghana, Guinée. *Série Repères Océan,* 5: Brest (IFREMER).

Moore, D.M., and Reynolds, R.C., Jr., 1989. *X-Ray Diffraction and the Identification and Analysis of Clay Minerals:* Oxford (Oxford Univ. Press).

Müller, P.J., 1977. C/N ratios in Pacific deep sea sediments: effect of inorganic ammonium and organic nitrogen compounds sorbed by clays. *Geochim. Cosmochim. Acta,* 41:765–776.

Mumpton, F.A., 1960. Clinoptilolite redefined. *Am. Mineral.,* 45:351–369.

Myhre, A.M., Thiede, J., Firth, J.V., et al., 1995. *Proc. ODP, Init. Repts.,* 151: College Station, TX (Ocean Drilling Program).

Odin, G.S., and Matter, A., 1981. De glauconarium origine. *Sedimentology,* 28:611–641.

Pisciotto, K.A., 1981. Distribution, thermal histories, isotopic compositions, and reflection characteristics of siliceous rocks recovered by the Deep Sea Drilling Project. *In* Warme, J.E., Douglas, R.G., and Winterer, E.L. (Eds.), *The Deep Sea Drilling Project: A Decade of Progress.* Spec. Publ.—Soc. Econ. Paleontol. Mineral., 32:129–148.

Poag, C.W., 1981. *Ecologic Atlas of Benthic Foraminifera of the Gulf of Mexico:* Stroudsburg, PA (Hutchinson Ross).

Prell, W.L., Niitsuma, N., et al., 1989. *Proc. ODP, Init. Repts.,* 117: College Station, TX (Ocean Drilling Program).

Reynolds, R.C., 1980. Interstratified clay minerals. *In* Brindley, G.W., and Brown, G. (Eds.), *Crystal Structures of Clay Minerals and their X-Ray Identification.* Mineral. Soc. London Monogr., 5:249–303.

Ruddiman, W.F., and Janecek, T.R., 1989. Pliocene-Pleistocene biogenic and terrigenous fluxes at equatorial Atlantic Sites 662, 663, and 664. *In* Ruddiman, W., Sarnthein, M., et al., *Proc. ODP, Sci. Results,* 108: College Station, TX (Ocean Drilling Program), 211–240.

Sage, F., 1994. Structure crustale d'une marge transformante et du domaine océanique adjacent: exemple de la marge de Côte d'Ivoire-Ghana [Ph.D. thesis]. Univ. Pierre et Marie Curie, Paris.

Srodon, J., and Eberl, D.D., 1984. Illite. *In* Bailey, S.W. (Ed.), *Micas.* Min. Soc. Am., Rev. Mineral., 13:495–544.

Stein, R., and Faugères, J.-C., 1989. Sedimentological and geochemical characteristics of the Upper Cretaceous and lower Tertiary sediments at Site 661 (eastern equatorial Atlantic) and their paleoenvironmental significance. *In* Ruddiman, W., Sarnthein, M., et al., *Proc. ODP, Sci. Results,* 108: College Station, TX (Ocean Drilling Program), 297–309.

van Morkhoven, F.P.C.M., Berggren, W.A., and Edwards, A.S., 1986. Cenozoic cosmopolitan deep-water benthic foraminifera. *Bull. Cent. Rech. Explor.-Prod. Elf-Aquitaine,* Mem. 11.

Verardo, D.J., and McIntyre, A., 1994. Production and destruction: control of biogenous sedimentation in the tropical Atlantic 0–300,000 years B.P. *Paleoceanography,* 9:63–86.

Weaver, C.E., and Broekstra, B.R., 1984. Illite-mica. *In* Weaver, C.E. (Ed.), *Shale-Slate Metamorphism in Southern Appalachians:* Amsterdam (Elsevier), 67–97.

Weaver, C.E., Highsmith, P.B., and Wampler, J.M., 1984. Chlorite. *In* Weaver, C.E. (Ed.), *Shale-Slate Metamorphism in Southern Appalachians:* Amsterdam (Elsevier), 99–139.

Weaver, P.P.E., and Raymo, M.E., 1989. Late Miocene to Holocene planktonic foraminifers from the equatorial Atlantic, Leg 108. *In* Ruddiman, W., Sarnthein, M., et al., *Proc. ODP, Sci. Results,* 108: College Station, TX (Ocean Drilling Program), 71–91.

Ms 159IR-107

NOTE: For all sites drilled, core-description forms ("barrel sheets") and core photographs can be found in Section 4, beginning on page 317. Smear-slide data can be found in Section 5, beginning on page 587. Scanned structural VCDs, structural data spreadsheets, and selected scanned microstructures are included on the CD-ROM in the back of this volume. Also presented on the CD-ROM are all processed logs (including FMS, dipmeter, BRG temperature, high-resolution density, and neutron data), sonic waveforms, and explanatory text.

Table 8. Index properties data at Site 961.

Core, section, interval (cm)	Depth (mbsf)	Lithologic unit	Water content: Total wet mass (%)	Water content: Mass of solids (%)	Density: Wet bulk (g/cm³)	Density: Solids-grain (g/cm³)	Density: Dry (g/cm³)	Porosity (%)	Void ratio (1)
159-961A-									
5R-2, 22	34.02	IB	43.44	76.80	1.60	2.70	0.91	67.99	2.03
8R-1, 66	61.86	IB	38.55	62.74	1.70	2.75	1.05	64.03	1.68
9R-1, 114	72.14	IB	39.89	66.36	1.67	2.69	1.01	65.19	1.75
12R-1, 54	100.44	IB	43.99	78.54	1.61	2.71	0.90	69.24	2.08
17R-CC, 2	148.41	IIB	6.62	7.09	2.15	2.10	2.00	13.85	0.15
19R-1, 15	167.55	IIB	37.52	60.04	1.69	2.43	1.06	62.02	1.43
20R-2, 81	179.31	IIB	47.09	89.00	1.54	2.52	0.81	70.55	2.19
21R-2, 94	189.14	III	20.37	25.59	2.11	2.77	1.68	41.99	0.69
22R-CC, 9	198.26	III	12.38	14.13	2.49	2.76	2.18	30.11	0.38
23R-1, 25	206.35	III	7.91	8.58	2.72	2.73	2.50	20.96	0.23
24R-1, 98	216.68	III	2.12	2.17	2.46	2.69	2.41	5.10	0.06
25R-1, 61	226.11	III	9.67	10.70	2.47	2.80	2.23	23.31	0.29
26R-1, 93	236.53	III	17.63	21.41	2.48	2.52	2.04	42.71	0.53
27R-1, 23	245.93	III	7.56	8.18	2.54	2.77	2.35	18.77	0.22
28R-1, 49	255.79	III	9.99	11.10	2.43	2.76	2.19	23.72	0.30
29R-1, 120	266.10	III	15.12	17.81	2.32	2.86	1.97	34.19	0.50
30R-2, 85	276.85	III	11.80	13.38	2.49	2.73	2.20	28.66	0.36
31R-1, 44	284.64	III	10.00	11.11	2.33	2.76	2.10	22.78	0.30
33R-1, 25	299.75	III	10.00	11.11	2.45	2.73	2.20	23.87	0.30
34R-1, 68	304.18	III	13.20	15.21	2.33	2.74	2.02	29.98	0.41
35R-1, 37	308.57	III	10.66	11.93	2.48	2.75	2.21	25.76	0.32
159-961B-									
1R-1, 110	217.40	III	7.87	8.54	2.35	2.75	2.17	18.05	0.23
2R-1, 44	226.44	III	8.54	9.33	2.34	2.72	2.14	19.52	0.25
3R-2, 44	237.94	III	2.29	2.34	2.27	2.77	2.22	5.07	0.06
4R-1, 86	260.76	III	9.07	9.97	2.86	2.81	2.60	25.30	0.27
5R-1, 95	268.45	III	13.41	15.49	2.39	2.83	2.07	31.28	0.43
5R-CC, 2	270.78	III	10.32	11.51	2.31	2.77	2.07	23.27	0.31
6R-1, 124	275.74	III	12.04	13.68	2.40	2.73	2.11	28.18	0.36
6R-2, 122	277.22	III	13.66	15.82	2.32	2.77	2.00	30.91	0.43
6R-3, 101	278.51	III	9.63	10.65	2.28	2.74	2.06	21.40	0.29
7R-1, 90	285.10	III	10.48	11.71	2.47	2.80	2.21	25.25	0.32
7R-2, 96	286.66	III	11.85	13.45	2.23	2.74	1.97	25.82	0.36
7R-3, 4	286.74	III	12.11	13.78	2.38	2.75	2.09	28.12	0.37
8R-1, 66	294.46	III	11.56	13.07	2.42	2.73	2.14	27.24	0.35
8R-2, 43	295.73	III	9.83	10.91	2.33	2.74	2.10	22.36	0.29
9R-1, 132	304.82	III	12.75	14.61	2.36	2.81	2.06	29.39	0.40
9R-2, 93	305.93	III	15.94	18.97	2.33	2.75	1.95	36.18	0.51
9R-CC, 10	307.40	III	13.12	15.10	2.38	2.78	2.07	30.49	0.41
10R-1, 44	313.64	III	14.37	16.78	2.37	2.73	2.03	33.27	0.45
10R-4, 53	318.23	III	14.11	16.43	2.32	2.73	2.00	31.99	0.44
11R-1, 31	317.71	III	12.79	14.67	2.38	2.78	2.07	29.68	0.40
12R-1, 55	322.95	III	22.06	28.31	2.79	2.73	2.17	59.98	0.76
13R-1, 74	332.84	III	10.57	11.82	2.32	2.75	2.08	23.97	0.32
13R-2, 73	334.33	III	10.64	11.90	2.27	2.75	2.03	23.55	0.32
13R-3, 15	334.75	III	10.56	11.80	2.34	2.74	2.10	24.15	0.32
15R-1, 80	352.20	III	11.41	12.87	2.35	2.78	2.08	26.15	0.35
15R-2, 44	353.34	III	9.36	10.33	2.33	2.75	2.11	21.28	0.28
16R-1, 44	356.14	III	12.45	14.22	2.47	2.94	2.16	29.96	0.41
16R-2, 125	358.45	III	12.65	14.48	2.36	2.80	2.06	29.15	0.40
16R-3, 112	359.82	III	12.14	13.82	2.44	2.83	2.14	28.90	0.38
16R-CC, 4	360.99	III	8.23	8.97	2.59	2.89	2.37	20.79	0.25
17R-CC, 10	362.60	III	7.91	8.59	2.54	2.74	2.34	19.65	0.23
18R-2, 62	364.64	III	8.30	9.05	2.39	2.74	2.19	19.38	0.24
19R-CC, 5	369.95	III	4.84	5.09	3.15	3.29	3.00	14.89	0.16

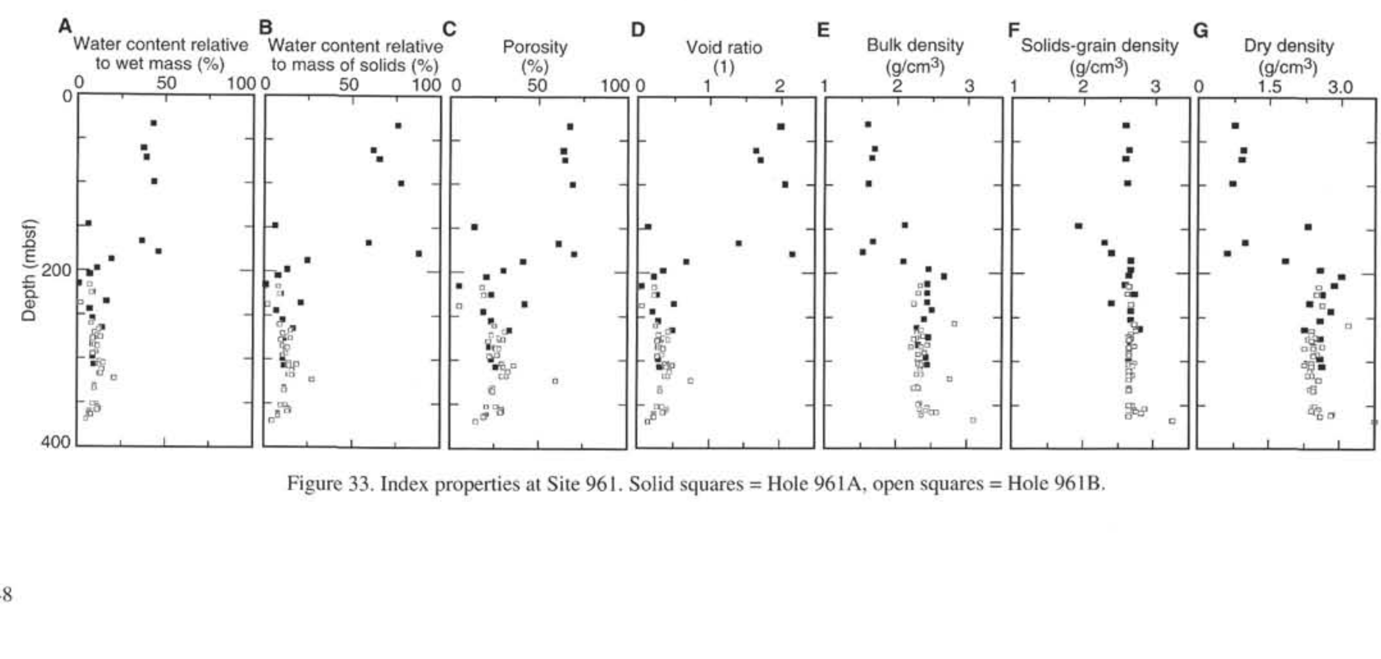

Figure 33. Index properties at Site 961. Solid squares = Hole 961A, open squares = Hole 961B.

Table 9. *P*-wave velocity and anisotropy data at Site 961.

Core, section, interval (cm)	Depth (mbsf)	Lithologic unit	Uncorrected velocity Vert (km/s)	Hor 1 (km/s)	Hor 2 (km/s)	Anisotropy Hor 1 (1)	Hor 2 (1)	Corrected velocity Vert (km/s)	Hor 1 (km/s)	Hor 2 (km/s)	DSV
159-961A-											
5R-2, 22.6	34.03	IB	—	1.542	—	—	—	—	1.538	—	3
5R-2, 23.5	34.03	IB	1.514	—	—	—	—	1.510	—	—	1
8R-1, 68.8	61.89	IB	1.560	—	—	—	—	1.559	—	—	1
8R-1, 70.8	61.91	IB	—	1.580	—	—	—	—	1.579	—	3
9R-1, 116.5	72.17	IB	1.553	—	—	—	—	1.554	—	—	1
9R-1, 118.3	72.18	IB	—	1.568	—	—	—	—	1.569	—	3
9R-2, 88.5	73.39	IB	—	1.557	—	—	—	—	1.558	—	3
12R-1, 52.8	100.43	IB	—	1.556	—	—	—	—	1.560	—	3
12R-1, 53.2	100.43	IB	1.540	—	—	—	—	1.544	—	—	1
12R-2, 33.8	101.74	IB	—	1.562	—	—	—	—	1.567	—	3
14R-2, 30.7	121.11	IB	—	1.529	—	—	—	—	1.534	—	3
16R-1, 122.5	139.73	IIA	—	1.611	—	—	—	—	1.615	—	3
17R-CC, 2.0	148.41	IIB	4.340	—	4.168	—	−0.04	4.359	—	4.185	3
19R-1, 16	167.56	IIB	—	1.733	—	—	—	—	1.752	—	3
20R-2, 86	179.36	IIB	—	1.625	—	—	—	—	1.639	—	3
21R-1, 78	187.48	IIB	—	1.748	—	—	—	—	1.762	—	3
21R-1, 78	187.48	IIB	—	1.696	—	—	—	—	1.709	—	3
21R-1, 78	187.48	IIB	—	1.762	—	—	—	—	1.776	—	3
22R-CC, 9	198.26	III	1.989	2.064	2.039	0.04	0.02	2.003	2.080	2.054	3
23R-1, 25	206.35	III	2.835	3.103	3.043	0.09	0.07	2.861	3.134	3.073	3
24R-1, 100	216.7	III	—	3.479	—	—	—	—	3.514	—	3
30R-2, 84	276.84	III	2.462	2.547	2.599	0.03	0.05	2.491	2.578	2.631	3
31R-1, 44	284.64	III	2.664	2.790	3.009	0.05	0.12	2.702	2.831	3.057	3
33R-1, 25	299.75	III	2.712	2.888	2.886	0.06	0.06	2.757	2.940	2.938	3
34R-1, 48.2	303.98	III	—	2.728	—	—	—	—	2.776	—	3
159-961B-											
1R-1, 110	217.4	III	3.176	3.181	3.103	0.00	−0.02	3.207	3.212	3.132	3
2R-1, 44	226.44	III	2.753	3.088	3.094	0.11	0.12	2.775	3.116	3.122	3
4R-1, 86	260.76	III	—	3.056	—	—	—	—	3.092	—	3
5R-CC, 2	270.78	III	2.375	2.619	2.600	0.10	0.09	2.400	2.650	2.630	3
6R-1, 101	275.51	III	—	2.747	—	—	—	—	2.783	—	3
6R-1, 101	275.51	III	—	2.952	—	—	—	—	2.993	—	3
6R-1, 101	275.51	III	—	3.135	—	—	—	—	3.182	—	3
7R-1, 90	285.1	III	2.647	2.838	2.966	0.07	0.11	2.684	2.881	3.013	3
7R-2, 96	286.66	III	2.672	2.659	2.855	0.00	0.07	2.711	2.697	2.899	3
7R-3, 4	286.74	III	2.614	2.607	2.695	0.00	0.03	2.651	2.644	2.734	3
8R-2, 43	295.73	III	2.792	2.616	2.797	−0.07	0.00	2.838	2.656	2.843	3
12R-1, 55	322.95	III	—	2.378	—	—	—	—	2.417	—	3
13R-1, 74	332.84	III	2.842	2.678	2.826	−0.06	−0.01	2.898	2.728	2.881	3
13R-1, 103.9	333.14	III	—	2.667	—	—	—	—	2.716	—	3
13R-2, 73	334.33	III	2.851	2.569	2.818	−0.10	−0.01	2.907	2.615	2.873	3
13R-2, 87.9	334.48	III	—	2.646	—	—	—	—	2.694	—	3
13R-3, 15	334.75	III	2.876	2.705	2.821	−0.06	−0.02	2.933	2.755	2.876	3
13R-3, 51.5	335.12	III	—	2.698	—	—	—	—	2.748	—	3
15R-1, 80	352.2	III	2.680	2.628	2.680	−0.02	0.00	2.725	2.671	2.725	3
15R-1, 80.8	352.21	III	—	2.541	—	—	—	—	2.581	—	3
15R-2, 44	353.34	III	2.838	2.675	3.064	−0.06	0.08	2.888	2.719	3.122	3
15R-2, 46.3	353.36	III	—	2.424	—	—	—	—	2.460	—	3
16R-CC, 4	360.99	III	2.806	2.893	3.085	0.03	0.09	2.850	2.939	3.138	3
17R-CC, 10	362.6	III	2.958	3.306	3.114	0.11	0.05	3.005	3.365	3.166	3
18R-2, 62	364.64	III	2.694	3.053	3.244	0.12	0.19	2.731	3.101	3.299	3

Note: Vert = vertical direction (along core); Hor 1 = horizontal direction (perpendicular to cut core face); Hor 2 = horizontal direction perpendicular to Hor 1; DSV 1 = Digital Sound Velocimeter; DSV 3 = Hamilton Frame Velocimeter.

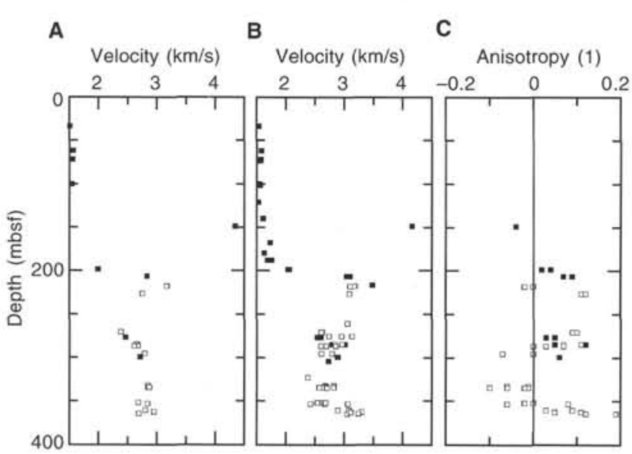

Figure 34. Results of discrete velocity measurements vs. depth at Site 961. **A.** *P*-wave velocity in vertical direction. **B.** *P*-wave velocity in horizontal direction. **C.** Anisotropy. Solid squares = Hole 961A, open squares = Hole 961B.

Table 10. Undrained shear strength data at Hole 961A.

Core, section, interval (cm)	Depth (mbsf)	Lithologic unit	Shear strength Vane shear (kPa)	Penetrometer (kPa)
159-961A-				
5R-2, 29.7	34.1	IB	22.4	—
5R-2, 33.6	34.14	IB	20.9	—
8R-1, 79.4	61.99	IB	37.7	—
9R-1, 123.6	72.24	IB	63.1	—
12R-1, 60.1	100.5	IB	72.1	—
14R-2, 21.3	121.01	IB	47.6	—
20R-2, 88	179.38	IIB	—	63.77
21R-2, 94	189.14	III	—	176.58